Universidad de Castilla-La Mancha

Escuela de Ingenieros de Caminos, Canales y Puertos

Doctoral Thesis

Advanced mechanical characterization of lime mortars and other materials of the civil and architectural patrimony

Lucía Garijo Alonso

Supervisors

Gonzalo Ruiz López

Xiaoxin Zhang

Pere Roca Fabregat

Ciudad Real, 2019

A mis padres y a José Joaquín

Agradecimientos

Quisiera agradecer de una forma especial a todas las personas que han hecho posible la realización de esta tesis doctoral.

Gracias a las instituciones que han financiado este trabajo. En primer lugar, al Ministerios de Educación, Cultura y Deporte por el contrato predoctoral FPU014/05186. Gracias también al Ministerio de Ciencia, Innovación y Universidades por el contrato 2018-COB-9144-2 a través del proyecto RTC-2017-6736-3. Agradezco también a la Universidad de Castilla-La Mancha (UCLM) la ayuda 2016/11635 para realizar una estancia de investigación en la Universidad de Miño, en Portugal. Finalmente, gracias a la meritoria ayuda del grupo de Mecánica de Sólidos de la Escuela de Caminos, C. y P. de Ciudad Real por financiar la asistencia a congresos y por todas las facilidades a través de equipos y materiales empleados en la investigación de esta tesis.

Pasando a un plano más personal, quisiera expresar mi más sincero agradecimiento a mis directores de tesis. Gracias al Prof. Gonzalo Ruiz por la oportunidad de trabajar en su equipo, por su dedicada atención a este trabajo y por su gran estímulo. Gracias por tu ejemplo de constancia en el trabajo y tu calidad humana. Gracias especialmente también al Dr. Xiaoxin Zhang por toda su paciencia y tiempo dedicado a esta tesis; gracias por tus preguntas y reflexiones que me han ayudado a profundizar y aprender del trabajo realizado. Gracias al Prof. Pere Roca, de la Universidad Politécnica de Cataluña, por los consejos sobre la dosificación de los morteros de cal y por lo aprendido junto a su equipo durante el año de trabajo previo a esta tesis.

Agradezco también a todos los miembros del grupo de Mecánica de Sólidos de la UCLM por el ambiente de trabajo tan acogedor que entre todos habéis creado. Gracias, en especial, a la Prof. Rena C. Yu por su ayuda con la simulación numérica y por estar siempre pendiente para coordinar todo aquello que necesitásemos. Gracias a los doctores Elisa Poveda y Manuel Tarifa por sus buenos consejos y ánimos; a mis compañeros de doctorado, Kaiming Pan y Ángel de la Rosa, al que además agradezco su ayuda con la técnica del porosímetro, el tiempo compartido en el despacho y las excursiones a Almagro. Gracias a los técnicos de laboratorio, Miguel Ángel Cámara, Juan Antonio Serrano y Miguel Ángel Cerezo por toda su ayuda durante la fabricación y ensayo de los morteros. Gracias también a Begoña Pérez por la colaboración en las gestiones.

Estoy muy agradecida también a todos aquellos que hicieron posible la realización de la estancia de investigación en la Universidad de Miño, en Portugal. A este respecto, agradezco a mi director, el Prof. Gonzalo Ruiz, habernos sugerido dicha universidad y ayudado en las gestiones. Gracias a los Profs. Paulo Lourenço y Miguel Azenha por su cálida acogida en Guimarães. Gracias además por su ayuda con el trabajo durante la estancia y con la redacción del artículo que surgió fruto de la misma. Gracias a mi compañera Meera Ramesh por el tiempo compartido en la Universidad de Miño, su ayuda en el laboratorio y su posterior y dedicada colaboración en dicho artículo.

Gracias a otros profesionales que de una manera u otra también han contribuído a esta tesis. Agradezco al Prof. Anselmo Acosta, de la UCLM, y a su equipo la ayuda en la

caracterización química y mineralógica de las cales. Gracias también al Dr. Carlos Leiva, de la Universidad de Sevilla, por ayudarnos con la técnica del porosímetro de mercurio. Agradezco al Dr. Ignacio Garrido Saénz, de la UCLM, la colaboración prestada en el análisis de microscopía de barrido, SEM, en los morteros de cal hidráulica natural y a *Iesmat*, Instrumentación Específica de Materiales por la ayuda en los ensayos por difracción láser para obtener la distribución granulométrica de las cales.

Doy las gracias también a toda mi familia por su apoyo constante. En especial, a mi tío Gonzalo por su gran ayuda y ánimo sobretodo en los comienzos de esta aventura, y a mis tíos Manolo y María por su apoyo de una u otra manera. Gracias a mis abuelos por el ejemplo que nos dieron, a los más pequeños de la casa por su entusiasmo y alegría contagiosos, a mis hermanos y cuñados por ayudarme siempre y por ser un referente para mí. Gracias de una manera especial a mis padres, José y Marisa, por todo el esfuerzo que habéis hecho para que yo pudiera llegar hasta aquí; gracias por vuestra entrega tan generosa. Para mí sois todo un ejemplo.

Finalmente, gracias a ese compañero de doctorado en el que me apoyé desde el principio porque siempre estaba disponible cuando le hacía alguna consulta y que se ha convertido en compañero de vida. Gracias, José Joaquín, por tu gran apoyo, tu ejemplo, tu tiempo, los planes compartidos y por toda tu ayuda a tantos niveles. Gracias por todo.

Ciudad Real, mayo de 2019

Acknowledgements

I would like to acknowledge all the people who have made possible the realization of this doctoral thesis.

Thanks to the institutions that have funded this work. Firstly, to the *Ministerio de Educación, Cultura y Deporte*, Spain, for the scholarship FPU014/05186. Thanks also to the *Ministerio de Ciencia, Innovación y Universidades* for the contract 2018-COB-9144-2 through the research project RTC-2017-6736-3. I also acknowledge the *Universidad de Castilla-La Mancha* (UCLM) for the help 2016/11636 to do a research stay at *Universidade do Minho*, in Portugal. Finally, thanks to the meritorious help from the group *Mecánica de Sólidos* of the *E.T.S.I. Caminos, C. y P. de Ciudad Real* for funding the attendance to conferences and for the facilities offered through the materials and equipment used during the research of this thesis.

From a more personal point of view, I would like to express my more sincerely gratitude to my thesis directors. Thanks to Prof. Gonzalo Ruiz for giving the opportunity to work in his group, for his dedicated attention to this work and for his stimulus. Thanks for your example of hard work and human quality. Thanks especially also to Dr. Xiaoxin Zhang for his great patience and for all the time devoted to this thesis; thanks for your questions and reflections that have helped me to deepen and learn more about the work done. Thanks to Prof. Pere Roca, from *Universidad Politécnica de Cataluña*, for his advice on the dosification of the lime mortars and for all that learnt within his group for a year previous to this thesis.

I acknowledge all the members of the group of *Mecánica de Sólidos* of UCLM; thanks for the warm environment of work that you have created. Thanks especially to Prof. Rena C. Yu for her help with the numerical simulation and for being always willing to coordinate everything we needed. Thanks to Drs. Elisa Poveda and Manuel Tarifa for their good advice and encouragement; to my colleges of Phd: Kaiming Pan and Ángel de la Rosa, from who I also appreciate the help with the mercury intrusion porosimeter tests, the time shared in the office and the journeys to Almagro. Thanks to the technicians of the laboratory, Miguel Ángel Cámara, Juan Antonio Serrano and Miguel Ángel Cerezo for their help with the fabrication and testing of the mortars. Thanks to Begoña Pérez for her support with administrative managements.

I also appreciate all help from the people that made it possible the realization of a research stay at *Universidade do Minho*, in Portugal. With this respect, I thank Prof. Gonzalo Ruiz for his suggestion of such a university and his help with the corresponding managements. Thanks to Prof. Paulo Lourenço and Dr. Miguel Azenha for their warm welcome in Portugal and their support both during the stay and the work afterwards to write and publish a research article. Thanks also to my college Meera Ramesh for all the time shared at *Universidade do Minho*, for her help in the laboratory and her detailled colaboration in the aforementioned paper.

Thanks to other professionals who in a way or another have also contributed to this thesis. I appreciate the help with the chemical and mineralogical characterization of the

limes from Prof. Anselmo Acosta and his research group in UCLM . Thanks also to Dr. Carlos Leiva, from *Universidad de Sevilla*, for his support with the technique of the mercury intrusion porosimeter. I appreciate the colaboration from Dr. Ignacio Garrido Sáenz, from UCLM, with the SEM analyses of the natural hydraulic lime mortars and *Iesmat, Instrumentación Específica de Materiales* for the laser particle size distribution of the limes.

I thank my family for their constant support. Especially to my uncle Gonzalo for his great help and encouragement at the beginning of this adventure and my uncle Manolo and my aunt María for their support in a way or another. Thanks to my grand parents for the example they showed us, to the youngest of home for the enthusiasm and happiness that they always transmit, to my siblings and their families for helping me always and for being a reference to me. Thanks in a especial manner to my parents, José and Marisa, for the great effort you have made so that I could reach this stage and for your great generosity and example to me.

Finally, thanks to that Phd college on who I relied since the beginning because he was always willing to answer all my doubts and who has become a life partner. Thanks, José Joaquín, for your great support, your example, your time, the plans together and your great help at many levels. Thanks for everything.

Ciudad Real, May 2019

Summary

The objective of the thesis is to provide an advanced and a deeper mechanical characterization of the lime mortars commonly used in the restoration field, which would be helpful for the numerical simulations of historical masonry structures. For the purpose, several aspects concerning the fracture and deformability behavior of lime mortars have been studied.

In the first place, it is found that there is still a lack of standardization on the dosage methodology of lime mortars. Thus, seven types of natural hydraulic and aerial lime mortar were fabricated and five factors which have an influence on their properties have been studied, in particular the water/lime ratio, the mold material, the aggregate size and type and the different curing conditions. Furthermore, an advanced mechanical characterization has been performed on these mortars, including the measurement of the fracture energy. Finally, some empirical equations for determining the relationships between these mechanical properties were proposed, which could be helpful when simulating the numerical models of historical constructions.

In the second place, the analysis of the time effect on the properties of lime mortars at early ages (up to 7 days) is analyzed. It is especially relevant the study of the deformability of lime mortars at early ages as it enables accommodation movements of masonry before cracking. However, the references focusing on the measurement of such property at early ages are inexistent. Then, in the thesis a novel technique developed recently for cement based materials is applied for the first time to natural hydraulic lime mortars. It is named as Elastic Modulus Measurement through Ambient Response Method (EMM-ARM) and it allows the automatic and continuous evaluation of the elastic modulus immediately after casting without demolding the specimen. For the purpose, various sealing and compacting procedures were studied through flexural and compressive strengths, density, ultrasound pulse velocity, open porosity, etc., in order to compare the procedure adopted for EMM-ARM (sealed and vibrated) with the standard one (unsealed and compacted). The range of elastic modulus obtained among the different mortars was between 2.5 and 4.1 GPa on day 7, which shows feasible potential of application of EMM-ARM to natural hydraulic lime mortars at early ages (under 3-7 days). It was also found that sealed specimens led to 50% and 25% lower compressive and flexural strengths, respectively, compared to unsealed ones.

Related to the previous aspect, it is also studied the time effect on the properties of natural hydraulic and aerial lime mortars in the long-term. This is of relevance because it is known that the flexural and compressive strengths of lime mortars continue evolving beyond 28 days as they require higher periods of time than cement-based materials to reach their maximum strengths. However, to our knowledge, there are no studies focusing on the measurement of the fracture energy, the splitting tensile strength or the static elastic modulus in the long-term in such materials. Thus, the third purpose of the thesis is to study the time effect in the mechanical properties of lime mortars. Moreover, these measurements are related to the evolution of the carbonation depth through the

phenolphthalein method on prisms to study the influence of the carbonation process on both lime mortars. The results show that there is a faster increase of the mechanical properties in both mortars up to 56 days, which ranges between 60% and 90% of their corresponding values at an age of 448 days depending on the mechanical property and type of mortar. After this age, there is a more moderate but progressive evolution up to 224 days. However, from this age to 448 days, the evolution of the mechanical properties is very slow for the aerial lime mortar and shows a slight increase for the natural hydraulic one. Furthermore, some empirical equations of such behaviors with time are proposed for both mortars.

The forth objective of the thesis is to analyze the loading rate effect on the fracture properties of lime mortars. This aspect is getting more attention recently as many historic masonry structures are situated in zones of seismic activity. For the purpose, three-point bending tests are performed on both natural hydraulic and aerial lime mortars under three various loading rates (loading-points displacement rates, 5.0×10^{-4} mm/s, 5.0×10^{-1} mm/s and 1.6×10^{1} mm/s). The results show that the peak load and the fracture are rate sensitive. The maximum dynamic increase factors (the ratio of the dynamic properties to their corresponding quasi-static values) of the peak load are 1.4 and 1.6 for the natural hydraulic and the aerial lime mortars, respectively, whereas it is 1.9 for the fracture energy for both mortars. Moreover, six specimens were dried and tested under the lowest and highest loading rates to study the phenomena of the rate sensitivity. It is found that it is mainly due to viscous effect of free water in the natural hydraulic lime mortar. However, for the aerial lime mortar, the rate effect is related chiefly to the crack growth and velocity. Moreover, through scanning electron microscope (SEM) analysis, it is observed intergranular failure.

Finally, among the mechanical properties measured on the natural hydraulic lime mortars, it was found a significant difference between the compressive strengths of standardized prisms (with 40 mm in depth) and cylinders (with 150 mm in height). Our hypothesis was that this difference was due to geometry and size effects. Then, in the thesis a numerical simulation of the compressive test on prisms is performed but assigning as intrinsic material compressive strength the one of the cylinders. The obtained numerical curves fit very well with the experimental ones, which means that the difference in the compressive strength of prisms and cylinders is due to geometry and size effects and that the compressive strength from the cylinders is roughly the intrinsic compressive strength of the material. Furthermore, two more numerical models were performed by doubling the size of the standard prisms once and twice. With the peak loads of the three models, it is possible to obtain the size effect laws of two natural hydraulic lime mortars. Furthermore, a cohesive simulation of the three-point bending test on such mortars is performed to verify that they behave as cohesive materials.

To conclude, this thesis provides improvements in the techniques to measure the mechanical properties of lime mortars. The analyses performed could be useful to define with more realism and precision the numerical simulation of masonry structures built with lime mortars. The techniques proposed in this research could also be applied to other cohesive materials of the civil and architectural patrimony, such as compressed earth blocks, rammed earth, stones or bricks.

Contents

Part I

Introduction

Chapter 1

Introduction

1.1. Motivation and objectives

Most of the civil and architectural patrimony present nowadays has been built with masonry structures. The intervention on such structures requires a deep knowledge of the characteristics of their components, mainly the stones, the blocks and the mortar that joins them. Recently, thanks to the effort made by researchers on the topic [1–5], some advanced computation models have been used to analyze the behavior and movements of such structures. These models are normally based on an advanced measurement of the mechanical properties of the masonry components.

It is well-known that the design of a good restoration intervention requires the usage of compatible materials so that the new ones do not cause neither spalling on the preexistent components nor further decay. In this sense, lime mortars are extensively used for restoration interventions due to their high compatibility with ancient masonry structures [6–9]. However, the references that characterize these materials often focus on their mineralogical and chemical behaviors, which is of great importance, but lack of a comprehensive analysis of their mechanical aspects. Then, when preparing a numerical model to simulate the behavior of a masonry structure, it is often to adopt highly simplified hypotheses and strong suppositions as for the mechanical parameters that define the component materials, especially when lime mortars are concerned. As a result, the validity and precision of such computational models are often compromised.

This thesis emerges from the need of an advanced and a deeper mechanical characterization of lime mortars with the objective of improving the material properties required for the numerical simulations of historical masonry structures. In view of such a need, several aspects have been studied regarding their effects on the mechanical properties of lime mortars.

1. In the first place, it was observed that the dosage methodologies of lime mortars are not so well defined as the ones of other important construction materials like concrete. In this sense, it is often observed that the amount of water required to fabricate the mortar is not always indicated, which has a relevant influence on the resulting mechanical properties. Other aspects, such as the raw component properties (like the density), are neither mentioned. For this purpose, the first objective of this thesis is to study the effect of different factors of the dosage and fabrication process of lime mortars on their resulting mechanical properties. These factors are the water/lime ratio, the material of the mold, the aggregate type and size and the curing conditions. Furthermore, some empirical relationships among the mechanical properties of the different mortars obtained are established.

2. In the second place, it is well known that lime mortars present such a deformability at early ages that it enables the accommodation movements of masonry before cracking [10]. However, to our knowledge, the references studying the early age behavior of lime mortars with especial focus on their deformability are inexistent. The second objective of the thesis is to study the mechanical and physical properties of lime mortars at early ages with especial attention to the evolution of their elastic modulus.

3. Moreover, it is well known that the flexural and compressive strengths of lime mortars change with time but there is little knowledge as for the evolution of other important mechanical properties such as the splitting tensile strength, the fracture energy or the static elastic modulus. With this respect, the third objective of the thesis is to analyze the evolution of such mechanical properties in the long term and to infer empirical relationships of such behaviors with time when possible.

4. Furthermore, most of historical masonry structures are situated in zones of seismic activity. However the dynamic mechanical behavior of lime mortars is not so studied as for other construction materials such as steel and concrete, especially as for the fracture energy in bending. For this reason, the fourth objective of the thesis is to study the loading rate effects in the fracture behavior of lime mortars.

5. Finally, two more aspects are studied. On the one hand, the fact that some mechanical tests performed in the laboratory, such as the standardized compression tests on prisms, are affected by size effects and the strength provided by them do not coincide with the intrinsic one of the material. Thus, the objective of this thesis is to analyze the possible geometry and size effect on the compressive strength of prisms. For the purpose, a numerical simulation of such tests with specimens of three different sizes is performed in order to obtain the size effect law for natural hydraulic lime mortars. On the other hand, these materials are supposed to present a cohesive behavior. The last objective of the thesis is to perform a numerical model of the three-point bending test on prismatic specimens of lime mortars to demonstrate their cohesive behavior.

With these purposes, the thesis is intended to provide a further contribution to the development of experimental and numerical techniques for the characterization of materials of the civil and architectural patrimony, such as lime mortars. An advanced mechanical characterization of new lime mortars, which reproduce the historical ones of old masonry structures, is performed. For this purpose, mechanical tests are performed to measure not only the flexural and compressive strengths, but also other important mechanical properties, not normally measured, such as splitting tensile strength, fracture energy and static elastic modulus. This contribution will be of great help for future works involving the mechanical behavior of historical masonry structures built with lime mortars; especially for the preparation of the numerical simulations that analyze their behavior. The techniques proposed in the thesis could also be applied to other cohesive materials of the civil and architectural patrimony, such as compressed earth blocks, as done in a recent work [11].

1.2. State of the art

According to the standard EN 459-1 [12], lime is a binding material formed by calcium oxide and/or hydroxide, and calcium-magnesium oxide and/or hydroxide produced by the calcinations (thermal decomposition) of calcium carbonate (such as limestone, chalk,

shells) or calcium magnesium carbonate (like dolomitic limestone, dolomite). The lime products can be classified as hydraulic or air ones (see Figure 1.1).

Among the hydraulic lime, there are several sub-families, such as natural hydraulic lime (NHL), formulated lime (FL) and hydraulic lime (HL). The first one is formed by burning argillaceous or siliceous limestones without additions. The second one is mainly composed by air lime and/or natural hydraulic lime with hydraulic and/or pozzolanic material. The last one is formed by lime and other materials such as cement, blast furnace slag, fly ash, limestone filler and some other constituents in very small proportions [12].

There also exist various types of air limes (commonly known as aerial ones). Among them, one can differentiate between calcium lime (CL) and dolomitic lime (DL). The former is mainly composed by calcium oxide and/or calcium hydroxide while the latter mainly by calcium magnesium oxide and/or calcium magnesium hydroxide; both of them without any hydraulic or pozzolanic additions. Likewise, these two types of aerial limes can be in the form of quicklime (Q) or as hydrated lime. The former is mainly in the oxide form and reacts exothermically with water; the second is mainly in the hydroxide form produced by slaking of quicklime. This last one can be formed as powder (S), putty (S PL) or slurry or milk of lime (S ML).

In this work it was used a natural hydraulic lime (NHL) and an aerial calcium lime (CL) in the hydroxide form slaked as powder (S). The former is classified according to its compressive strength at 28 curing days as: NHL 2 (2 MPa $\leq f_c \leq$ 7 MPa), NHL 3.5 (3.5 MPa $\leq f_c \leq$ 10 MPa) and NHL 5 (3.5 MPa $\leq f_c \leq$ 15 MPa)[12]. The latter can be classified according to their (CaO + MgO) content into CL 90-S (with a proportion higher than 90%), CL 80-S (with corresponding proportion higher than 80%) and CL 70-S (with corresponding one higher than 70%). The work of this thesis focuses on a NHL 3.5 and a CL 90-S (Figure 1.1). From a mineralogical point of view, both limes are composed by portlandite, $Ca(OH)_2$, in a proportion higher than 80% for the aerial lime mortar and around 30% for the natural hydraulic lime, according to their respective technical sheets. They can also contain some amount of calcite, $CaCO_3$, produced by the transformation of portlandite with the carbon dioxide, CO_2, from the atmosphere [13]; NHL, instead, also presents calcium silicates (C_2S in a much higher proportion than C_3S) [13–16]. The mortars produced with both types of lime differ in the way of hardening. Both of them can harden by the reaction of portlandite with carbon dioxide from the atmosphere, named as "carbonation"; while natural hydraulic limes also harden by hydration of its mineral compounds, mainly dicalcium silicates, C_2S, with water to produce C-S-H and portlandite [8, 17]. These processes can be better understood within the cycle of each lime, see Figures 1.2 and 1.3, respectively, for the aerial and the natural hydraulic limes and the mortars produced with corresponding limes.

The cycle of the aerial lime (Figure 1.2) [18] implies the transformation of the limestone into calcium oxide (quicklime), CaO, when it is burned at high temperatures (around 900°C) in the limekiln. In this process, carbon dioxide and water vapor are emitted to the atmosphere. Then, the quicklime can be slaked with water. There exist several slaking procedures [19], such as water spraying, water immersion or just spreading the lime in the ground and leave it to react in contact with the vapor of the atmosphere. The slaking of the quicklime, also called, hydration, produces hydrated lime, mainly calcium hydroxide, $Ca(OH)_2$. As mentioned previously, such a lime can be in the form of powder, putty, slurry or milk of lime depending of the amount of water used in the slaking process. Thus, this calcium hydroxide can be mixed with sand and water to fabricate aerial lime mortar. As already explained, such a mortar hardens by air drying and by carbonation, which is the reaction of the $Ca(OH)_2$, also called portlandite, with the carbon dioxide from

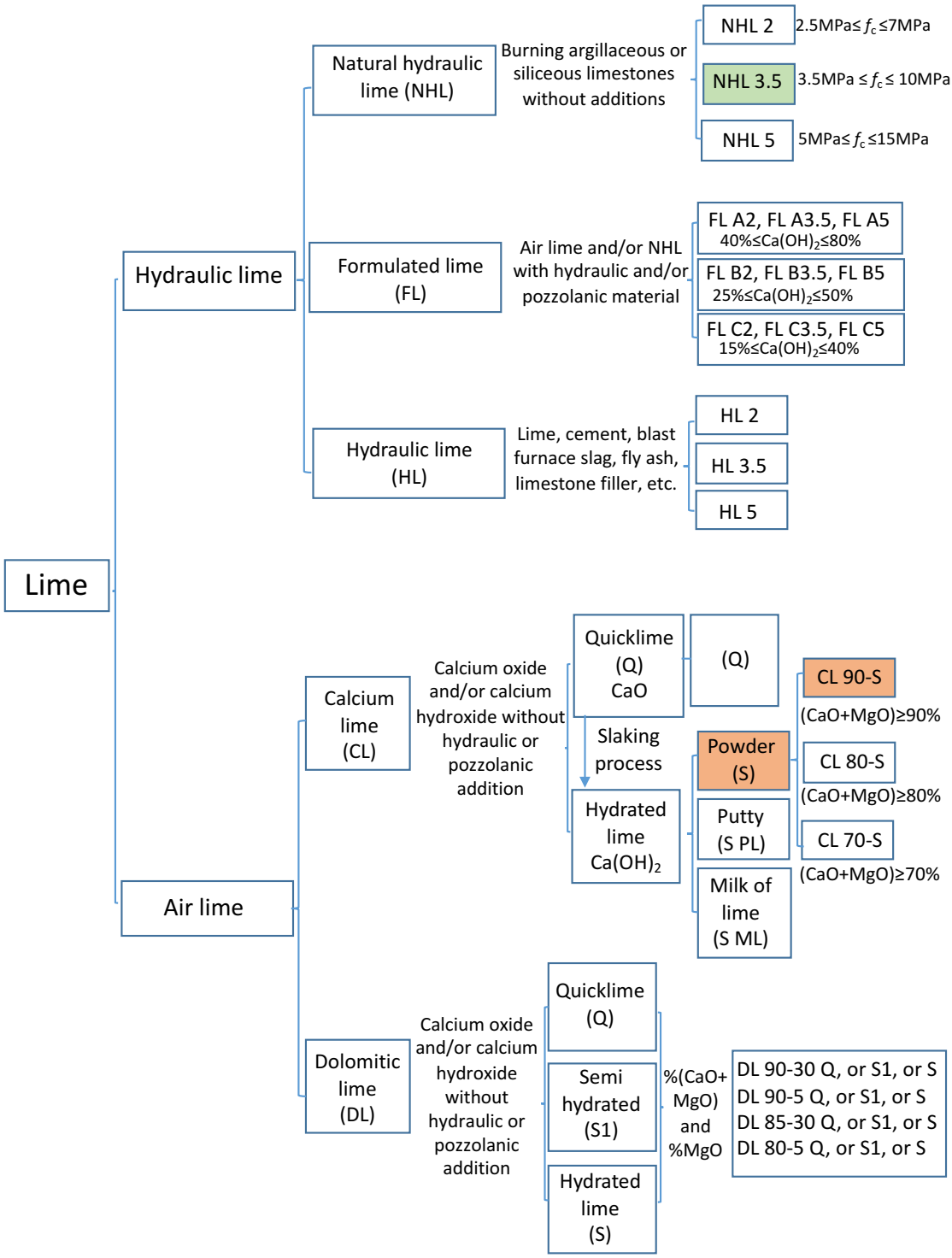

Figure 1.1: Classification of the different types of lime according to EN 459-1 [12].

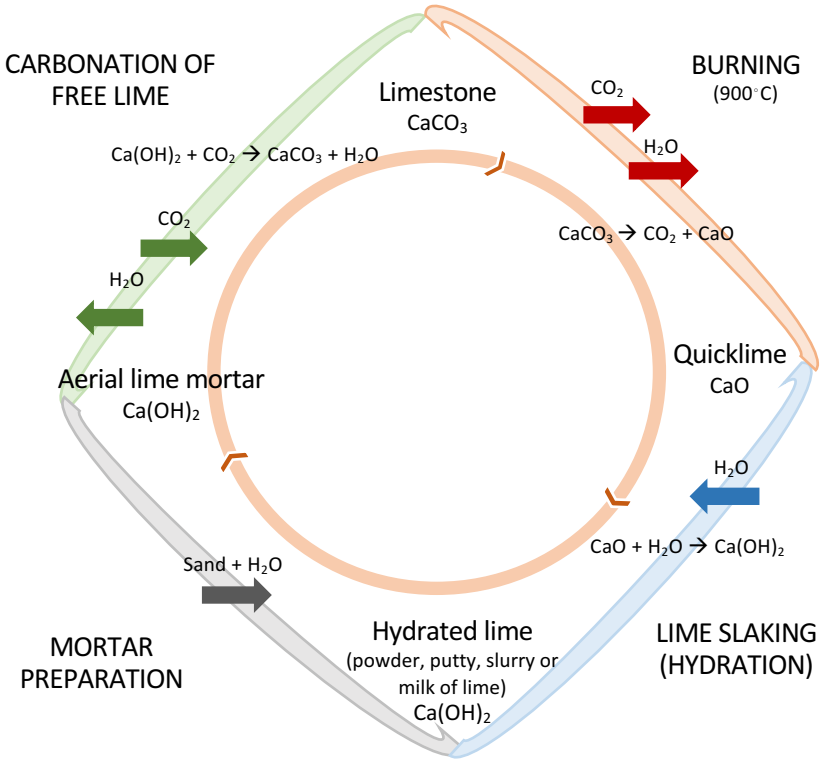

Figure 1.2: Cycle of aerial lime adapted from [18].

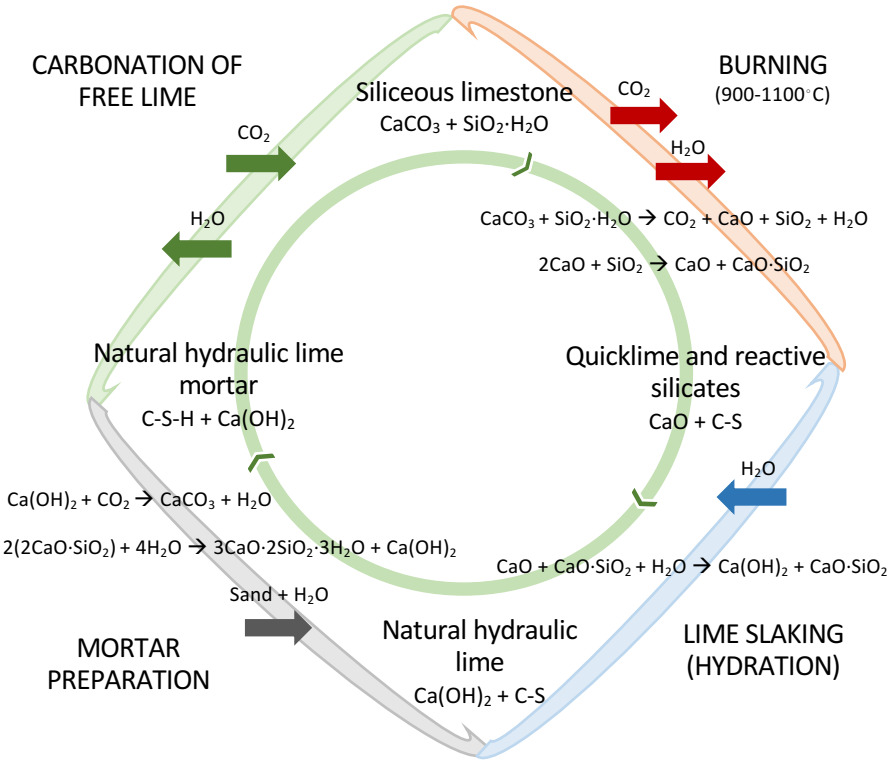

Figure 1.3: Cycle of natural hydraulic lime adapted from [8, 17, 18, 20].

the atmosphere to produce calcite, $CaCO_3$, and water. In this process, carbon dioxide is absorbed from the atmosphere. For this main reason, lime mortars are considered as eco-efficient materials. Afterwardas, the cycle can start again.

The cycle of the natural hydraulic lime (Figure 1.3) [8, 17, 18, 20] is similar to the one of the aerial lime with the difference that now the limestone can be a more or less argillaceous or siliceous one [12]. With the burning process, the siliceous limestone transformes into calcium oxide (quicklime) and reactive silicates, C-S. Then, the hydration of the material produces the natural hydraulic lime, NHL, which is mainly formed by portlandite, $Ca(OH)_2$, and calcium silicates, mainly belite, C_2S. The mixture of the NHL with sand and water originates the natural hydraulic lime mortar. Such a mortar hardens by carbonation and hydration. With the former process, the portlandite transforms into calcite by the reaction of the carbon dioxide of the atmosphere. With the hydration, the calcium silicates, mainly (belite), transforms into calcium silicates hydrates (C-S-H) and portlandite. As time passes, the process continues.

Considering the aplicability of both lime mortars, it is relevant their use to join stones and blocks in structural masonry walls [7, 14, 17, 21–26]. The natural hydraulic lime mortars are usually adopted when early strength gain and faster setting time are necessary [6] or when it is required to present better behavior under soluble salts or under high humid conditions [27]. Instead, the aerial lime mortars are also used as renders and plasters to protect walls from water and impacts, to bond material for mosaics and ceramic tiles or

for decorative purposes [7]. In any case, the use of both lime mortars is increasing for restoration works due to their high compatibility with the substrate material in terms of chemical, physical and mechanical performance [6–8]. Furthermore, both lime mortars are eco-efficient materials as they require low amount of energy during their production process, generate reduced carbon dioxide emissions and absorb carbon dioxide during carbonation [6]. For all these reasons, their study results fundamental.

Particularly, knowledge on the mechanical properties of mortar is crucial to ensure a good performance of masonry structures [28]. According to Binda *et al.* [29], there exist different ways to test old mortars. On the one hand, there are on-site tests, such as the pointing hardness test and the penetration test. The former is a non-destructive test (NDT) intended for cement mortars so it requires new calibration for lime based ones. The latter can be considered as a NDT or as a minor destructive test (MDT) as the damage induced in the masonry wall is minimal. It provides a value of penetration force of the drill along certain distance from the surface of the masonry wall [26]. On the other hand, there are the laboratory-based tests on sample mortars. In this group, one can find the compression tests on thin sampled joints or the so-called double punch test (according to DIN 18555-9 [29, 30]). It can be performed with new mortar joints reproducing the old ones or with on-site samples and in both cases the test does not require the standardized specimen thickness of 40 mm. A scheme of the double punch test from DIN 18555-9 [29, 30] is presented in Figure 1.4. This test provides the compressive strength of the mortar in the joints [23]. There also exist the standardized flexural and compression tests, according to EN 1015-11 [31], on new mortar specimens of 40 mm × 40 mm × 160 mm. These two last tests are well extended among researchers of lime mortars [6–9, 15, 25, 32].

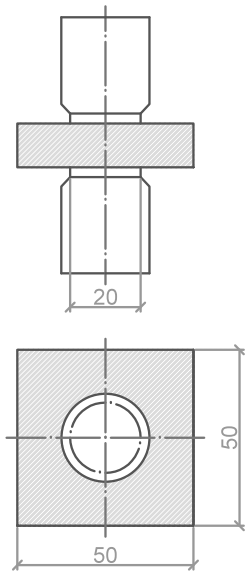

Figure 1.4: Scheme of the double punch test from DIN 18555-9 [29, 30].

However, there is a need of measuring other important mechanical properties such as the splitting tensile strength, the elastic modulus and the fracture energy. In this sense, Marastoni *et al.* [23] proposed a method to estimate the material's strength envelope by representing the mortar's state of failure on the Mohr's plane. Experimental data were obtained from Brazilian tests on core drilled masonry samples with one diametral mortar joint and from double punch tests on extracted mortar joints. They pointed out that the

compressive strength from the latter type of tests was 10% higher than that obtained from standard tests on prisms, mainly due to the different boundary conditions of the two types of tests.

The direct measurement of quasi-static elastic modulus of lime mortars is not so well documented. Maravelaki-Kalaitzaki *et al.* [33] studied the modulus of elasticity in NHL mortars with pozzolanic additions and Drougkas *et al.* [21] obtained indirectly the elastic modulus of lime based mortars from the masonry and brick characteristics. They also derived relations between the compressive strength and the elastic modulus and compared their results with those in the standards. They observed discrepancies among the results obtained from various types of specimens and recommended using cylinders to measure mechanical properties, provided proper curing throughout the specimen was achieved. Others, like Rosell and Cantalapiedra [34] measured the dynamic Young's modulus by using ultrasonic impulse velocity and the static Young's modulus by performing conventional bending tests in lime and cement mortars. Nežerka *et al.* [35] studied the dynamic Young's modulus of lime based pastes using the resonance method, Pozo-Antonio [36] measured the dynamic Young's modulus in lime based and lime-cement based mortars with pure limestone aggregate and Veiga [7] gathered some references about air lime mortars with different measurements of dynamic elastic modulus.

Regarding the study of the fracture energy of pure lime mortars, especially through the three-point bending test, there is hardly any research so far, despite of the fact that it is an important parameter to characterize the ductility and fracture behavior of the material. Pereira *et al.* [37] studied the fracture energy of lime-cement mortars produced with different binders and sands. They concluded that the fracture energy was higher for artificial sand mortars for all classes and all types of binders. Also, Pereira and Lourenço [38] measured the compressive fracture energy of a pre-mixed mortar and Asprone *et al.* [39] measured the fracture energy of NHL mortar with siliceous fine aggregate through a Hydropneumatic machine and a Modified Hopkingson bar.

All things considered, we can say that there are several aspects concerning the mechanical characterization of lime mortars, especially regarding their fracture behavior and deformability, that require further analysis in order to improve the comprehension of their role within masonry structures. These aspects comprise the effect of different production and dosage factors on the physical and mechanical properties of lime mortars with especial attention to properties not normally measured such as fracture energy, splitting tensile strength and static elastic modulus. Furthermore, it is also relevant to know the time effect on mechanical properties of lime mortars at early ages and in the long-term, as well as the loading rate effect on the fracture properties of lime mortars, which can happen under dynamic loads such as earthquakes, wind gust or impacts. Finally, the study of the size effect on the compressive strength of lime mortars as well as the verification of their cohesive behavior are relevant matters for the mechanical role of the material within masonry structures. The state of the art concerning all these topics is analyzed as follows to understand better to what extent each aspect requires further analysis.

1.2.1. The effects of production process and dosage on the physical and mechanical properties of lime mortars

Nowadays there is no a strong dosage methodology for lime mortars like the one present for other important building materials such as concrete. In many occasions relevant aspects such as the amount of water used or the densities of the raw materials are neither indicated.

Referring the lime/aggregate ratio, many researchers, such as Moropoulu *et al.* [40, 41] coincide that the appropriate ratio for lime mortars used in restoration could be 1:3

by volume. More specifically, for NHL mortars, Lanas *et al.* [8] studied the influence of lime/aggregate ratios and aggregate attributes on the mechanical properties of NHL mortars. They prepared five different lime/aggregate ratios from 1:1 to 1:5 in terms of volume and four different types of aggregates. The consistencies ranged from 128 mm to 159 mm of diameter in the flow-table test by varying the water/lime ratio. They observed that specimens with more lime content had higher compressive and flexural strengths and, additionally, the highest strengths were reached with limestone aggregates. Kalagri *et al.* [6] investigated the effect of aggregate size and the lime type on microstructure and mechanical properties, the water/lime ratio by weight was between 0.49 and 0.61, the consistency was 160 mm of diameter for all the mixes. The experimental results showed that the inclusion of coarse aggregates (in that case a 0/6 mm grain size aggregate) enhanced the compressive and flexural strengths, increased the packing density, decreased the water demand and consequently, reduced the open porosity. They also proposed an equation in regard to the compressive strength and the median pore radius.

As for the aerial lime mortars, Lanas and Alvarez [9] prepared various of these mortars with different lime/aggregate ratios, ranging from 1:1 to 1:5 by volume and studied their influence on the mechanical properties. In order to obtain normal consistency and good workability, the corresponding water/lime ratios were ranged from 0.5 to 1.2. They observed a correlation between lime amount and mortar strength. However, in the case of high lime contents, the increase in voids led to strength reduction. They also concluded that angular limestone improved the strength of the mortar. Gameiro *et al.* [42] studied the influence of lime/aggregate ratio on the physical and chemical properties of air lime-metakaolin mortars. The water/lime ratios were also varied to get adequate workability (consistency range: 129 mm -144 mm, from dry to plastic lime mortars). They found that mortars with low lime/aggregate ratio (1:3 by volume) seemed to develop carbonation sooner and therefore reach their highest strength relatively early while mortars with higher lime/aggregate ratio (1:1) presented lower carbonation rates. The latter is not appropriate for use in conservation works due to its high shrinkage and strong mechanical properties, which is incompatible with substrate material. Referring the aggregate type and shape, it has been pointed out that the limestone aggregates present a structure similar to the calcitic binder matrix which leads to a reduction of the discontinuities between the lime matrix and the aggregates [9, 43], moreover, calcitic particles growing over the limestone grains increase also the crystallographic continuity between limestone aggregates and the lime matrix [44, 45]. These facts cause strength increase in the aerial lime mortars when using limestone aggregates in comparison to siliceous ones [9, 43]. Furthermore, the shape of aggregates contributes to the strength as well; angular aggregates produce better cohesion degree between the aggregate surface and binder, thus, the strength increases [43]. As for the grain size of the aggregates, it has been explained that the best aggregate is a well-graded sharp sand (medium to coarse sand) that generates a good interlocking [46]. Stefanidou and Papayianni [47] showed that the inclusion of coarse aggregates was advantageous for long term strength. They observed that at later ages, cracks appeared to be blocked by the coarse aggregates [47] and the highest strength values were reached with lime mortars of low lime/aggregate ratio and aggregates of 0/4 mm of maximum grain size in the long term. They recommended that compaction was necessary when using coarse aggregates to reduce the voids and the bond between the lime paste and the pebbles.

Considering the influence of the water content, a general tendency was observed by Papayianni and Stefanidou [32] on lime pozzolan mortars and Xu *et al.* [48] for NHL pastes. As the water/lime ratio increases, the porosity increases and as a consequence, the mechanical properties decrease, that is to say, the material becomes weaker. Considering

the influence of the water/lime ratio on the mechanical properties of aerial lime mortars, the references are scarcer. For example, Lawrence and Walker [49] showed that aerial lime mortars did not follow Abrams' rule, which is applicable to cement mortars and states that when a cement mortar is fully compacted, its strength is inversely proportional to the water/cement ratio [50]. They reported that the water/lime ratio has a minimal effect on the mechanical properties of aerial lime mortars compared with the influence of lime and aggregate types. They tested aerial lime mortars with different water/lime ratios, ranging from 0.500 to 0.875 by volume, at curing ages of 28, 56 and 91 days. They observed that the compressive strength of the mortars decreased with the water/lime ratio but this decrease was neither linear nor so abrupt as for the natural hydraulic lime mortars with similar consistencies; and even for high water/lime ratios, the compressive strength seemed to be almost constant. Moreover, they proposed an equation to predict the compressive strength based on a relationship among the form of lime, type of aggregate, water/lime ratio and age of the mortar. They also urged on the need for more work to understand the mechanisms producing differences in the compressive strength of aerial lime mortars. Raposo Pacheco Algarvio [51] measured flexural and compressive strength of five aerial lime mortars with different water/lime ratio, ranging from 1.48 to 1.68, which provided a range of consistencies between 144 mm and 188 mm, respectively. They observed that both the flexural and the compressive strengths decreased with the water/lime ratio. The flexural and compressive strengths were between 0.26 MPa and 0.33 MPa, 0.73 MPa and 0.79 MPa, respectively, corresponding to the lowest and highest water/lime ratios.

Furthermore, there are other aspects, such as the material of the molds used and the different curing conditions, which also affect the fabrication process of lime mortars. No research has been performed on the former. However, for the latter, Lanas *et al.* [52] fabricated aerial and hydraulic lime-based mortars and subjected them to different environments. They concluded that, in general, higher relative humidity (RH) increased the mechanical properties of NHL mortars. Grilo *et al.* [25] studied the mechanical and mineralogical properties of natural hydraulic-metakaolin mortars under different curing conditions. They observed that lower humid conditions favored a carbonation reaction (which governed aerial lime mortars), while high humid curing aided a hydration reaction (which partially governed NHL mortars). Thus, they concluded that humid conditions (95% ± 5%) favored compound hydration reactions, which were relevant for the development of mechanical properties of NHL mortars. Grilo *et al.* [53] also agreed that higher RH curing regimes benefited these processes and also contributed to void infilling.

Moreover, some researchers have coincided on the great influence of the curing conditions on the carbonation process of the aerial lime mortars and therefore on their mechanical properties. It is known that the carbonation process is highly influenced by the CO_2 concentration, moisture content and permeability of the material [54]. Achieving an adequate moisture content is determinant for the development of the carbonation process. For example, Moorehead [54] observed that for cement lime mortars, the adequate moisture content of the sample to maximize carbonation was when 50% of their pore volume was filled with water. Van Balen and Van Gemert [55] showed for lime mortars that the carbonation was retarded when the specimen was saturated with water as the diffusion of CO_2 is prevented and therefore, a first phase of drying was required. At the same time, a certain level of moisture content was required for the dissolution of CO_2 with the water to form carbonic acid so that later the lime could react with it [54, 56, 57]. They pointed out that the optimum water content for carbonation is the one that corresponds to "maximum adsorption on the surface of the pores before capillary condensation". Other authors have also outlined the influence of moisture on the carbonation of aerial lime mortars [58–62].

The thesis of Oliveira [62], at University of Minho, studies the relationship between carbonation progress and humidity diffusion and proposes a numerical model to study both phenomena on quicklime aerial lime mortars. In relation to this, Ferretti and Bažant [63] had created a similar model for masonry towers on moisture diffusion and carbonation reaction. They found that both processes influenced the behavior of multiple-leaf ancient masonry walls, producing during centuries a redistribution of stresses that could induce long-time damage of some ancient masonry walls [63]. Concerning the influence of the curing conditions on the carbonation process, it is also known that the temperature has an impact on it. Increasing temperatures of the CO_2: reduces the solubility of this gas in water and then the reaction slows down, the concentration of CO_2 decreases at constant pressure and hot CO_2 may help evaporation of free water in the pores, which can reduce the amount of water necessary for the diffusion of CO_2 inside the material [54, 58].

However, the influence of all these aspects on the fracture properties of lime mortars, like fracture energy, splitting tensile strength and characteristic length are not studied yet, even though they are important properties to define the ductility and fracture behavior of the material. Therefore, further studies with such a concern are still required.

1.2.2. Time effect on the physical and mechanical properties of lime mortars at early ages; stiffness evolution

From the mechanical point of view, lime mortars are also very suitable for restoration works because they are able to accommodate minor differential movement of masonry over time without cracking [10]. However, despite awareness of the importance of the early age conditions of application, curing and stiffness build-up in the actual behavior of lime mortars, little research is found about the behavior of these mortars at early ages. For instance, Lanas *et al.* [8] performed flexural and compression tests and thermogravimetric analyses (TGA) on mortars with NHL type 5 at 3 and 7 days. Arandigoyen and Alvarez [44] tested aerial lime mortars with cement in bending and compression after 3 and 7 days. However, we did not encounter any study focused on the stiffness evolution of lime mortars at early ages, particularly including the first 48 h of hardening. This is of crucial importance because the behavior of lime mortars at early ages has a direct influence on the supporting capability and ability to accomodate movements of masonry during construction or repairing operations. This behavior is especially relevant for interventions in historic structures, where an appropriate large deformation before failure of the new additions helps to avoid brittle breakage when restrained by preexistent elements.

1.2.3. Time effect on the physical and mechanical properties of lime mortars in the long-term

In the long-term, the research of the mechanical properties of lime mortars is also important because it is known that they require higher periods of time than cement-based materials to reach their maximum strengths [21]. It is well known that the carbonation and hydration processes of natural hydraulic and aerial lime mortars can be long lasting [9, 58, 64] and it is therefore frequent that their strengths at early ages is lower than the corresponding ones in the long term. For this reason, there is an urgent need for quantifying the corresponding increase of important mechanical properties such as the fracture energy, the splitting tensile strength or the elastic modulus with time.

With this respect, Drougkas *et al.* [21] measured the flexural and compressive strengths of one natural hydraulic and an aerial lime mortars at different curing ages, from 7 up to 49 days in the case of the former and from 14 up to 49 days for the latter. They obtained

that the flexural strength increased around 87% for the natural hydraulic lime mortar while it was around 75% in the case of the aerial one within the corresponding testing periods. Regarding the compressive strength from prisms, the increase was of 22% for the natural hydraulic lime mortar and of 50% for the latter. Furthermore, they provided logarithmic adjustments for them and also observed that the increase between 28 and 49 days for lime mortars was significant in comparison to Portland cement based materials.

Kalagri *et al.* [6] obtained flexural and compressive strengths, dynamic modulus of elasticity (through ultrasonic pulse velocity method), open porosity and mean pore radius on four types of mortars fabricated with NHL 5 and NHL 3.5-Z (with pozzolanic or cementitious additives up to 20%). The mortars presented a lime/aggregate ratio of 1:2.3 by weight. They counducted tests at 28, 90 and 270 days and established some relationships between the aforementioned parameters.

Karaveziroglou-Weber and Papayianni [65] studied the evolution of flexural and compressive strengths and dynamic modulus of elasticity determined by ultrasonic pulse velocity method of eighteen mortars and ten grouts up to 1540 days. The results show that the compressive strength of mortars without ceramic material or cement presented an increase in their compressive strength with time, while it decreased slightly after one year; the flexural strength gained up to 60% from 28 days to one year, the modulus of elasticity followed almost the same tendency as the compressive strength.

Stefanidou and Papayianni [47] analyzed the role of aggregates on the structure and properties of aerial lime mortars at different ages up to 730 days. They observed that the aggregates of 0/4 mm of particle size distribution had a positive impact on the strength in the long-term and coarse aggregates improved volume stability of aerial lime mortars.

Lanas *et al.* [17] measured compressive strengths on different mortars fabricated with aerial and natural hydraulic limes up to 365 days. They discovered different stages of hardening in the mortars with the two types of limes. Aerial lime mortars presented two main stages: one at early ages characterized by the water excess loss, the other consisting on the carbonation process. These phenomena was also observed in the reference [9]. However, in the case of the natural hydraulic lime mortars, they presented three phases of hardening as a function of their chemical composition, according to the reference [17]. The first one, up to 28 days of age with the hydration of several hydraulic compounds that formed hydrated calcium silicates (C-S-H) and an increase of the strength due to the presence of C_3S; secondly, up to 182 days approximately with a slight increase of the strengths as C_3S was almost finished and, finally, up to 365 days with an increase of the long-term strengths due to the carbonation process and the contribution of C_2S. In the reference [8], Lanas *et al.* measured flexural and compressive strengths of several mortars fabricated with NHL 5 with different lime/aggregate ratios. They observed that NHL mortars with high lime/aggregate ratios, such as 1:1 and 1:2 followed the three stages of hardening as mentioned previously, while in mortars with lower lime/aggregate ratios, such as 1:3, 1:4 and 1:5, the last stage presented lower increase of the strength as the carbonation process and the presence of C_2S were lower.

Manita and Triantafillou [66] studied the compressive strength of mortars with lime, pozzolana, cement and brick fragments up to 1095 days. They checked that some fluctuations may appeared in the long-term in the compressive strength of mortars with time, resulting in an increase, stabilization or decrease of the strength. They explained that this behavior depended mainly on the amount of portlandite, $Ca(OH)_2$, that stayed uncarbonated. Lanas *et al.* [8, 9] also observed a similar behavior for pure lime mortars.

Likewise, there is still a need for measuring the evolution of other important properties such as the fracture energy, the splitting tensile strength and the static elastic modulus.

1.2.4. Loading rate effect on the fracture properties of lime mortars

Recently, the dynamic mechanical behavior of lime mortars [38, 39, 67–69] is getting more attention due to the fact that many historic masonry structures are situated in zones of seismic activity, such as Lisbon (Portugal), L'Aquila (Italy), Lorca (Spain), Kathmandu (Nepal) and Nairobi (Kenya). Compared with the extensive research on the rate effect on steel and concrete [70–76], such information on lime mortars is limited. For example, Apostolopoulou *et al.* [27] studied the compatibility criteria of masonry mortars to resist better under earthquakes. They explained that restoration mortars, even the ones with low compressive strength, could achieve an improvement in terms of possible damage occurrence in the case of an earthquake and that this improvement was higher with the increase of damage severity.

Pereira and Lourenço [38] studied the dynamic compressive behavior of masonry specimens, clay brick and mortar prisms by using a drop-weight tower. The corresponding strain rate range was from 2 s^{-1} to 200 s^{-1}. A commercial ready-mix mortar (MAPEI MAPE-ANTIQUE MC) was used for the fabrication of masonry and mortar specimens. A Dynamic Increase Factor (DIF, a ratio of the dynamic response over the corresponding quasi-static one) of 2.73 was obtained for the compressive fracture energy of the mortar specimens.

Asprone *et al.* [39] analyzed the tensile behavior of a basalt fiber-reinforced natural hydraulic lime mortar at medium and high strain-rates, using a Hydro-pneumatic machine and a Modified Hopkinson bar apparatus, respectively. The DIF for tensile strength was 5.11 at the strain rate of 90 s^{-1}.

For bending behavior, Chan and Bindiganavile [67] studied the strain rate sensitivity of plain and fiber-reinforced hydraulic lime mortar by adopting a universal testing machine and a drop-weight impact machine at strain rate range from 10^{-6} to 10 s^{-1}. Impact tests on notched beams with dimensions of 100 mm × 100 mm × 350 mm were conducted, the notch depth was 12.5 mm and 2 mm in width and the span was 300 mm. For plain hydraulic lime mortar, the results show that the DIF for modulus of rupture was 12 at the drop height of 500 mm (corresponding to strain rate 10 s^{-1}), while it was 53 for fracture toughness. Moreover, the flexural behavior of hydraulic lime mortar is more sensitive to strain rate than fiber reinforced hydraulic lime mortar. Later, the bond behavior between the stone masonry block and the plain and fiber-reinforced hydraulic lime mortar was also investigated by Bindiganavile *et al.* [68, 69]. The results show that there was an improvement in the bond strength due to polypropylene micro-fibers (20 mm in length) but a difference in the fracture performance between the Portland cement-lime and hydraulic lime mortars. Whereas with the former, the fibers promoted failure through fracture in the stone block especially under dynamic loading conditions, with the latter, the fibers moved the failure plane from the interface to within the bulk mortar.

However, the studies on the dynamic mechanical behavior of lime mortars are scant, especially for fracture energy, though it is an important parameter to characterize the ductility and fracture behavior of the material.

1.2.5. Geometry and size effects on the compressive strength of lime mortars

Finally, it is well known that for other quasi-brittle materials like concrete, the compressive strength is affected by geometry and size effects and the results of some mechanical tests do not represent the real compressive strength of the material. Therefore, size effect implies that the nominal strength of a structure depends on its size (dimension) when

compared to another geometrically similar structure [77, 78].

Geometry and size effect was also found among compression results for cement-lime mortars [28, 79]. Particularly, Haach *at al.* [28] used a cement mortar with NHL type 5. They measured compressive strength from standardized prisms (measuring 40 mm × 40 mm × 160 mm) and also from cylinders (with 50 mm in diameter and 100 mm in length). They found that the ratio of compressive strength obtained from both tests could reach 1.9. To our knowledge for pure NHL mortars such phenomenon is not already analyzed and further research is required to obtain the corresponding size effect laws.

On the other hand, lime mortars are supposed to present a cohesive behavior. This would imply that there is a zone, referred as Fracture Process Zone (FPZ), in which damage is generated and related to the crack propagation. Such zone would be governed by a softening law that is a constitutive function relating the tension transmission across the lips of the crack with the crack opening. The validation of such cohesive behavior on NHL mortars through a numerical model would allow the applicability of a softening law for this material [80].

1.3. Contents of the thesis

In this thesis an advanced mechanical characterization of natural hydraulic and aerial lime mortars is presented. Several mechanical tests are performed to measure the flexural, compressive and splitting tensile strengths, the fracture energy and the static elastic modulus. Different influencing aspects on such an advanced mechanical characterization are analyzed.

Chapters 2 and 3 study the influence of five factors affecting the dosage methodology and fabrication process of natural hydraulic and aerial lime mortars, respectively, on several mechanical properties. The factors analyzed are the water/lime ratio, the material of the mold, the aggregate type and size and the curing conditions. Results of other physical tests both in fresh and in harden state, such as consistency, apparent density, water retention capacity, capillary water absorption coefficient and open porosity by hydrostatic methods and Mercury Intrusion Porosimetry (MIP), are included as well. Furthermore, some empirical relationships were obtained among some resulting mechanical properties and the standardized compressive strength from prisms for the first time.

Chapter 4 focuses on the early age behavior of three NHL mortars, with different water/lime ratios. Special attention is paid to the evolution of the elastic modulus since casting through a novel technique proposed recently by Azenha *et al.* [81], named as Elastic-Modulus Measurement through Ambient Response Method (EMM-ARM). With it, it is possible to record the early age stiffness and kinetics of evolution of the three mortars. These results show good comparability with the ones obtained with cyclic compression tests on cylinders. Furthermore, some empirical relationships are stablished concerning the evolution of flexural and compressive strengths with time of the different mortars up to 7 curing days. Different fabrication and curing methods are studied in order to compare standard procedures with the ones followed in EMM-ARM. Results of other tests, such as Ultrasound Pulse Velocity (UPV), density, open porosity by hydrostatic methods and thermodravimetric analysis (TGA) are also related to better characterize the material at early ages. This research was performed during a research stay at University of Minho under the supervision of Prof. Paulo B. Lourenço and Dr. Miguel Azenha. As already explained, this Chapter focuses on three NHL mortars with different water/lime ratios. We decided not to use aerial lime mortars, as the technique of EMM-ARM involves the specimens to be sealed inside PVC tubes, and therefore, carbonation of such mortars will

not be allowed, as explained in detail in Chapter 4. Anyhow, there is another ongoing research focused on the early age characterization of the stiffness evolution of blended aerial lime mortars with cement [82]. Further research on the possibilities of application of the technique of EMM-ARM to pure aerial lime mortars will be of interest.

Chapter 5 analyzes the evolution of several mechanical properties, such as flexural, compressive and splitting tensile strengths, fracture energy and elastic modulus, which are not normally measured, with time up to 448 curing days. One natural hydraulic and an aerial lime mortars with plastic consistencies were studied. Furthermore, empirical formulas are proposed to describe the mechanical behavior of such materials with time up to 448 days. The evolution of such mechanical properties is related to the development of density and carbonation depth by means of the phenolphthalein method.

Chapter 6 studies the loading rate effect on the fracture properties of one natural hydraulic lime mortar and an aerial one. For this purpose, three different loading rates (loading-point displacement rates), from the quasi-static one, 5.0×10^{-4} mm/s to rate sensitive ones, 5.0×10^{-1} mm/s and 1.6×10^{1} mm/s were applied by using a servo-hydraulic testing machine up to its maximum rate range. The results show that the peak load and the fracture energy are rate sensitive, which is mainly due to the viscous effect caused by the presence of free water in the porous structure. Furthermore, empirical equations are proposed to describe such rate dependent behavior of lime mortars. Also, the nature of failure (intergranular or transgranular) is analyzed by means of pictures of the crack surface and SEM analyses.

Finally, in view of the difference found in the compressive strength from standardized prisms (measuring 40 mm $\times$ 40 mm $\times$ 160 mm) and cylinders (with 75 mm of diameter and 150 mm length) in the NHL mortars, in Chapter 7 of the thesis, a numerical simulation of the compressive test on prisms is performed to verify that such difference is mainly due to geometry and size effects. Two different NHL mortars with dry and fluid consistencies, respectively, are simulated with prism of three different sizes (40 mm $\times$ 40 mm $\times$ 80 mm, 80 mm $\times$ 80 mm $\times$ 160 mm and 160 mm $\times$ 160 mm $\times$ 320 mm). The results show that the material is affected by geometry and size and that the compressive strength of the cylinders is close to the intrinsic compressive strength of the material. Furthermore, another numerical simulation of the three-point bending test on prisms measuring 40 mm $\times$ 40 mm $\times$ 160 mm is performed to demonstrate the cohesive behavior of NHL mortars. This chapter does not include the analysis of the size effect on aerial lime mortars as this material will presumably be affected by the different possible carbonation process between prisms and cylinders. Further research with the objective of creating a model to analyze geometry and size effects on pure aerial lime mortars in combination with effect of carbonation process and humidity diffusion will be of interest. Other researchers [62, 63] have already proposed similar models for the analyses of quicklime mortars and masonry towers, respectively.

It is concluded that the advanced mechanical characterization of lime mortars performed in the thesis will be helpful to define with more realism and precision the numerical simulations of historical masonry structures built with such materials.

1.4. Work plan

The thesis includes the following tasks and procedures. They are mainly shown in the work plan (see Figure 1.5).

1. Revision of the bibliography concerning different aspects of lime mortars: fabrication procedures, dosage, raw materials, etc. and the advance mechanical characterization

of materials of the civil and architectural patrimony. Revision of theses and articles in scientific journals. This task is performed during the whole period of the thesis extension so it is not included in the work plan for simplicity.

2. Design of the experimental techniques: loading systems, instrumental tools, accessories, etc., to be used in the different experimental campaigns of the thesis. This was performed mainly for the first three months of the thesis with the help of the research group of Solid Mechanics of the University of Castilla-La Mancha in Ciudad Real (Spain) as most of the techniques were adapted from previously validated ones for concrete.

3. Selection of the necessary materials for the fabrication of the mortars: different types of limes (aerial and natural hydraulic) and different types of aggregates (crushed limestone one and silica sand). Analysis of the different possible dosage, fabrication procedures and characterization of the component materials (aggregates grading curve, water content, physical characterization of the limes). This was mainly performed during the first two months of the thesis and it is not included either on the work plan for simplicity.

4. Development of the different experimental campaigns to analyze the corresponding different aspects already mentioned. Each one is marked with an "X" and a different color in the work plan.

5. Development of the numerical simulation of the compression tests of mortar prisms with different sizes to study the size effect on lime mortars. Also, numerical simulation of the three-point bending test to confirm the cohesive behavior of lime mortars (indicated in the work plan).

6. Writing of the different articles, each one corresponding approximately with a chapter of the thesis. And, finally, preparation of the document of the thesis.

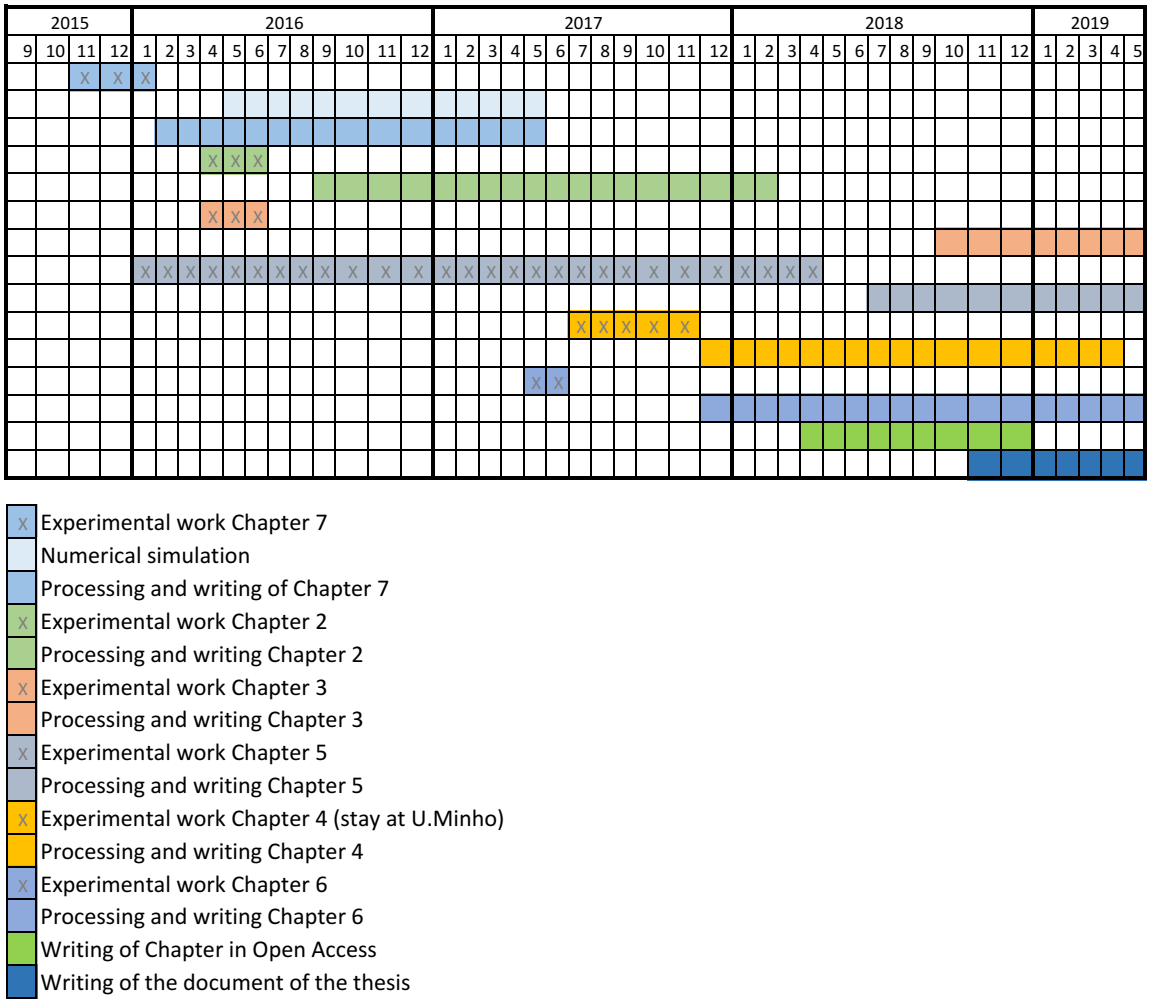

Chapter 2-article: *The effects of dosage and production process on the mechanical and physical properties of natural hydraulic lime mortars*
Chapter 3-article: *The influence of dosage and production process on the physical and mechanical properties of aerial lime mortars*
Chapter 4 (stay at U.Minho)-article: Stiffness evolution of natural hydraulic lime mortars at early ages measured through EMM-ARM
Chapter 5-article: *Age effects on the physical and mechanical properties of a natural hydraulic and an aerial lime mortars*
Chapter 6-article: *Loading rate effect on the fracture behavior of natural hydraulic and aerial lime mortars*
Chapter 7-article: *Advanced mechanical characterization of NHL mortars and cohesive simulation of their failure behavior*
Chapter in Open Access: *Mechanical behavior of natural hydraulic lime mortars*

Figure 1.5: Work plan of the thesis.

Part II

Experimental contributions and analyses

Chapter 2

The effects of production process and dosage on the physical and mechanical properties of natural hydraulic lime mortars

Article title: The effects of dosage and production process on the mechanical and physical properties of natural hydraulic lime mortars
Authors: Lucía Garijo, Xiaoxin Zhang, Gonzalo Ruiz, José J. Ortega, Zhimin Wu
Journal: Construction and Building Materials
Submitted: 10/12/2017
Accepted: 01/03/2018
DOI: 10.1016/j.conbuildmat.2018.03.016
Available at: https://doi.org/10.1016/j.conbuildmat.2018.03.016

Natural Hydraulic Lime (NHL) mortars are well-extended in restoration works presently. However, there is still a lack of standardization on their dosage methodology. Thus, seven types of mortar were fabricated and five factors which have an influence on their properties have been studied, in particular the water/lime ratio, the mold material, the aggregate size and type and the different curing conditions. Furthermore, an advanced mechanical characterization has been performed on these mortars, including the measurement of the fracture energy. Finally, some empirical equations for determining the relationships between these mechanical properties were proposed, which could be helpful when simulating the numerical models of historical constructions.

Keywords: NHL mortar, Dosage, Mechanical Characterization, Fracture Energy, Empirical equations.

2.1. Introduction

The study of the influence of the factors affecting the dosage methodology of lime mortars on their mechanical properties, such as, fracture energy and characteristic length is not so well-documented. In addition, there are no empirical equations for the mechanical properties of these mortars as the ones proposed by FIB Model Code [73] and ACI Building Code [83] for concrete. Thus, the aim of the chapter is to determine the influence of different factors (water/lime ratio, type and size of the aggregates, curing conditions and materials of the molds) affecting the dosage and fabrication process of NHL mortars on the mechanical properties, including the compressive strength of prisms and cylinders, the flexural strength, the splitting tensile strength, the elastic

modulus and the fracture energy. Furthermore, some empirical formulas determining a relationship between these properties and the compressive strength are proposed for the first time. Such formulas could be useful for the numerical simulations of masonry structures presenting natural hydraulic lime mortars.

The rest of the chapter is organized as follows. The next section describes the experimental procedure. In Section 2.3 a thorough analysis of the results and discussion are provided in addition to formulas which establish relationship between the mechanical properties of NHL mortars. Finally, our conclusions are presented in Section 2.4.

2.2. Experimental procedure

2.2.1. Raw materials

The binder used for all seven types of NHL mortar was a commercial lime of class NHL 3.5, in accordance with EN 459-1 [12] and was supplied by "Socli, Italcementi Group" (France). It had a density of 2580 kg/m^3 and an apparent density of 850 kg/m^3. Both chemical and mineralogical analyses of the lime were performed by corresponding X-ray fluorescence (XRD) and X-ray diffraction (XRD) analyses. It was used for each test a Philips (PANALYTICAL) Magis Pro X-ray fluorescence spectrometer, and a Philips (PANALYTICAL) X'Pert MPD diffractometer, respectively. The results show that the NHL presents a content of portlandite higher than 30%, see Table 2.1 and Figure 2.1. Moreover, the laser particle size distribution curve of the NHL (Figure 2.2) was obtained by means of a PSD Mastersizer 3000 from Malvern Instruments.

Table 2.1: Chemical and mineralogical compositions of the natural hydraulic lime, NHL 3.5.

Chemical composition (%)	
Na_2O	0.125
MgO	3.078
Al_2O_3	2.051
SiO_2	13.606
P_2O_5	0.044
SO_3	0.990
K_2O	0.456
CaO	59.949
TiO_2	0.132
MnO	0.014
Fe_2O_3	0.994
NiO	0.014
CuO	0.007
ZnO	0.004
SeO_2	0.002
Rb_2O	0.003
SrO	0.169
CO_2	18.365
Mineral phases (%)	
Portlandite, $Ca(OH)_2$	40-45
Calcite, $CaCO_3$	40-45
Calcium silicates	5-10

Different aggregates were used as well. The common one was a commercial crushed limestone with a maximum grain size of 4 mm. In addition, crushed limestone with a maximum grain size of 2 mm and river sand with a maximum grain size of 4 mm were also used in the fabrication of various mortars. The particle-size distribution curve of aggregates, determined according to

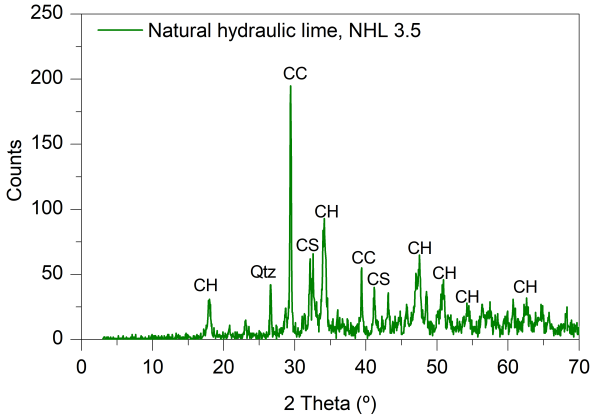

Figure 2.1: X-ray diffraction patterns of the natural hydraulic lime, NHL 3.5. CH = portlandite, CC = calcite, CS = calcium silicates, Qtz = quartz.

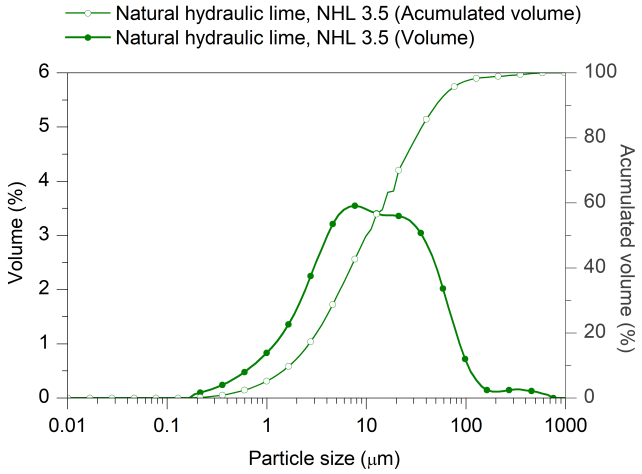

Figure 2.2: Laser particle size distribution curves of the natural hydraulic lime, NHL 3.5.

EN 1015-1 [84] (Figure 2.4a), is presented in Figure 2.3.

The apparent particle density and the apparent density of each type of aggregate are listed in Table 2.2, in accordance with the standards EN 1097-6 [85] (Figure 2.4 b) and EN 1097-3 [86] (Figure 2.4 c), respectively.

Table 2.2: Apparent particle density and apparent density of each type of aggregate.

	Apparent particle density (kg/m^3)	Apparent density (kg/m^3)
Standards	EN 1097-6 [85]	EN 1097-3 [86]
Crushed limestone 0/4 mm	2680	1820
Crushed limestone 0/2 mm	2740	1810
River sand 0/4 mm	2590	1460

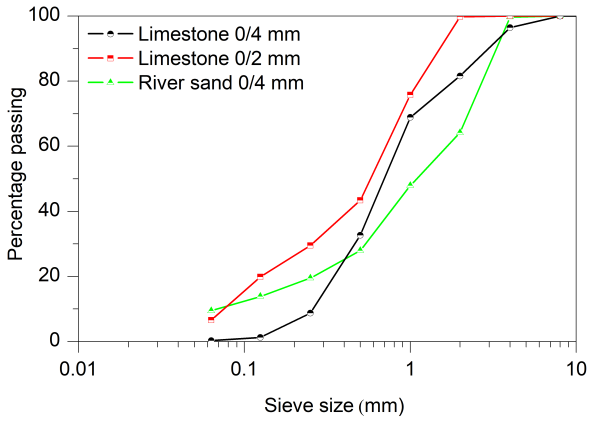

Figure 2.3: Aggregates grading curves.

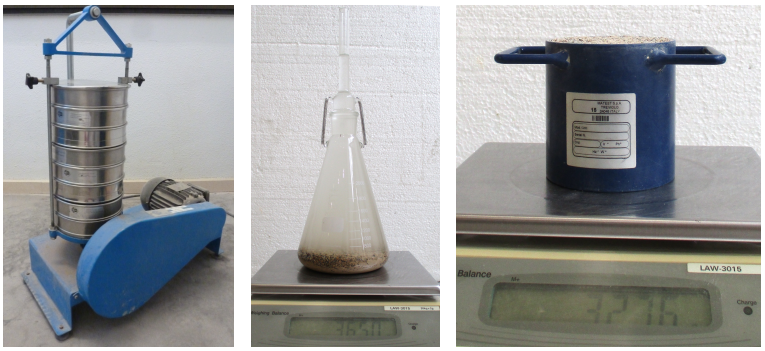

(a) (b) (c)

Figure 2.4: Test setup to obtain: (a) the grading curves, (b) the apparent particle densities and (c) the apparent densities of the aggregates.

2.2.2. NHL mortar preparation

In total, seven types of NHL mortar were prepared and tested (see Table 2.3). First, as a reference material, a NHL mortar with a lime/aggregate ratio of 1:3 by volume was fabricated according to the traditional treatises and the recommendations of the references mentioned in the Introduction [25, 32, 40, 87]. A water/lime ratio of 0.9 by volume for the mortar was selected to obtain a plastic consistency from 140 mm to 200 mm, determined by the flow table test, in accordance with the standards EN 1015-3 [88] and EN 1015-6 [89]. It should be noted that the volume proportions of the compounds were converted to weight in order to obtain a convenient measurement for the mixing process. In addition, a crushed limestone aggregate with a maximum grain size of 4 mm and a metallic mold were used. For purpose of simplification, this benchmark NHL mortar was labeled H09C04M, where "H" stands for hydraulic. The other mortar compositions were obtained by modifying an aspect of this material. For instance, H08C04M and H11C04M were achieved by changing the water/lime ratio of the benchmark to 0.8 and 1.1, respectively. Thus, dry, plastic and fluid mortars were obtained.

In order to disclose the influence of the type and size of sand, materials of mold and curing conditions on the mechanical properties of mortars, the water/lime ratio was kept constant as 0.9 to isolate and quantify the function of each factor. It is worth noting that we did not follow the conventional ideas for studying the effect of the type and size of sand, that is, maintaining the consistencies of mortars approximately constant by varing the water/lime ratios [6, 8, 9, 42, 52]. H09C04W was fabricated in wooden (plywood) molds (see Figure 2.5) instead of the metallic one

Table 2.3: Characteristics of the seven mortar compositions.

Mortar composition	Water/lime ratio (by volume)	Type of aggregate	Maximum grain size (mm)	Material of the mold	Curing conditions
H09C04M	0.9	Crushed limestone	4	Metallic	56 days at HC
H08C04M	0.8	Crushed limestone	4	Metallic	56 days at HC
H11C04M	1.1	Crushed limestone	4	Metallic	56 days at HC
H09C04W	0.9	Crushed limestone	4	Wooden	56 days at HC
H09C02M	0.9	Crushed limestone	2	Metallic	56 days at HC
H09R04M	0.9	River sand	4	Metallic	56 days at HC
H09C04MA	0.9	Crushed limestone	4	Metallic	7 days at HC and 49 days at AC

Note. HC: Humid chamber (RH: 97 ± 0.5%, 20 ± 0.5°C), AC: Ambient laboratory conditions (RH: 50 ± 10%, 23 ± 3°C)

required by the standard EN 1015-11 [31]. H09C02M had the same type of crushed limestone aggregate, but with a maximum grain size of 2 mm. H09R04M was prepared with river sand. H09C04MA had the same composition as H09C04M, but was cured under the ambient laboratory conditions (RH of 50 ± 10% and 23 ± 3°C) until the day of testing, after an initial seven days curing period in a humid chamber at RH of 97 ± 0.5% and 20 ± 0.5°C by following recommendations in the standard EN 1015-11 [31]. The remainder were cured in the humid chamber until the day of testing.

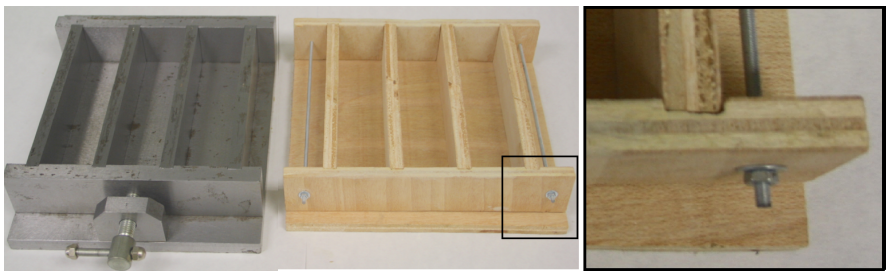

(a) (b)

Figure 2.5: Different types of molds for the fabrication of mortar: (a) metallic mold, (b) wooden mold

Prior to the mixing process, the aggregates were heated at 105°C for 24 hours and then cooled down to room temperature so as to remove any moisture content.The mixing process was then performed according to the standard EN 1015-2 [90]. For the purpose, a vertical axis mortar mixer with sufficient capacity was used so as to cast one batch per mortar type within this chapter. For each NHL mortar, 18 prisms (40 mm × 40 mm × 160 mm) and 6 cylinders (75 mm in diameter and 150 mm in height) were fabricated, followed by 126 prismatic specimens and 42 cylinders in total. All the molds were previously lubricated with mineral oil to prevent the mortar from adhering

to the mold walls. The mortar was poured in two layers when using the prismatic molds and in three layers instead when using the cylindrical ones and each was compacted with 25 strokes of the tamper. All the specimens were removed from the molds in two days after the fabrication following the standard EN 1015-11 [31].

2.2.3. Test of the NHL mortar in a fresh state

In a fresh state, the apparent density was measured following the standard EN 1015-6 [89] (Figure 2.6 a). The water-retention capacity was obtained according to the standard EN 459-2 [91] (Figure 2.6 b),which was determined as the percentage of water that remained in the mortar after a suction time of 5 minutes on ten layers of filter paper model "Resma" of 73 g/m^2. In addition, the consistency was measured using the method mentioned in Section 2.2.2 by the flow diameter test (Figure 2.6 c).

(a) (b) (c)

Figure 2.6: Test of mortar in fresh state for: (a) apparent density, (b) water retention capacity and (c) consistency.

2.2.4. Mechanical tests on the NHL mortars

All the specimens were weighed and measured prior to testing so as to obtain the apparent density of the material. The flexural, compressive and splitting tensile strengths, the elastic modulus and fracture energy were obtained through various types of tests as shown in Figure 2.7, at an age of 56 days.

Flexural and compressive strengths

The flexural and compressive strengths were determined according to the standard EN 1015-11 [31] by using an Instron 1011 testing machine. The flexural strength was measured by a three point-bending test on three beams (40 mm × 40 mm × 160 mm) at a loading rate of 10 N/s and a span of 100 mm, see Figure 2.7 a. It is worth noting that the beam rests on two rigid-steel cylinders placed on two supports which permit rotation out of the plane of the beam and rolling along the longitudinal axis of the beam with negligible friction. That is, the anti-torsion supports were used for the test, which is specially important for quasi-brittle materials, like NHL mortars.

The compressive tests were conducted on the six half-prisms remaining from the bending tests at a loading rate of 50 N/s, as shown in Figure 2.7 b. The load was centered in the middle of the longest side by using a steel plate (40 mm × 40 mm × 10 mm). Moreover, an individualized ball-and-socket joint over the steel plate was used to reduce the eccentricity during the loading process.

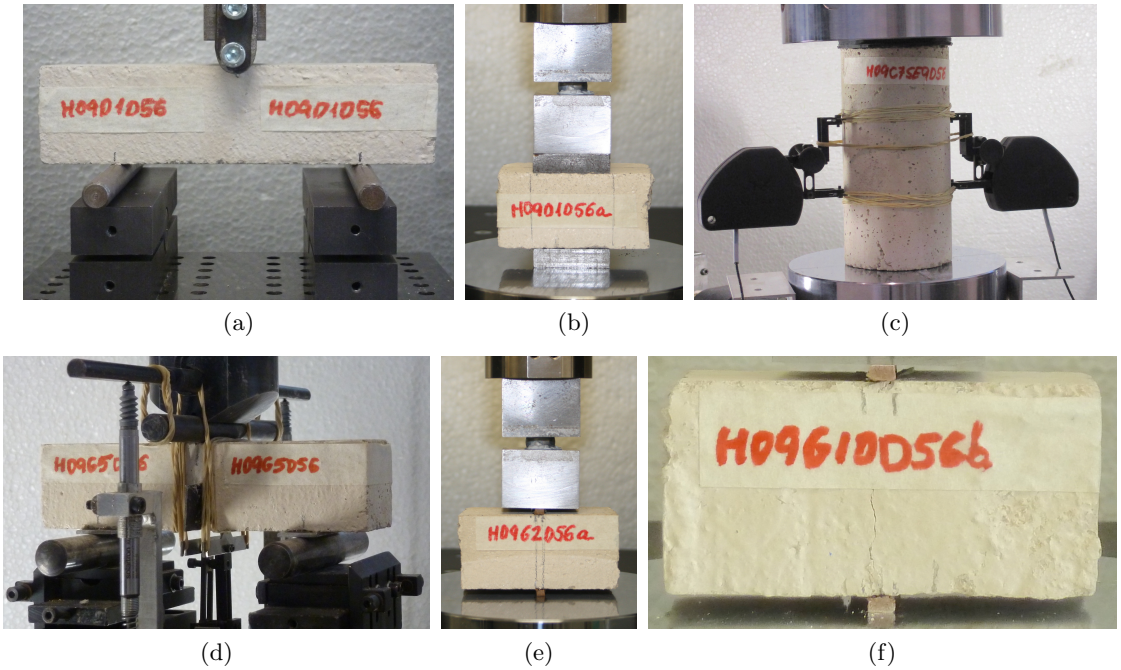

Figure 2.7: Tests for: (a) flexural strength, (b) compressive strength, (c) elastic modulus and compressive strength, (d) fracture energy, (e) splitting tensile strength. (f) Crack pattern after splitting tensile test.

Compressive strength on cylinders and elastic modulus

In order to study the size and shape effects on compressive strength, compressive tests were also carried out on four cylinders (75 mm in diameter and 150 mm in height) at a loading rate of 10 N/s by using an Instron 8805 testing machine. In addition, the elastic modulus was measured in accordance with the principles of the standard EN 12390-13 [92], see Figure 2.7 c. Two clips (strain gauge extensometers Instron 2630) centered on opposite generatrices were used to measure the axial deformation. The clips were placed covering a span of 50 mm so that local constrictions caused by the friction between the steel platens and the cylinder surface did not influence the measurement of the elastic modulus. Two rubber layers with 2 mm thickness each were used between the upper surface of the sample and the steel platen to avoid contact problems due to the irregular roughness of the sample. In order to obtain a stable value, five repeat monotonic tests were conducted up to 30% of the maximum load; the mean of the last three values measured were taken as the elastic modulus. After measuring the elastic modulus, the specimens were broken to obtain the compressive strength.

Fracture energy

The fracture energy, G_F, was measured by a three-point bending test following the procedure recommended by RILEM [93] and the improvements proposed by Planas, Guinea and Elices [94–96]. For sake of convenience, the prisms were the same size as those used for the flexural tests. A pre-cast notch in the middle of the specimens was introduced by using a cardboard piece (2 mm thickness and 20 mm in depth) during the fabrication. Four tests were conducted for each mortar.

The tests were performed by using an Instron 8805 testing machine as shown in Figure 2.7 d. G_F was obtained as:

$$G_F = \frac{W_m + W_{um}}{B\,(D-a)} \tag{2.1}$$

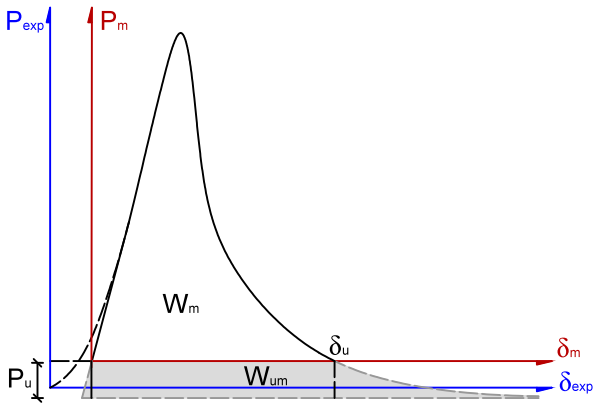

Figure 2.8: Determination of the fracture energy.

where W_m, measured energy, is the area under the experimental load–displacement curve (P_m – δ_m), and W_{um} is the unmeasured energy that corresponds to the portion of the ligament that is still unbroken when the test is stopped. B and D are the specimen width and depth, respectively. a is the notch depth.

We assume that the crack propagation obeys a cohesive model, which leads to a hyperbolic tail in the $P - \delta$ curve when displacement is very large and the ligament is very short [95, 97, 98]. Figure 2.8 shows the process used to obtain complete fracture energy, where δ_u and P_u correspond to the termination point of the bending test. It should be emphasized that the kinetic energy of the specimen is very small and insignificant compared with the fracture energy in our tests [98]. The procedure described above allows getting a size independent value for G_F [97, 99].

The weight-compensation technique was followed during the test in order to obtain complete failure information from the specimen, i.e. rubber bands were used to hold the specimen at all times, as shown in Figure 2.7 d. The specimen was placed over two rigid steel cylinders that could roll along the longitudinal axis of the specimen over supports that permit rotation out of the plane of the specimen. These supports were affixed to a steel beam attached to the machine frame. The loading point displacement in relation to this steel beam was measured by using two LVDTs (linear variable differential transducers) affixed to it. The tests were performed in position-control at a loading rate of 5.0×10^{-4} mm/s until a displacement equal to 0.3 mm and at 2.5×10^{-3} mm/s during the rest of the test (until reaching a displacement of 3 mm in total).

In addition, an extensometer (strain gauge extensometer Instron 2620) attached to the lower surface of the beam was used to obtain the crack-mouth opening displacement (CMOD). For span/depth (S/D) ratios (β) between 2.5 and 16, the elastic modulus obtained from prisms (E_{pr}) could be calculated by general Eqs. (2.2) and (2.3) according to the reference [100].

$$E_{pr} = 6\frac{Sa}{C_i B D^2} \upsilon_\beta(\alpha) \tag{2.2}$$

$$\upsilon_\beta(\alpha) = \upsilon_\beta(a/D) = 0.8 - 1.7\alpha + 2.4\alpha^2 + \frac{0.66}{(1-\alpha)^2} + \frac{4}{\beta}(-0.04 - 0.58\alpha + 1.47\alpha^2 - 2.04\alpha^3) \tag{2.3}$$

where C_i is the initial compliance determined from Load-CMOD curve, $\upsilon_\beta(\alpha)$ is a dimensionless shape function depending on β and the relative notch/depth ratio α. The other parameters of the beam have been previously defined.

It is worth noting that Eq. (2.3) changes to Eq. (2.4), which is recommended by RILEM TC 89-FMT [101] for calculating the shape parameter when the span/depth ratio β equals 4.

$$\upsilon_4(\alpha) = \upsilon_4(a/D) = 0.76 - 2.28\alpha + 3.87\alpha^2 - 2.04\alpha^3 + \frac{0.66}{(1-\alpha)^2} \tag{2.4}$$

Splitting tensile strength

Splitting tensile strength (indirect tensile strength) was measured through quasi-static splitting tensile tests (Brazilian tests) on four prismatic halves resulting from the preceding bending test for measuring fracture energy, in accordance with the procedures recommended by the standard EN 12390-6 [102]. To perform the test, the Instron 1011 testing machine was used, and the loading rate was set at 50 N/s. The proportion between the load-bearing width and the height of the specimens was maintained as low as 1/10 following the recommendations in [103–105]. The bearing strips were made of plywood, and they were placed in the middle of the longest side of the halves. The observed fracture mechanisms are indicative of the test validity and they can be studied through the crack pattern, which is a single crack [106] (Figure 2.7 f). The splitting tensile strength is obtained as:

$$f_t = \frac{2F}{\pi BD} \tag{2.5}$$

where f_t is the splitting tensile strength, F is the maximum load, B and D are the specimen width and depth, respectively, as mentioned previously.

Characteristic length

Once splitting tensile strength (f_t), elastic modulus (E) and fracture energy (G_F) are obtained, the characteristic length, l_{ch}, can be calculated according to Eq. (2.6). It is a parameter proposed by Hillerborg *et al.* [107] for fracture behavior. It is related to the length of the Fracture Process Zone and could be used to predict the brittleness of a material. As it decreases, brittle nature dominates and vice versa [107].

$$l_{ch} = \frac{EG_F}{f_t^2} \tag{2.6}$$

2.2.5. Porosity and capillary water absorption measurements

Porosity is a key parameter for the evaluation of compatibility between original and restoration materials due to the fact that it mainly affects water movement and evaporation [108]. In the study, the open porosity at an age of 56 days was measured by a hydrostatic method following the standard UNE 83980 [109]. In such a test, the dry weight of the samples m_1, the weight after two days of water immersion m_2, the weight after 5 hours of water saturation by boiling m_3 and the apparent weight with a hydrostatic scale m_4, were obtained respectively.
Then, the open porosity, OP, is expressed in percentage as:

$$OP = \frac{m_3 - m_1}{m_3 - m_4} 100 \tag{2.7}$$

Note that in Eq. 2.7, m_2 is not used. Standard UNE 83980 [109] includes the procedure to obtain such a parameter to calculate latter the absorption after immersion, which is not included in this study.

Furthermore, by means of the Mercury Intrusion Porosimetry (MIP) method, the pore-size distribution was obtained by using a Micromeritics 9500 Poresizer mercury porosimeter (Figure 2.9). This technique is based on the principle that a sample surrounded by mercury, a non-wetting liquid, fills its pores with mercury by applying pressure. The volume of the intruded mercury is subsequently recorded. At the lowest filling pressure, intrusion is considered zero and no pore volume of interest is filled. The volume of mercury required to fill all accessible pores is considered the total pore volume [110]. The percentage of porosity, P, is obtained as Eq. (2.8).

$$P = 100\left(\frac{V_{Pt}}{V}\right) \tag{2.8}$$

where V is the bulk volume of a sample (obtained from the bulk density) and V_{Pt} is the total intrusion volume [110]. Moreover, the pore size ranging from 0.005 to 360 µm can be detected by the MIP method [111].

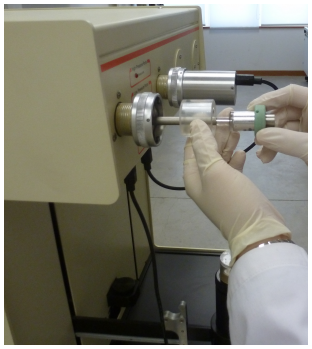

Figure 2.9: Micromeritics 9500 Poresizer mercury porosimeter.

The capillary water-absorption coefficient was measured according to the standard EN 1015-18 [112] (Figure 2.10). This test consists of drying halves of the prismatic samples, then, painting the four lateral surfaces with paraffin wax, and finally, immersing the cut surface in water for a period of time. Thus, the water-absorption coefficient, C, can be calculated according to Eq. (2.9):

$$C = 0.1(M2 - M1) \tag{2.9}$$

where $M1$ and $M2$ are the mass in grams of the sample after 10 and 90 minutes of immersion, respectively. The unit of C is kg/(m^{2}min$^{0.5}$).

Figure 2.10: Test to measure capillary water absorption coefficient.

2.3. Results and discussion

In this section the results of the experimental campaign described in Section 2.2 are presented. Table 2.4 provides a comparison between some of the experimental results obtained from other researchers and the results of this chapter. Table 2.5 exhibits the properties of NHL mortars in a fresh state, while Table 2.6 presents the mechanical and

physical properties of the seven NHL mortars in a hardened state. Std. Dev. is the standard deviation, and CV is the coefficient of variation.

Before analyzing the results, it was checked that they were repeatable; it was obtained a difference up to 5% on the compressive strengths of mortars belonging to different batches. Although, as mentioned in Section 2.2.2, it had been used a vertical axis mortar mixer with sufficient capacity so as to cast one batch per mortar type within mortars used in this chapter and avoid then repeatability inconveniences. On Chapters 4, 5, 6 and 7, mortars of the same types as those presented in this chapter were fabricated and repeatability was then checked among natural hydraulic lime mortars belonging to different chapters.

From Table 2.4, it is important to note that the experimental results are similar among mortars which resemble one another in composition. For instance, the mortars tested by Drougkas *et al.* [21] and the mortar H09C04MA in the current work, were both mainly cured under ambient laboratory conditions. For the former, the flexural strength and the compressive strength are 0.8 MPa and 1.9 MPa, respectively, while they are 0.91 MPa and 2.4 MPa for the latter. Only a small difference is observed, which could be due to the different curing conditions during the first 7 days of maturation. In our case, it was cured in a climate chamber instead of under laboratory conditions. Moreover, similar mechanical properties were obtained by Grilo *et al.* in [25] compared with H09R04M in the current work, both of which had the same type of siliceous river sand. Furthermore, Maravelaki-Kalaitzaki *et al.* [33] prepared and tested a NHL mortar with pozzolanic additions by reproducing the original mortars from a historic masonry in Crete, Greece. The overall similarities obtained on the mechanical and physical properties of H09C04M may show that the fabricated mortar is also suitable for repairing historic masonry.

From Table 2.6, it is obvious that there is considerable difference between the compressive strength from prisms and cylinders. For example, for H09C04M, they are 3.2 MPa and 2.0 MPa, respectively. The ratio between prism and cylinder strengths is 1.6, which is much larger than that of concrete [78]. The variations of density and open porosity of both specimens are around 1% and 0.4%, respectively, which confirms that the fabrication process should not result in a such large difference. In Chapter 7 of the thesis, it is shown that this difference is mainly due to geometry and size effects [78, 80]. Similar tendency was also observed by Haach *et al.* [28] for cement-lime mortars, the ratio could reach 1.9. Moreover, for H09C04M, the elastic moduli are 5.0 GPa and 5.2 GPa measured from cylinders and prisms, respectively. The variation of both measurements is only 4%. However, for H11C04M, the difference is greater(2.8 GPa versus 3.8 GPa),which may be mainly due to the quality or imperfections of the pre-notches. Nevertheless, they are still of the same order.

Regarding open porosity, due to the different ranges of pore-size detected, the values obtained by using the hydrostatic method are always greater than the ones measured by using the MIP method as presented in [14].

2.3.1. Effect of the water/lime ratio

Three types of mortars were tested in order to study the influence of the water/lime ratio on mechanical properties (H08C04M, H09C04M and H11C04M, with corresponding water/lime ratios of 0.8, 0.9 and 1.1). Their consistencies were dry, plastic and fluid, as shown in Table 2.5. In addition, the apparent density in a fresh state and the water-retention capacity increase as the water/lime ratio decreases. For example, for H08C04M, the apparent density and water-retention capacity are 2290 kg/m^3 and 90.9%, respectively, compared with 2240 kg/m^3 and 76.7% for H11C04M. In Table 2.6, it is observed that as the water/lime ratio increases, the open porosity increases as well, which causes a weakening

Table 2.4: Comparison of experimental results.

	Drougkas *et al.*, 2015, [21]	Current work H09C04MA (ambient curing)	Grilo *et al.*, 2014, [25]	Current work H09R04M (river sand)	Maravelaki-Kalaitzaki *et al.*, 2005, [33]	Current work H09C04M (benchmark)
NHL type	NHL 3.5	NHL 3.5	NHL 3.5	NHL 3.5	NHL-Z 3.5(*)	NHL 3.5
Aggregate type	Crushed limestone	Crushed limestone	Siliceous river sand	Siliceous river sand	Siliceous sand	Crushed limestone
Maximum grain size (mm)	5	4	-	4	5	4
Binder/aggregate ratio	1:3 by volume	1:3 by volume	1:3 by volume	1:3 by volume	6:14 by weight	1:3 by volume
Consistency (mm)		150-155	151-153	180-187	155	150-155
Curing conditions	(70.2% , 22.5°C)	7 days at (RH 97±0.5%, 20±0.5°C) and (RH 50±10%, 23±3°C) until testing	(RH 95±5%, 20±3°C)	(RH 97±0.5%, 20±0.5°C)	3 days at (RH 95±1%, 20±1°C) and (RH 60±1%, 20±1°C) until testing	(RH 95±5%, 20±3°C)
Age of testing	49 days	56 days	90 days	56 days	31 days	56 days
Flexural strength, f_{flex} (MPa)	0.8	0.91	1.2	0.96	-	1.3
Compressive strength, f_{cpr} (MPa)	1.9	2.4	2.4	2.3	3.48	3.2
Elastic modulus, E_{cy} (GPa)		1.5	-	4.2	7.12	5.0
Capillary water absorption coefficient ($kg/(m^2 min^{0.5})$)	-	1.57	-	1.69	1.87	1.36
Open porosity (hydrostatic) (%)	-	29.0	-	29.4	26.23 (at 365 days)	27.7
Open porosity (MIP) (%)	-	23.8	-	24.0	-	23.4

(*) Natural hydraulic lime with pozzolanic additions.

Table 2.5: Properties of NHL mortars in a fresh state.

	H09C04M (benchmark)	H08C04M (water/lime: 0.8)	H11C04M (water/lime: 1.1)	H09C02M (maximum grain size: 2 mm)	H09R04M (river sand)
Flow diameter (consistency) (mm)	150-155	130-135	238-240	120-125	180-187
Category (consistence)	Plastic	Dry	Fluid	Dry	Plastic
Apparent density (kg/m^3)	2250	2290	2240	2250	2110
Water retention (%)	83.5	90.9	76.7	91.6	78.7

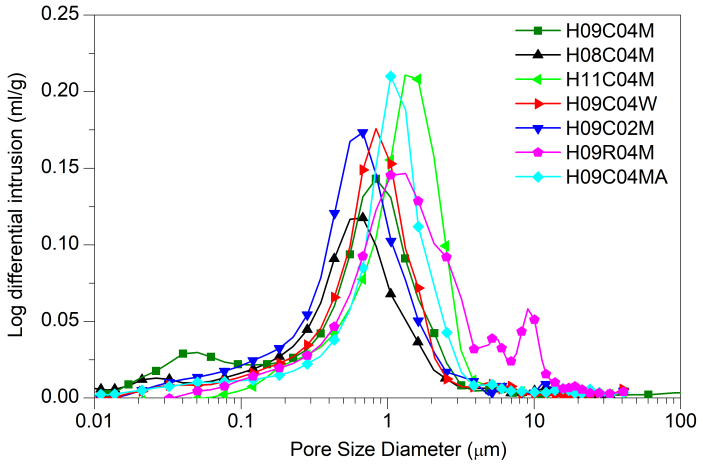

Figure 2.11: Pore-size distribution of NHL mortars as measured by MIP.

of the material structure and its mechanical properties. This is attributed to the fact that both the carbonation rate of calcium hydroxide and calcium silicates hydrates in NHL paste present a downward tendency with an increase in the water/lime ratio [48].

Figure 2.11 shows the pore-size distribution of seven types of NHL mortars measured by MIP. It is obvious that most of the mortars present a single narrow peak between 0.5 and 2 µm. A shift of the pore-size distribution towards a finer diameter is observed in mortar H08C04M, while in mortar H11C04M, there is a shift towards a larger one. Namely, with an increase in the water/lime ratio, the median pore radius also increases as shown in Table 2.6. This results in an increase of the capillary water-absorption capacity, which is the main controlling factor for determining service life. The higher the capillary absorption coefficients, the more vulnerable they are to the effect of ambient water and soluble salts [113, 114].

In Figure 2.12 it is observed the pore-size distribution of the seven NHL mortars by means of bar charts (representing percentage of pore area). The classification of the pore size range is given in [43], where gel pores are between 0.005 µm and 0.01 µm, medium

Table 2.6: Properties of NHL mortars in a hardened state at an age of 56 days.

		H09C04M (benchmark)	H08C04M (water/ lime: 0.8)	H11C04M (water/ lime: 1.1)	H09C04W (wooden mold)	H09C02M (maximum grain size: 2 mm)	H09R04M (river sand)	H09C04MA (ambient curing)
Apparent density from prisms, ρ_{pr} (kg/m^3)	Mean	**2050**	**2091**	**1964**	**2070**	**2016**	**1856**	**2003**
	Std. Dev.	20	3	30	8	15	10	8
	CV (%)	1	0.2	1.5	0.4	0.7	0.5	0.4
Apparent density from cylinders, ρ_{cy} (kg/m^3)	Mean	**2054**	**2113**	**1983**	**-**	**1994**	**1869**	**2014**
	Std. Dev.	5	10	4		12	8	5
	CV (%)	0.3	0.5	0.2		0.6	0.4	0.3
Flexural strength, f_{flex} (MPa)	Mean	**1.3**	**1.3**	**0.89**	**1.7**	**1.1**	**0.96**	**0.91**
	Std. Dev.	0.1	0.1	0.04	0.1	0.1	0.06	0.02
	CV (%)	8	7	5	6	10	6	2
Compressive strength from prisms, f_{cpr} (MPa)	Mean	**3.2**	**4.2**	**1.7**	**3.5**	**3.2**	**2.3**	**2.4**
	Std. Dev.	0.1	0.3	0.1	0.1	0.2	0.1	0.1
	CV (%)	3	6	4	4	6	6	5
Compressive strength from cylinders, f_{ccy} (MPa)	Mean	**2.0**	**2.7**	**1.4**	-	**2.0**	**1.5**	**1.5**
	Std. Dev.	0.2	0.3	0.1		0.1	0.1	0.1
	CV (%)	9	12	8		7	8	3
Fracture energy, G_F (N/m)	Mean	**12**	**13**	**4.9**	-	**12**	**10**	**8**
	Std. Dev.	3	1	0.8		1	2	1
	CV (%)	22	9	17		10	19	10
Splitting tensile strength, f_t (MPa)	Mean	**0.39**	**0.51**	**0.24**	**0.57**	**0.49**	**0.38**	**0.34**
	Std. Dev.	0.02	0.01	0.03	0.05	0.05	0.03	0.03
	CV (%)	6	1	12	9	11	7	9
Elastic modulus from cylinders, E_{cy} (GPa)	Mean	**5.0**	**5.4**	**2.8**	-	**4.6**	**4.2**	**2.8**
	Std. Dev.	0.2	0.6	0.7		0.2	0.2	0.4
	CV (%)	4	10	25		4	6	7
Elastic modulus from prisms, E_{pr} (GPa)	Mean	**5.2**	**6.0**	**3.8**	-	**5.1**	**4.4**	**3.2**
	Std. Dev.	0.5	0.2	1.0		0.6	0.4	0.6
	CV (%)	11	3	27		11	8	18
Characteristic length l_{ch} (mm)		**390**	**260**	**240**	-	**220**	**280**	**190**
Capillary water absorption coefficient (kg/(m^{2}min$^{0.5}$))	Mean	**1.36**	**0.95**	**1.70**	**1.83**	**1.84**	**1.69**	**1.57**
	Std. Dev.	0.06	0.07	0.07	0.03	0.03	0.07	0.06
	CV (%)	4	7	4	1	1	4	4
Open porosity (hydrostatic) (%)	-	**27.7**	**25.0**	**29.9**	**24.1**	**27.8**	**29.4**	**29.0**
Open porosity (MIP) (%)	-	**23.4**	**19.7**	**24.3**	**22.5**	**24.8**	**24.0**	**23.8**
Median pore radius (MIP) (µm)	-	**0.36**	**0.28**	**0.66**	**0.39**	**0.31**	**0.66**	**0.52**

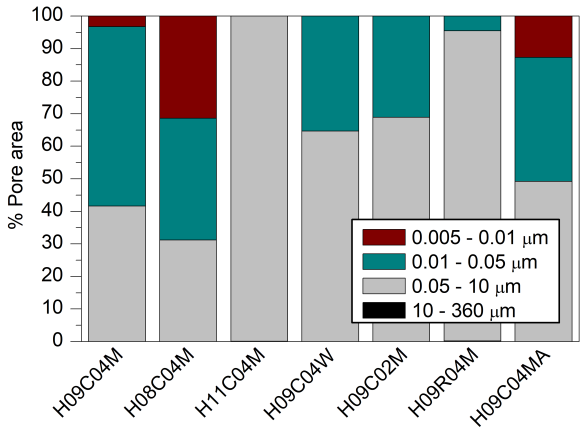

Figure 2.12: Pore-size distribution of NHL mortars as measured by MIP (percentage of pore area)

capillaries or large mesopores range between 0.01 µm and 0.05 µm, large capillary pores or macropores between 0.05 µm and 10 µm, and finally, air voids are bigger than 10 µm. The predominant pore size range is the one corresponding to large capillary pores or macropores (0.05 µm and 10 µm) [43, 115–117]. This pore range influences the strength and transport processes [115–117]. It is followed by the medium capillaries or large mesopores (range between 0.01 µm and 0.05 µm), which affect strength and permeability trough the mortar structure [43]. Moreover, gel pores (below 0.01 µm) are present in H09C04M (benchmark mortar), H08C04M (with a water/lime ratio of 0.8) and H09C04MA (cured in the ambient conditions). Such pores are formed inside the binder crystal lattice and influence the hydration rate [43, 110]. Finally, It is remarkable that H09R04M present a quite small amount (around 0.20%) of air voids (larger than 10 µm), while they are almost negligible for the rest of the NHL mortars.

2.3.2. Effect of the material of the molds

In order to determine the influence of the material of the mold on the properties, a comparison was made between H09C04M and H09C04W mortars, fabricated with metallic and wooden molds respectively. The elastic modulus and the compressive strength of cylinders were not measured, as we did not make cylindrical wooden molds. In general, H09C04W exhibits a better mechanical behavior, see Table 2.6. For example, it has a flexural strength of 1.7 MPa and a compressive strength from prisms of 3.5 MPa. However for H09C04M they are instead 1.3 MPa and 3.2 MPa, respectively. This difference could be due to the fact that wooden molds absorb the excess of water from the mortar. Accordingly, the water content of the specimens decreases compared with metallic molds. Thus, as mentioned in section 2.3.1, H09C04W has higher mechanical properties. Moreover, the median pore radius (measured by MIP) is 0.39 µm for H09C04W (inside wooden molds), while 0.36 µm for H09C04M (benchmark mortar). Considering that the sample for MIP is taken from the inner of the specimen, this difference could probably be associated with the fact that the water absorption of the wooden molds is local and non-uniform resulting in a drier material in the borders than in its core.

Moreover, due to the demolding process for the wooden molds (see Figure 2.5), the nuts had to be removed from the steel wires, which caused damage in all the notched specimens. Thus, the fracture energy and the elastic modulus from prisms were not

measured. Furthermore, all these molds were only used once for the fabrication of NHL mortars, as they supposedly change their absorption capability with each use, and therefore this would affect the comparison. Nevertheless, the influence of the material of the mold on the properties of mortars needs further study in order to examine the type of plywood used, the improvement of the demolding system and the possibility of reusing the molds.

2.3.3. Effect of the maximum aggregate size

Mortars H09C04M and H09C02M were prepared with the same composition but different maximum aggregate size (4 mm and 2 mm, respectively). The water/lime ratio was maintained at 0.9 for both. Thus, mortar H09C02M had a lower consistency (see Table 2.5) and a higher water demand in a fresh state, due to the fact that small aggregates could absorb more water during the fabrication process, i.e., it induces higher capillary water absorption coefficients in a hardened state [6, 118] (Table 2.6). The influence of the aggregate size is coupled with the effect of the water/lime ratio. According to reference [6], larger coarse aggregates (in that case a 0/6 mm grain size aggregate) improve the resistance in a comparison among mortars with similar consistencies. However, this is achieved by means of adding water to mortars with smaller aggregates, as they have a higher water demand, which modifies the water/lime ratio. In our case, this proportion has been kept for H09C04M and H09C02M mortars, which results, respectively, in a plastic and a dry consistency in a fresh state (see Table 2.4). As both have similar mechanical properties, this could be explained by the positive effect of a lower water/lime ratio offsetting the possible lower capacity of smaller aggregates. Moreover, if more water were added to H09C02M to obtain a plastic mortar instead of a dry one, the mechanical properties should be weaker.

2.3.4. Effect of the aggregate type

The influence of two types of aggregate was studied by comparing H09C04M (the benchmark mortar) and H09R04M, fabricated with crushed limestone and river sand, respectively. In a fresh state, H09R04M has a higher consistency (180-187 mm) than H09C04M (150-155 mm) for the same water/lime ratio. In addition, H09R04M has a lower apparent density and water-retention in a fresh state, see Table 2.5.

In a hardened state (see Table 2.6), H09R04M also presents lower mechanical properties than H09C04M. Moreover, the open porosity and the mean pore radius are higher for the former. Furthermore, H09R04M shows a high dispersion of the pore-size distribution with a broad curve (see Figure 2.6) and presents the highest content of pores larger than 0.05 µm as well (see Figure 2.12). These differences in the mechanical behavior and the size of the pores are mainly due to the interlocking of aggregate particles. Crushed limestone aggregates exhibit better interlocking behavior than river sands with round particles [9]. Undoubtedly, if less water were added to H09R04M to get similar consistency as H09C04M, the mortar would be stronger.

2.3.5. Effect of the curing conditions

The influence of the curing conditions has been studied between mortars H09C04M, cured in the humid chamber (RH: 97 ± 0.5% and 20 ± 0.5°C), and H09C04MA, cured under the ambient laboratory conditions (RH: 50 ± 10% and 23 ± 3°C). It is observed in Table 2.6 that high RH favors lime hydration, which results in higher mechanical properties. H09C04MA shows 25% less compressive strength and 30% less flexural strength

compared with those of H09C04M. Moreover, it has higher open porosity and median pore radius, between 5% or 2% (depending on the method) and 31%, respectively. Similar tendencies are also found in [25, 52, 53].

2.3.6. Characteristic length

As mentioned in Section 2.2.4, characteristic length is an indicator of brittleness of quasi-brittle materials. The shorter it is, the more brittle the material is. For all mortars studied in this chapter, their range is from 190 mm to 390 mm, which is quite similar to the one of normal strength concrete (250 mm to 300 mm). Moreover, maximum grain size has a great impact on the parameter. For example, H09C04M and H09C02M, which have different maximum grain sizes (4 mm and 2 mm, respectively), present characteristic lengths of 390 mm and 220 mm, see Table 2.6. It is obvious that the smaller the aggregate size, the more brittle the mortar. Furthermore, using river sand in fabrication and curing under ambient laboratory conditions also make the mortar more brittle.

2.3.7. Empirical equations among mechanical properties

For the principal construction material, concrete, there are some recognized codes, such as the FIB Model Code [73] and ACI Building Code [83], which present empirical formulas relating compressive strength to other mechanical properties. These equations are quite helpful for numerical simulation and structural design when only compressive strength is measured due to the convenience of conducting the test, although relative error may be as high as 90% [119]. To our knowledge, there are still no empirical equations on mechanical properties of lime mortar, thus, according to the experimental results of seven types of mortar several equations are proposed as follows, see Eq. (2.10) and corresponding coefficients on Table 2.7. It should be emphasized that the compressive strength of prisms is used as the basis of all empirical equations as it is a normalized property in lime mortars and easier to be measured.

$$Y = e f_{cpr}^{g} \tag{2.10}$$

Table 2.7: Coefficients of Equation (2.10).

Y	e	g
f_{ccy}	0.76	0.85
f_{flex}	0.60	0.62
f_t	0.18	0.78
G_F	4.19	0.82
E_{cy}	1.89	0.75
E_{pr}	2.46	0.61

The determination coefficient, R^2, is calculated according to Eq.(2.11), where y_i is the i^{th} value of the variable to be predicted, x_i is the i^{th} value of the explanatory variable, $f(x_i)$ is the predicted value of y_i and $\overline{y}$ is the mean.

$$R^2 = 1 - \frac{\sum_i \left(y_i - f(x_i)\right)^2}{\sum_i \left(y_i - \overline{y}\right)^2} \tag{2.11}$$

In most cases, R^2 is over 75% while, for the flexural strength, it is only 56%, due to the fact that the result of the specimens fabricated in the wooden mold does not follow the trend.

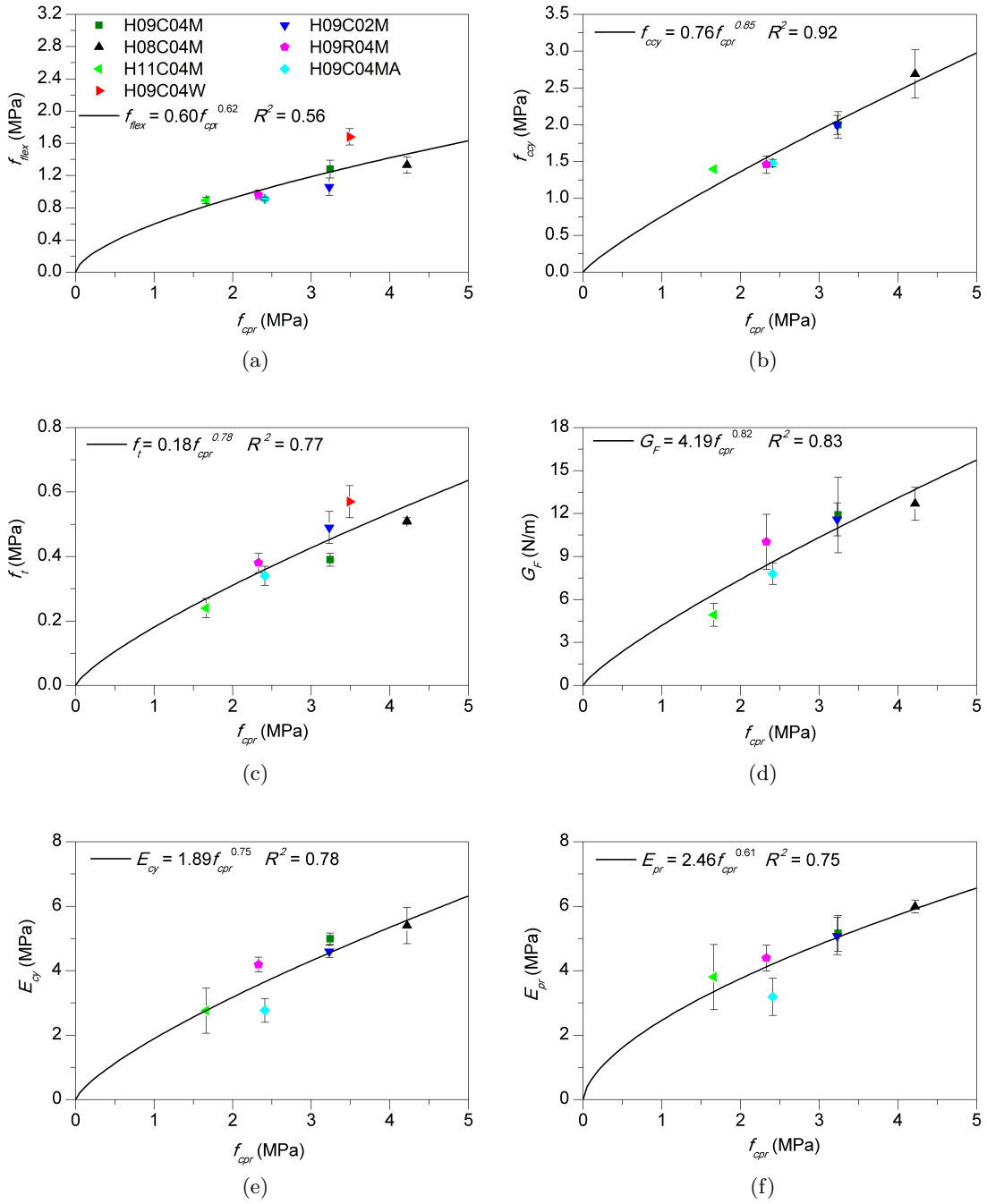

Figure 2.13: Relationship between the compressive strength from prisms and other mechanical properties: (a) compressive strength from cylinders, (b) flexural strength, (c) splitting tensile strength, (d) fracture energy, (e) elastic modulus from cylinders and (f) elastic modulus from prisms.

Figure 2.13 shows the relationship among the mechanical properties, such as the com-

pressive strength from cylinders, flexural strength, tensile strength, fracture energy and elastic modulus with respect to the compressive strength from prisms. It is worth noting that only the flexural strength and the splitting tensile strength are included for the mortar H09C04W, the specimen fabricated with wooden molds, as the rest were not measured.

2.4. Conclusions

This work studied the influence of five factors affecting the dosage and fabrication process of NHL mortars on their physical and mechanical properties, such as water/lime ratio, wooden or metallic molds, aggregate type and size and curing condition. In total, seven types of NHL mortars have been fabricated and tested to obtain their mechanical properties, i.e., compressive strength from prisms and cylinders, flexural strength, elastic modulus from cylinders and prisms, fracture energy and splitting tensile strength. Moreover, some physical properties were also measured, such as open porosity, pore size distribution and capillary water absorption.

The experimental results show that high water/lime ratios produce structural weakening, increase the open porosity and reduce mechanical properties. High relative humidity ($97 \pm 0.5\%$) is more suitable than ambient laboratory conditions for the hydration of the compounds of NHL mortars and for the increase of its ductility. Moreover, it has been shown that the mortars fabricated with wooden molds obtain higher mechanical properties due to the fact that the molds absorb the excess of free water. However, this results in a non-homogeneous material, since the beneficial effect can be restricted to the material close to the mold surface.

When the water/lime ratio is fixed instead of maintaining the consistencies approximately constant by varying the water/lime ratios, the influence of type and size of aggregate on mechanical properties would be isolated and quantified. The mortar with an aggregate size of 2 mm has a lower consistency in a fresh state and smaller pore-sizes in a hardened state compared with the one with an aggregate size of 4 mm, due to the fact that small aggregates are more water demanding. Mortars with river sand have lower mechanical properties, higher pore radius and open porosity in comparison with the ones with crushed limestone aggregates. Undoubtedly, if the water/lime ratios varied as well, the tendency could be different.

Furthermore, some empirical equations which describe the relationship between the mechanical properties of the mortars and the compressive strength of the prisms are proposed. They are helpful for the characterization of lime mortars with a lime/aggregate ratio of 1:3, as one of the main components of masonry, when simulating the mechanical behavior of historical constructions and monuments.

Chapter 3

The effects of production process and dosage on the physical and mechanical properties of aerial lime mortars

Article title: The influence of dosage and production process on the physical and mechanical properties of aerial lime mortars
Authors: Lucía Garijo, Xiaoxin Zhang, Gonzalo Ruiz, José J. Ortega
Journal: Construction and Building Materials
Submitted: 11/07/2019

This chapter studies the influence of five different factors affecting the dosage and fabrication process of seven types of aerial lime mortars on their physical and mechanical properties. Such factors comprise the water/lime ratio, the aggregate type and size, the material of the mold and the curing conditions. Moreover, some mechanical properties, not usually measured on aerial lime mortars, are obtained, such as splitting tensile strength, fracture energy and elastic modulus measured through prisms. Furthermore, empirical equations showing the relationship of the mechanical properties are proposed, which could be useful for numerical simulations of historical constructions with aerial lime mortars.

Keywords: Aerial lime mortar, Dosage, Mechanical Characterization, Fracture Energy, Empirical equations.

3.1. Introduction

The study of the influence of the dosage factors on the properties of aerial lime mortars is still scarce, especially, considering elastic modulus, splitting tensile strength and fracture energy. Thus, the aim of this chapter is to quantify the effect of five various factors affecting the dosage process of aerial lime mortars on their physical and mechanical properties. As studied for natural hydraulic lime mortars in Chapter 2, such factors are the water/lime ratio, aggregate type and size, curing conditions and material of the molds. Moreover, empirical equations relating these mechanical properties are proposed for these mortars similar to the ones presented by FIB Model Code [73] and ACI Building Code [83] for concrete. The results could be helpful for the numerical simulations of masonry structures with aerial lime mortars.

The rest of the chapter is organized as follows. The next section describes the experimental procedure. Section 3.3 proposes a thorough analysis of the results and discussion in addition to formulas which establish relationships between the mechanical properties of aerial lime mortars. Finally, some conclusions are presented in Section 3.4.

3.2. Experimental procedure

3.2.1. Raw materials

The lime used for the seven types of mortars was a commercial aerial one of class CL 90-S, according to EN 459-1 [12] and was supplied by "Calcasa, Calcinor" (Spain). It had an apparent density of 490 kg/m^3. Chemical and mineralogical analyses of the lime were performed as indicated in Chapter 2. The results are shown in Table 3.1 and Figure 3.1. The laser particle size distribution curve is presented in Figure 3.2.

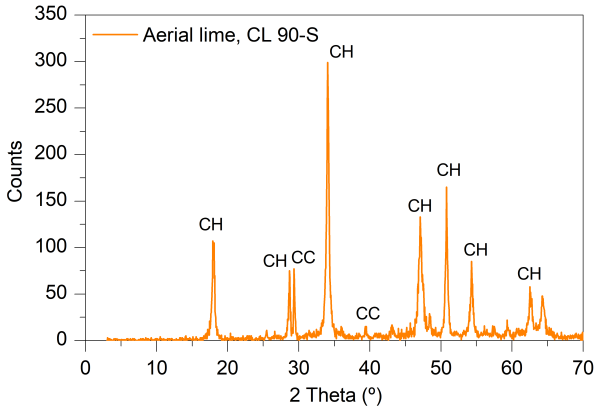

Figure 3.1: X-ray diffraction patterns of the aerial lime, CL 90-S. CH = portlandite, CC = calcite.

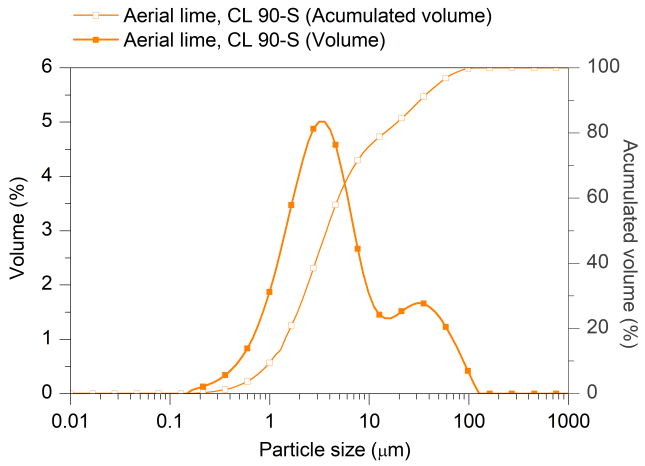

Figure 3.2: Laser particle size distribution curves of the aerial lime, CL 90-S

The aggregates used were commercial crushed limestones with a maximum grain size of 4 mm and 2 mm, respectively, a river sand with a maximum grain size of 4 mm. The particle-size distribution curves of the aggregates are shown in Chapter 2, see Figure 2.3, while the corresponding apparent particle density and apparent density, determined according to EN 1097-6 [85] and EN 1097-3 [86], respectively, are listed in Table 2.2 of Chapter 2.

Table 3.1: Chemical and mineralogical compositions of the aerial lime, CL 90-S.

Chemical composition (%)	
Na_2O	0.070
MgO	0.545
Al_2O_3	0.336
SiO_2	0.944
P_2O_5	0.020
SO_3	1.022
Cl	0.006
K_2O	0.039
CaO	70.609
TiO_2	0.029
V_2O_5	0.017
Fe_2O_3	0.164
NiO	0.017
CuO	0.009
Br	0.002
SrO	0.034
CO_2	26.137
Mineral phases (%)	
Portlandite, $Ca(OH)_2$	90-95
Calcite, $CaCO_3$	5-10

3.2.2. Aerial lime mortar preparation

Similar to the procedure followed for NHL mortars in Chapter 2, seven types of aerial lime mortars were prepared and tested, which are listed in Table 3.2, where "A" stands for the aerial lime mortar. Mortar A09C04M is the benchmark one. It had a lime/aggregate ratio of 1:3 by volume and a water/lime ratio of 0.9 that provided a consistency from 140 mm to 150 mm according to EN 1015-3 [88] and EN 1015-6 [89]. The aggregate used was a crushed limestone one with maximum grain size of 4 mm as indicated in Table 3.2. Also a metallic mold was adopted. The other mortars were obtained by modifying one aspect of this benchmark. All mortars were cured for seven initial days in the humid chamber and the rest 49 days in the ambient laboratory conditions (RH: 52 $\pm$ 12%, 22 $\pm$ 3°C) except for A09C04MC, which was cured 56 days in the humid chamber (RH: 97 $\pm$ 0.5%, 20 $\pm$ 0.5°C).

As done in Chapter 2, the water/lime ratio was kept constant to disclose the influence of the type and size of sand, material of the mold and curing conditions on the mechanical properties, instead of maintaining the same consistency by varying the water/lime ratio at the same time as presented in the references [9, 42, 43]. In this way, the effect of each factor could be isolated and quantified.

The mixing process was performed according to EN 1015-2 [90]. For the purpose, a vertical axis mortar mixer with sufficient capacity was used so as to cast one batch per mortar type within this chapter. For each type of aerial lime mortar, 18 prisms measuring 40 mm $\times$ 40 mm $\times$ 160 mm were fabricated; in total 126 prismatic specimens. All the specimens were removed from the molds in five days after the fabrication as established by EN 1015-11 [31] for such mortars. We decided not to fabricate cylindrical specimens as the possible different carbonation processes of both specimens could presumably have a significant effect in aerial lime mortars in comparison to the natural hydraulic ones of Chapter 2.

3.2.3. Tests of the aerial lime mortars in a fresh state

Different tests were performed on the aerial lime mortars in a fresh state: the apparent density according to EN 1015-6 [89] (Figure 2.6 a), the water-retention capacity following EN 459-2 [91] (Figure 2.6 b), which was determined as the percentage of water that remained in the mortar after

Table 3.2: Characteristics of the seven mortar compositions.

Mortar composition	Water/lime ratio (by volume)	Type of aggregate	Maximum grain size (mm)	Material of the mold	Curing conditions
A09C04M	0.9	Crushed limestone	4	Metallic	7 days in HC and 49 in AC
A08C04M	0.8	Crushed limestone	4	Metallic	7 days in HC and 49 in AC
A11C04M	1.1	Crushed limestone	4	Metallic	7 days in HC and 49 in AC
A09C04W	0.9	Crushed limestone	4	Wooden	7 days in HC and 49 in AC
A09C02M	0.9	Crushed limestone	2	Metallic	7 days in HC and 49 in AC
A09R04M	0.9	River sand	4	Metallic	7 days in HC and 49 in AC
A09C04MC	0.9	Crushed limestone	4	Metallic	56 in CC

Note. HC: Humid chamber (RH: 97 ± 0.5%, 20 ± 0.5°C), AC: Ambient laboratory conditions (RH: 52 ± 12%, 22 ± 3°C).

a suction time of 5 minutes on ten layers of filter paper, and the consistency in accordance with EN 1015-3 [88] and EN 1015-6 [89] through the flow table test (Figure 2.6 c).

3.2.4. Mechanical tests on the aerial lime mortars

Various types of mechanical tests were performed at an age of 56 days to obtain the flexural, compressive and splitting tensile strengths, fracture energy and elastic modulus measured through prisms. All these mechanical tests were performed according to the procedures indicated in Chapter 2 for natural hydraulic lime mortars, see Section 2.2.4.

Characteristic length

As explained in Chapter 2, the characteristic length, l_{ch}, is a parameter proposed by Hillerborg *et al.* [107] for fracture behavior. It is calculated according to:

$$l_{ch} = \frac{EG_F}{f_t^2} \tag{3.1}$$

where E in this study refers to the elastic modulus measured through prisms, E_{pr}, as we did not fabricate cylinders.

3.2.5. Porosity and capillary water absorption measurements

The open porosity was measured by hydrostatic method according to UNE 83980 [109] and by Mercury Intrusion Porosimetry (MIP) method with a Micromeritics 9500 Poresizer mercury porosimeter, as done for natural hydraulic lime mortars in Chapter 2, see Section 2.2.5.

Finally, the capillary water-absorption coefficient was also measured as indicated in Chapter 2 by following standard EN 1015-18 [112] (see Figure 2.10).

3.3. Results and discussion

In this section, the results of the experimental campaign described in the previous one are presented. Table 3.3 shows a comparison between some of the experimental results obtained from

other researchers and the ones of this work. Table 3.4 presents the properties measured in a fresh state, while Table 3.5 exhibits the mechanical and physical properties of the seven aerial lime mortars in a hardened state. In this Table, Std. Dev. is the standard deviation, and CV is the coefficient of variation.

From Table 3.3, it is observed that the experimental results of mortars are similar where the components are comparable. For example, the mortar tested by Margalha [7, 120] and the benchmark A09C04M in the current work present flexural strengths of 0.52 MPa and 0.54 MPa, and compressive strengths of 1.33 MPa and 1.30 MPa, respectively. Moreover, one of the mortars fabricated by Lanas and Alvarez [9], with a limestone of 2 mm of maximum grain size, shows similar mechanical properties as the mortar A09C02M of the current work with similar type of aggregate. Furthermore, the mortar with river sand tested by Ramalho [7, 121] also has comparable properties as A09R04M of this work. In addition, the comparison confirms that the mortars fabricated in the current work are also suitable for repairing historic masonry.

In Tables 3.4 and 3.5, it is observed that the apparent density of the mortars, measured in the fresh state at the fabrication moment and at 56 days in hardened state, respectively, decreases due to the water evaporation of the material during samples air drying process [55, 58]. As for the results of open porosity shown in Table 3.5, it is clear that the values from the hydrostatic method are always greater than the ones obtained by the MIP method. This is mainly due to the different ranges of pore-size detected by both methods [14, 41], as it was also observed for natural hydraulic lime mortars in Chapter 2.

3.3.1. Effect of the water/lime ratio

The influence of the water/lime ratio was studied through three mortars: A08C04M, A09C04M and A11C04M, corresponding to the water/lime ratios of 0.8, 0.9 and 1.1, respectively. As shown in Table 3.4, their consistencies were dry, plastic and fluid. As also observed for NHL mortars in Chapter 2, the apparent density in a fresh state and the water-retention capacity increase as the water/lime ratio decreases. For example, they are 2290 kg/m^3 and 90.9%, respectively, for A08C04M while 2160 kg/m^3 and 75.3% for A11C04M instead. In hardened state, see Table 3.5, the results show that with an increase in the water/lime ratios, the mechanical properties decrease. The same tendency was also observed by Raposo Pacheco Algarvio [51]; however, to verify that aerial lime mortars do not follow exactly Abrams' rule, as found by Lawrence and Walker [49], more different mortars with varying water/lime ratios should be tested. From Table 3.5, it is also observed that the porosity and mean pore radius increase for mortars with higher water/lime ratios. For example, the porosity measured by MIP is 19.7% and 24.3%, respectively, for mortars A08C04M and A11C04M, while their mean pore radius are, respectively, 0.28 µm and 0.66 µm.

Figure 3.3 shows the pore-size distribution of the seven aerial lime mortars. Most of them present two peaks similar to findings in the reference [43]: the first one between 0.5 and 2 µm and the second one between 7 and 11 µm. This is quite different to that of natural hydraulic lime mortars, as observed in Chapter 2 and the reference [41], where all the mortars, except the one with river sand, presented only a single narrow peak. However, as it also happened for natural hydraulic lime mortars, there is a shift of the pore-size distribution towards a finer diameter for mortar A08C04M, while in mortar A11C04M it is towards larger diameter.

Figure 3.4 shows the pore size distribution as means of bars charts (representing percentage of pore area) of the seven aerial lime mortars of the current work. The classification of the pore size range is the same one followed for the NHL mortars in Chapter 2 and the given in [43]. Such a classification comprises gel pores (between 0.005 µm and 0.01 µm), medium capillaries or large mesopores (between 0.01 µm and 0.05 µm), large capillary pores or macropores (between 0.05 µm and 10 µm), and finally, air voids (bigger than 10 µm). The pore size distribution of the aerial lime mortars seem to be more uniform than that of NHL mortars. The predominant pore size range is the one corresponding to large capillary pores or macropores (0.05 µm and 10 µm) [43, 115–117], which influences the strength and transport processes as mentioned in Chapter 2 [115–117]. It is followed by the medium capillaries or large mesopores (range between 0.01 µm and 0.05 µm), which affect strength and permeability trough the mortar structure [43]. Moreover, it is observed that A09R04M present a quite small amount (around 0.91%) of air voids (larger than 10 µm), similar to what happened for H09R04M of Chapter 2, while they are almost negligible for the rest

Table 3.3: Comparison of experimental results.

	Margalha, 2010, [7, 120]	Current work A09C04M (benchmark)	Lanas and Alvarez, 2003, [9]	Current work A09C02M (maximum grain size of 2 mm)	Ramalho, 2013, [7, 121]	Current work A09R04M (with river sand)
Type of aerial lime	CL 90-S	CL 90-S	CL 90-S	CL 90-S	CL 90	CL 90-S
Aggregate type	-	Crushed limestone	Crushed limestone	Crushed limestone	River sand	River sand
Maximum grain size (mm)	-	4	2	2	-	4
Lime/aggregate ratio (by volume)	1:3	1:3	1:3	1:3	1:3	1:3
Consistency (mm)	-	140-150	140-200	120-125	-	150-155
Curing conditions	-	7 days at (RH 97±0.5%, 20±0.5°C) and (RH 52±12%, 22±3°C) until testing	(RH 60±10%, 20±5°C)	7 days at (RH 97±0.5%, 20±0.5°C) and (RH 52±12%, 22±3°C) until testing	-	7 days at (RH 97±0.5%, 20±0.5°C) and (RH 52±12%, 22±3°C) until testing
Age of testing	90 days	56 days	91 days	56 days	90 days	56 days
Flexural strength, f_{flex} (MPa)	0.52	0.54	0.40	0.44	0.33	0.23
Compressive strength, f_{cpr} (MPa)	1.33	1.30	1.10	1.23	0.63	0.64
Static elastic modulus, E (GPa)	-	2.71	-	2.32	-	1.78
Capillary water absorption coefficient (kg/($m^2 min^{0.5}$))	0.77	1.27	-	1.58	1.49	1.38
Open porosity (hydrostatic) (%)	-	25.7	24.50	27.5	-	29.40
Open porosity (MIP) (%)	-	20.2	-	22.7	-	21.37

Table 3.4: Properties of aerial lime mortars in a fresh state.

	A09C04M (benchmark)	A08C04M (water/lime: 0.8)	A11C04M (water/lime: 1.1)	A09C02M (maximum grain size: 2 mm)	A09R04M (river sand)
Flow diameter (consistency) (mm)	140-150	120-125	210-215	120-125	150-155
Category (consistency)	Plastic	Dry	Fluid	Dry	Plastic
Apparent density (kg/m^3)	2230	2290	2160	2230	2060
Water retention (%)	84.2	90.9	75.3	84.3	83.1

Table 3.5: Properties of aerial lime mortars in a hardened state at an age of 56 days.

		A09C04M (benchmark)	A08C04M (water/ lime: 0.8)	A11C04M (water/ lime: 1.1)	A09C04W (wooden mold)	A09C02M (maximum grain size: 2 mm)	A09R04M (river sand)	A09C04MC (humid chamber)
Apparent density from prisms, ρ_{pr} (kg/cm^3)	Mean	**2000**	**2000**	**1944**	**1983**	**1960**	**1786**	**1984**
	Std. Dev.	7	4	11	30	6	4	8
	CV (%)	0.4	0.2	0.6	1.5	0.3	0.2	0.4
Flexural strength, f_{flex} (MPa)	Mean	**0.54**	**0.55**	**0.34**	**0.58**	**0.44**	**0.31**	**0.23**
	Std. Dev.	0.01	0.09	0.02	0.04	0.03	0.02	0.05
	CV (%)	2	17	7	6	6	5	23
Compressive strength from prisms, f_{cpr} (MPa)	Mean	**1.30**	**1.49**	**0.64**	**1.43**	**1.23**	**0.63**	**0.64**
	Std. Dev.	0.03	0.07	0.01	0.08	0.08	0.02	0.02
	CV (%)	2	4	2	6	6	3	4
Fracture energy, G_F (N/m)	Mean	**3.2**	**4.5**	**2.8**	-	**2.7**	**1.8**	**2.1**
	Std. Dev.	1.2	0.3	0.8		0.3	0.3	0.6
	CV (%)	36	6	27		10	15	30
Splitting tensile strength, f_t (MPa)	Mean	**0.18**	**0.20**	**0.10**	**0.19**	**0.18**	**0.11**	**0.08**
	Std. Dev.	0.01	0.02	0.01	0.01	0.02	0.01	0.01
	CV (%)	6	9	10	7	13	10	4
Elastic modulus, E_{pr} (GPa)	Mean	**2.7**	**2.6**	**2.2**	-	**2.3**	**1.8**	**1.5**
	Std. Dev.	0.3	0.2	0.2		0.5	0.3	-
	CV (%)	12	7	8		20	15	-
Characteristic length, l_{ch} (mm)		**261**	**281**	**611**	-	**190**	**239**	**485**
Capillary water absorption coefficient (kg/(m^{2}min$^{0.5}$))	Mean	**1.27**	**1.15**	**1.38**	**1.55**	**1.58**	**1.38**	**1.37**
	Std. Dev.	0.03	0.07	0.07	0.05	0.04	0.04	0.08
	CV (%)	2	6	4	4	3	3	6
Open porosity (hydrostatic) (%)	-	**25.7**	**25.0**	**27.7**	**25.3**	**27.5**	**29.4**	**26.9**
Open porosity (MIP) (%)	-	**20.2**	**19.6**	**21.0**	**20.6**	**22.7**	**21.7**	**21.4**
Mean pore radius (MIP) (µm)	-	**0.39**	**0.33**	**0.58**	**0.40**	**0.40**	**0.56**	**0.37**

of the aerial lime mortars. It is also remarkable that gel pores (below 0.01 µm) are not common among aerial lime mortars as they are in hydraulic lime ones, as they influence the hydration rate [43, 110].

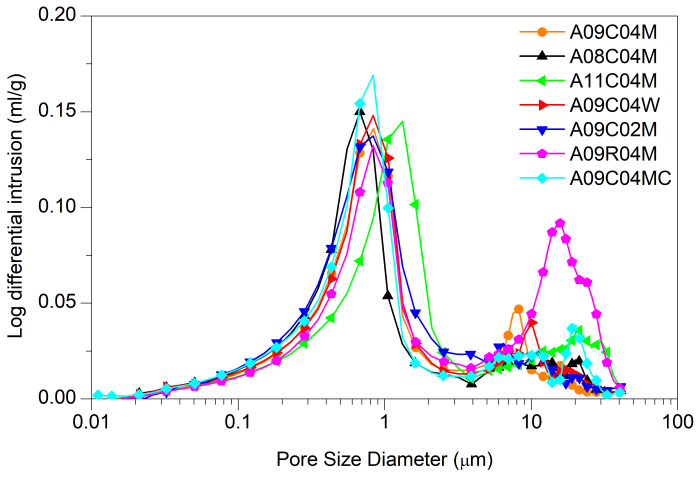

Figure 3.3: Pore-size distribution of the seven aerial lime mortars measured by MIP.

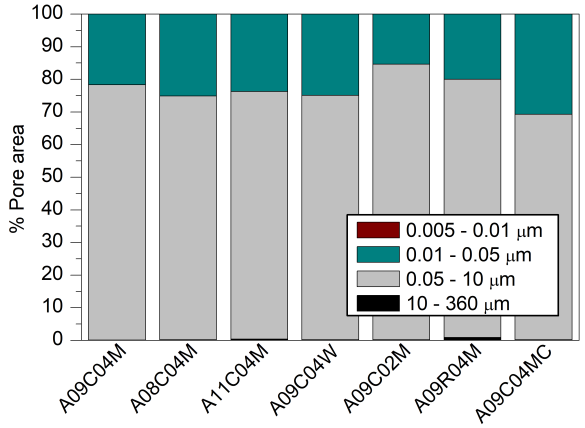

Figure 3.4: Pore-size distribution of seven aerial lime mortars measured by MIP (percentage of pore area).

3.3.2. Effect of the material of the molds

In order to determine the effect of the material of the mold on the properties of the aerial lime mortars, a comparison was made between A09C04M and A09C04W, fabricated with metallic and wooden molds, respectively. The fracture energy and the elastic modulus could not be measured as the prismatic notch specimens were damaged due to the demolding system of the wooden molds [41]. Observing the rest of the mechanical properties, the results show that they are higher for A09C04W than for the benchmark mortar. For example, the flexural strength is 0.58 MPa for the former and 0.54 MPa for the latter, while the compressive strengths are 1.43 MPa and 1.30 MPa instead, respectively. This difference could be due to the fact that the wooden molds absorb the excess of free water from the mortar. In general, the water content of the mortar decreases in comparison to the mortars with metallic molds and therefore, as mentioned before, with lower water content the mechanical properties increase. Regarding the mean pore radius, it is observed that it is slightly higher for A09C04W in comparison to A09C04M (0.40 µm against 0.39 µm). This is due to the fact that the mortar with wooden molds presents its second narrow peak at around 10 µm instead of at around 8 µm of the benchmark mortar (see Figure 3.3). Considering that the sample for MIP is taken from the inner of the specimen, this difference could probably be

associated with the fact that the water absorption of the wooden molds is local and non-uniform resulting in a drier material in the borders than in its core as it was also observed for the natural hydraulic lime mortars of Chapter 2.

It is also remarkable that the molds were used only once as the degree of absorption would change with each use. Therefore, the influence of the material of the molds, as commented for the NHL mortars in Chapter 2, needs further research as for the effect of reusing the molds, the type of wooden mold used or the improvement of the demolding system [41].

3.3.3. Effect of the maximum aggregate size

Two types of aerial lime mortars, A09C04M and A09C02M, were prepared with the same composition but different maximum aggregate sizes (4 mm and 2 mm, respectively). As indicated by their names, both have the same water/lime ratio: 0.9 by volume. As mortar A09C02M was fabricated with finer aggregates, it presented a higher water demand in a fresh state [47] and therefore lower consistency for the same water/lime ratio (120 – 125 mm versus 140 – 150 mm of the benchmark mortar, see Table 3.4). In a hardened state, the use of finer aggregates induces higher capillary water absorption coefficient (1.58 kg/($m^2 min^{0.5}$) against 1.27 kg/($m^2 min^{0.5}$), see Table 3.5. As for the mechanical properties, it is observed that they are slightly higher for A09C04M in comparison to A09C02M, although this difference is within the margin of error for most of the mechanical properties. For example, their compressive strength are, respectively, 1.30 ± 0.03 MPa and 1.23 ± 0.08 MPa (Table 3.5). Stefanidou and Papayianni [47] observed that mortars with a lime/aggregate ratio of 1:3 fabricated with aggregates of sizes of 0/4 mm provided higher mechanical properties than the ones with aggregates of 0/2 mm in the long term (around 730 curing days; at earlier ages they were very similar). In their case, they did not keep a constant water/lime ratio but maintained similar consistencies by adding more water to the mortar with finer aggregates. Obviously, if more water were added to mortar with finer aggregates to reach a similar consistency with the benchmark mortar, the mechanical properties would be different.

3.3.4. Effect of the aggregate type

The effect of two different types of aggregate was analyzed by comparing aerial lime mortars A09C04M and A09R04M, which were fabricated with crushed limestone and river sand, respectively. In a fresh state, see Table 3.4, A09R04M presents larger consistency (150-155 mm) than that of A09C04M (140-150 mm) for the same water/lime ratio. Moreover, A09RC04M, in comparison to the benchmark mortar, has lower apparent density (2060 kg/m^3 versus 2230 kg/m^3) and water-retention in a fresh state (83.1% versus 84.2%).

In a hardened state (see Table 3.5), A09R04M shows lower mechanical properties than A09C04M. For example, their compressive strengths are, respectively, 0.63 MPa and 1.30 MPa. In addition, their open porosity and mean pore radius are higher for the former (29.4% in comparison to 27.7% and 0.66 µm with respect to 0.36 µm). From Figure 3.3, it is also observed that A09R04M presents a broad peak at the pore size of around 11 µm, and it is the mortar presenting the higher content of air pores (around 0.9%) (Figure 3.4). All these observations are in agreement with the findings of the references mentioned in the Introduction. That is to say, in general, aerial lime mortars fabricated with crushed limestone aggregates present higher strength than mortars with round river sand [9, 43], due to the fact that the limestone aggregates present a structure similar to the calcitic binder that reduces the discontinuities between the lime matrix and the aggregates [9, 43] and also the calcitic particles grow over the limestone grains increasing the crystallographic continuity between them [43–45]. In addition to this, angular aggregates improve the cohesion degree between the aggregate surface and the binder reducing the porosity and increasing the strength of the mortars [43]. It is obvious that if the water content of the mortar with river sand is decreased to reach similar consistencies, the tendency would be different.

3.3.5. Effect of the curing conditions

In this current work, based on the references mentioned in the Introduction and standard EN 1015-11 [31], it was decided to cure the benchmark aerial lime mortar for 7 initial days in the

humid chamber and later for 49 curing days in the ambient laboratory conditions (RH 52 ± 12% and 22 ± 3°C) until the moment of testing. This is different to the procedure followed for NHL mortars of Chapter 2, where most of them were cured for 56 days in the humid chamber. Then, the benchmark aerial lime mortar was compared with A09C04MC, cured in the humid chamber (RH: 97 ± 0.5% and 20 ± 0.5°C) for the entire time. From the comparison of their results in Table 3.5, it is observed that the mechanical properties of the aerial lime mortar cured in the humid chamber, under high humid conditions, are lower than the ones of the mortar cured under ambient laboratory conditions (the flexural and compressive strength decrease around 57% and 51%, respectively). This is due to the fact that there is an optimum humid condition that favors carbonation of aerial lime mortar [55]. It is known that in a first phase, aerial lime mortars harden by drying the excess of water of the material. This allows, once the material is not saturated in water, the diffusion of CO_2 inside the mortar. At the same time, it is required a certain level of moisture so that the CO_2 can be dissolved with water inside the pores of the material [56, 57]. Considering all these facts, it is concluded that high humid conditions (like the ones inside the humid chamber) are not favorable owing to the fact that the aerial lime mortars require a first phase of drying. Meanwhile, too low humid conditions (below 40% [56]) are not favorable either as it could prevent the CO_2 from being dissolved with the water. Some other authors, such as Paulina Faria and Ana Martins [59, 60] have also observed that aerial lime mortars cured under 20°C and 50% and under 20°C and 65% provided corresponding compressive strengths at the age of 60 days 20% higher for the latter. Also Cyzer [61] found that hydration was enhanced under moist conditions for natural hydraulic lime mortars, while carbonation was improved under dryer conditions (in that case at 60% RH) for the aerial ones.

3.3.6. Characteristic length

As presented in Section 2.2.4, characteristic length is an indicator of brittleness of quasi-brittle materials. The shorter it is in a material, the more brittle the material is. In the current work, their values range between 190 mm and 611 mm, which is a bit wider than that of normal strength concrete (250 mm to 300 mm) and NHL mortars of Chapter 2 (190 mm to 390 mm). However, as observed for NHL mortars, the characteristic length decreases with mortars containing finer aggregates. For example, A09C02M and A09C04M, with maximum grain sizes of 2 mm and 4 mm, respectively, present corresponding values of 190 mm and 261 mm, see Table 3.5. Obviously, the former mortar is more brittle. Moreover, curing under high humid conditions or using river sand in the fabrication also make the aerial lime mortar become more brittle.

3.3.7. Empirical equations among mechanical properties

As explained in Chapter 2, for other building materials, such as concrete, there exist some recognized codes, such as FIB Model Code [73] and ACI Building Code [83], that present empirical equations among the mechanical properties of the material. These formulas are quite useful for structural design and numerical simulations when only the compressive strength is measured, although the relative error might be as high as 90% [119]. In this work similar equations relating some mechanical properties of the aerial lime mortars to their compressive strength from prisms are proposed, see Equation 3.2 and Table 3.6. It should be highlighted that the compressive strength is used as the basis of all empirical formulas as it is a normalized property in masonry mortars and easier to be obtained.

Figure 3.5 shows the relationship among the mechanical properties, such as the flexural (f_{flex}) and splitting tensile strengths (f_t), fracture energy (G_F) and elastic modulus measured through prisms (E_{pr}) with respect to the compressive strength of prisms. As presented in Section 3.3.2, the results of fracture energy and elastic modulus measured through prisms do not include the corresponding value of the mortar fabricated with wooden molds due to the fact that the specimens were damaged during the demolding process. It is also worth noting that in most cases, the correlation coefficient R^2, is around 75% or even higher, except for the case of the fracture energy (Figure 3.5c) (with R^2 equal to 52%), where the standard deviation (error bars) of each mortar is also larger.

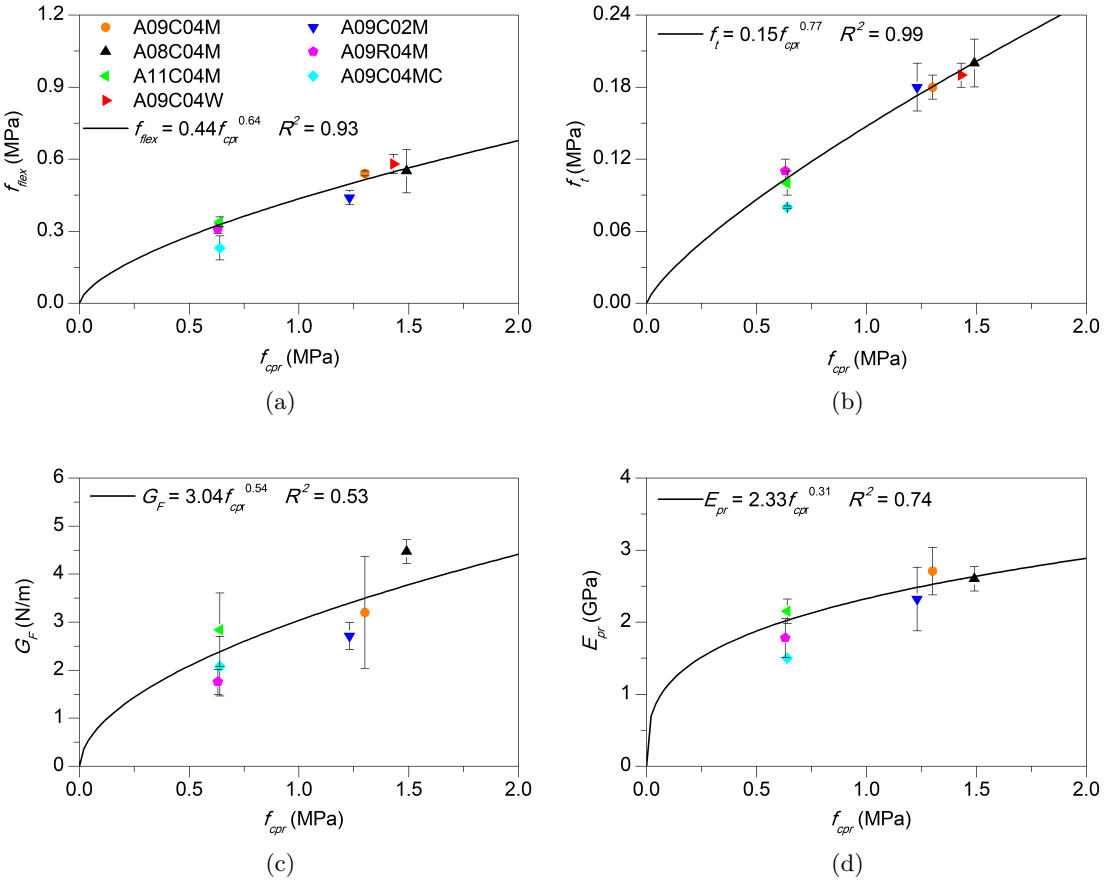

Figure 3.5: Relationship between the compressive strength from prisms and other mechanical properties: (a) flexural strength, (b) splitting tensile strength, (c) fracture energy and (d) elastic modulus.

Table 3.6: Values of parameters in Equation (3.2).

Y	h	j
f_{flex}	0.44	0.64
f_t	0.15	0.77
G_F	3.04	0.54
E_{pr}	2.33	0.31

$$Y = h f_{cpr}^{j} \tag{3.2}$$

3.3.8. Comparison between aerial and natural hydraulic lime mortars

Figure 3.6 and Table 3.7 show a comparison of the physical and mechanical properties between aerial and natural hydraulic lime mortars of Chapter 2. As a general observation, it is obvious that the mechanical properties of aerial lime mortars are much lower than that of natural hydraulic lime mortars. As it will be explained in Chapter 5, this is mainly due to the different mineralogical compositions and hardening processes of both materials. Aerial lime mortars are mainly composed

by portlandite and harden by carbonation. However, besides portlandite and carbonation, natural hydraulic lime ones are also composed by calcium silicates and harden by hydration. Furthermore, the open porosity measured by hydrostatic methods and by MIP is, in general, higher for the aerial lime mortars, although their mean pore radii (measured by MIP) are not always like that.

Moreover, the influence of each factor for both materials is different in most cases as well. For example, the effect of the water/lime ratio on aerial lime mortars is less than that of natural hydraulic ones, see Table 3.7 and Figure 3.6 a-e. It is obvious that the compressive strength from prisms diminishes approximately 60% in the natural hydraulic lime mortars with water/lime ratios of 0.8 and 1.1, while for the aerial lime mortars it decreases approximately 38%. Observing the fracture energy, it diminishes around 62% and 38% for the natural hydraulic and the aerial lime mortars, respectively. A similar tendency was also observed by Lawrence and Walker [49] when comparing the compressive strength of both natural hydraulic and aerial lime mortars.

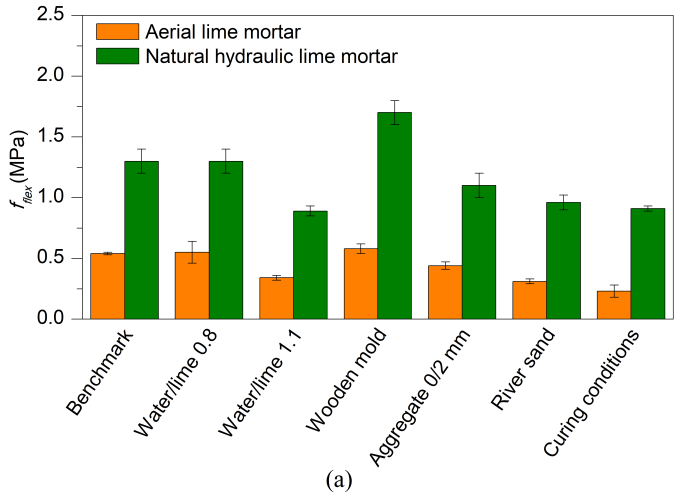

(a)

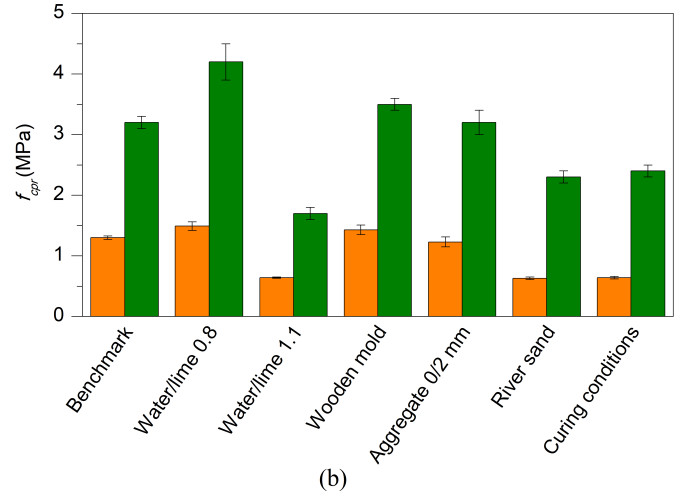

(b)

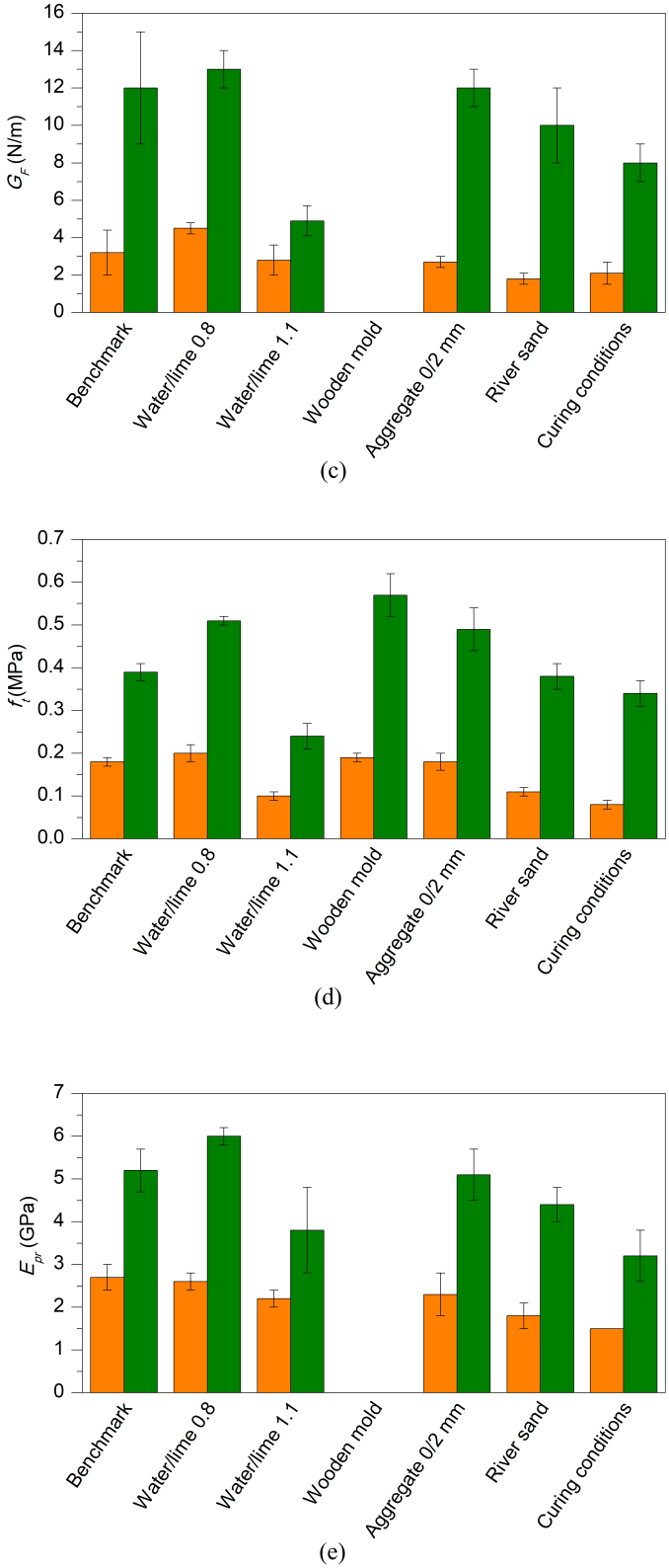

Figure 3.6: Comparison of mechanical properties between aerial and natural hydraulic lime mortars: (a) flexural strength, (b) compressive strength from prisms, (c) fracture energy, (d) splitting tensile strength, and (e) elastic modulus.

Table 3.7: Properties of aerial and natural hydraulic lime mortars in a hardened state at an age of 56 days.

	Type of lime mortar	Benchmark	Water/ lime: 0.8	Water/ lime: 1.1	Wooden mold	Aggregate 0/2 mm	River sand	Curing conditions
Apparent density from prisms, ρ_{pr} (kg/cm^3)	**Aerial**	**2000**	**2000**	**1944**	**1983**	**1960**	**1786**	**1984**
	Natural hydraulic	2050	2091	1964	2070	2016	1856	2003
Flexural strength, f_{flex} (MPa)	**Aerial**	**0.54**	**0.55**	**0.34**	**0.58**	**0.44**	**0.31**	**0.23**
	Natural hydraulic	1.3	1.3	0.89	1.7	1.1	0.96	0.91
Compressive strength from prisms, f_{cpr} (MPa)	**Aerial**	**1.30**	**1.49**	**0.64**	**1.43**	**1.23**	**0.63**	**0.64**
	Natural hydraulic	3.2	4.2	1.7	3.5	3.2	2.3	2.4
Fracture energy, G_F (N/m)	**Aerial**	**3.2**	**4.5**	**2.8**	-	**2.7**	**1.8**	**2.1**
	Natural hydraulic	12	13	4.9	-	12	10	8
Splitting tensile strength, f_t (MPa)	**Aerial**	**0.18**	**0.20**	**0.10**	**0.19**	**0.18**	**0.11**	**0.08**
	Natural hydraulic	0.39	0.51	0.24	0.57	0.49	0.38	0.34
Elastic modulus from prisms, E_{pr} (GPa)	**Aerial**	**2.7**	**2.6**	**2.2**	-	**2.3**	**1.8**	**1.5**
	Natural hydraulic	5.2	6.0	3.8	-	5.1	4.4	3.2
Characteristic length, l_{ch} (mm)	**Aerial**	**261**	**281**	**611**	-	**190**	**239**	**485**
	Natural hydraulic	390	260	240	-	220	280	190
Capillary water absorption coefficient (kg/(m^{2}min$^{0.5}$))	**Aerial**	**1.27**	**1.15**	**1.38**	**1.55**	**1.58**	**1.38**	**1.37**
	Natural hydraulic	1.36	0.95	1.70	1.83	1.84	1.69	1.57
Open porosity (hydrostatic) (%)	**Aerial**	**25.7**	**25.0**	**27.7**	**25.3**	**27.5**	**29.4**	**26.9**
	Natural hydraulic	27.7	25.0	29.9	24.1	27.8	29.4	29.0
Open porosity (MIP) (%)	**Aerial**	**20.2**	**19.6**	**21.0**	**20.6**	**22.7**	**21.7**	**21.4**
	Natural hydraulic	23.4	19.7	24.3	22.5	24.8	24.0	23.8
Mean pore radius (MIP) (µm)	**Aerial**	**0.39**	**0.33**	**0.58**	**0.40**	**0.40**	**0.56**	**0.37**
	Natural hydraulic	0.36	0.28	0.66	0.39	0.31	0.66	0.52

Concerning the influence of using wooden molds instead of metallic ones, a similar effect is observed in both natural hydraulic and aerial lime mortars. The mechanical properties of the mortars fabricated with wooden molds are higher than that of mortars with metallic ones. For instance, the compressive strength increases 10% and 9%, respectively in both aerial and natural hydraulic lime mortars. Moreover, the open porosity remains similar or decreases slightly in mortars with wooden molds, while the mean pore radius increases in both materials (from 0.39 to 0.40 µm in the aerial lime mortars and from 0.36 to 0.39 µm in the natural hydraulic ones). As explained in Chapter 2, this could be due to the fact that the material is not homogenous when the wooden molds are used and it presents higher water content inside the specimen than that fabricated with the metallic molds.

Regarding the effect of using different aggregate sizes, the reference [46] explain that the best aggregates are those with a well-graded particle size. Furthermore, adding aggregates with higher grain size improves the compressive strength on natural hydraulic lime mortars, which is also related to the packing density of the aggregates, according to Kalagri *et al.* [6]. For aerial lime mortars, Stefanidou and Papayianni [47] observed that mortars with a lime/aggregate ratio of 1:3 and aggregates of sizes of 0/4 mm provided higher mechanical properties in the long term than the ones with aggregates of 0/2 mm. They varied the water/lime ratio to achieve similar consistencies. In this research a similar phenomenon is observed for the aerial lime mortars when maintaining constant water/lime ratio; their compressive strength can decrease by 5% when using aggregates with maximum grain size of 2 mm. However, in this case this difference seems to be within the margin of error in most of the mechanical properties. For the natural hydraulic lime mortars of Chapter 2, the effect of using aggregates with smaller grain size seems to be coupled with the influence of different consistencies due to the fact that the water/lime ratio id fixed as 0.9. Thus, the obtained mechanical properties are almost constant. Concerning the characteristic length, a clear tendency is observed for both aerial and natural hydraulic lime mortars: the ones with smaller aggregates size are more brittle than those with aggregates containing higher grain size.

As for the shape and nature of the aggregates, it is shown in this research that using river sand provides lower mechanical properties than those with limestone aggregates. For example, the compressive strength and the fracture energy decrease approximately 52% and 44%, respectively

for aerial lime mortars, while they diminish approximately 28% and 17% for natural hydraulic lime mortars [41]. For both materials such influence is due to the better cohesion among the particles of crushed angular limestone aggregates. Moreover, in the case of the aerial lime mortars the effect is more pronounced due to the similar calcitic nature of the lime and the aggregates, which improves the crystallographic continuity and enhance even more the mechanical properties [9, 43–45]. Obviously, if less water was added to the mortars with river sand to achieve similar consistency, the mechanical properties would be improved.

Finally, the curing condition affect in a very different way to both aerial and natural hydraulic lime mortars. For the aerial ones, the compressive strength and the fracture energy decrease approximately 51% and 34%, respectively, when comparing a mortar cured for seven initial days in the humid chamber and the rest under ambient laboratory conditions (RH 52 ± 12% and 22 ± 3°C) with a mortar cured the entire time inside the humid chamber (RH: 97 ± 0.5% and 20 ± 0.5°C). However, in the case of the natural hydraulic lime mortars, the compressive strength and the fracture energy decrease by 25% and 33% [41], respectively, when comparing a mortar cured inside the humid chamber with another cured for seven initial days in the humid chamber and the rest under ambient laboratory conditions. This also proves that the carbonation process of the aerial lime mortar is favored under relative humidity conditions ranging between 40% and 80% according to Saetta *et al.* [56]; meanwhile, for the natural hydraulic lime mortar, higher humid conditions favour the hydration of their mineral compounds [41, 53].

3.4. Conclusions

This work aims at the analysis of the effect of five factors, such as water/lime ratio, wooden or metallic molds, aggregate type and size and curing conditions on the physical and mechanical properties of seven aerial lime mortars. Different physical properties, such as: open porosity, pore size distribution, capillary water absorption; and mechanical ones: flexural, compressive and splitting tensile strengths, fracture energy and elastic modulus measured through prisms were measured at the age of 56 days.

The results show that under the three different water/lime ratios tested, the material experiences a structural weakening, an increase of the open porosity and a reduction of the mechanical properties with increasing water/lime ratios, although this effect is not so pronounced as for natural hydraulic lime mortars. Contrary to observances for NHL mortars, ambient curing conditions (RH: 52 ± 12%, 22 ± 3°C) were more favorable for aerial lime mortars than high humid ones (RH: 97 ± 0.5%, 20 ± 0.5°C), as the former favored carbonation process of this material. Moreover, it is observed that fabrication with wooden molds provided higher mechanical properties as they absorbed the free water, although this effect was probably local and resulted in a non-homogenous material.

As performed in Chapter 2, in order to study the type and size of the aggregates on the mechanical properties, the water/lime ratio was fixed instead of maintaining similar consistencies to isolate and quantify the effect of each factor. The results show that the aerial lime mortar with aggregate size of 2 mm had lower consistency in a fresh state as finer sands were more water demanding. The mechanical properties of this mortar were slightly lower than those of mortar with aggregate sizes of 0/4 mm. Furthermore, using limestone aggregates improved the continuity between the lime and the matrix. This fact resulted in higher mechanical properties of the mortars with limestone aggregates in comparison to those with river sand when maintaining the same water/lime ratios.

Finally, some empirical formulas are proposed relating some mechanical properties, such as the flexural and splitting tensile strengths, fracture energy and elastic modulus with the compressive strengths. They could be helpful for the numerical simulations of masonry structures with aerial lime mortars presenting a lime/aggregate ratio of 1:3 as ones of the most widespread in the restoration field.

Chapter 4

Time effect on the physical and mechanical properties of natural hydraulic lime mortars at early ages; stiffness evolution through EMM-ARM

Article title: Stiffness evolution of natural hydraulic lime mortars at early ages measured through EMM-ARM
Authors: Lucía Garijo, Miguel Azenha, Meera Ramesh, Paulo. B. Lourenço, Gonzalo Ruiz
Journal: Construction and Building Materials
Submitted: 23/09/2018
Accepted: 27/04/2019
DOI: 10.1016/j.conbuildmat.2019.04.258
Available at: https://doi.org/10.1016/j.conbuildmat.2019.04.258

This chapter focuses on the mechanical characterization of the early age behavior of three NHL mortars with different water/lime ratios. A vibration-based technique with continuous data recording (Elastic Modulus Measurement through Ambient Response Method - EMM-ARM) was used to measure stiffness of the different mortars that were found to range between 2.5 and 4.1 GPa on day 7. Other physical and mechanical properties such as strength and density were measured as a function of sample preparation protocols: vibrated, compacted, sealed and unsealed. After 7 days, sealed specimens led to 50% lower compressive strength and 25% lower flexural strength compared to unsealed specimens.

Keywords: Natural Hydraulic Lime (NHL) mortars, Elastic Modulus Measurement through Ambient Response Method (EMM-ARM), Stiffness evolution, Ultrasonic pulse velocity test (UPV), Sample preparation.

4.1. Introduction

The study of the stiffness evolution of NHL mortars at early ages, particularly including the first 48h of hardening is of crucial importance because the behavior of NHL mortars at early ages has a direct influence on the supporting capability and ability to accommodate movements of masonry during construction or repairing operations. This behavior is especially relevant for interventions in historic structures, where an appropriate large deformation before failure of the new additions helps to avoid brittle breakage when restrained by preexistent elements.

For these reasons, the objective of this research is to study the behavior of three NHL mortars at early ages (same binder, with three distinct water/lime ratios). An exhaustive mechanical and physical characterization of these mortars was performed, including the measurement of the elastic modulus through two methods: Elastic Modulus Measurement through Ambient Response Method (EMM-ARM) [81], and conventional compression test (CC) on cylinders. Furthermore, the following tests and property assessments have also been deployed: penetration resistance test

to study the initial setting time of the mortars; density and normalized flexural and compressive strength tests on prisms at days 2, 4 and 7; open porosity and, finally, thermogravimetric analysis on the corresponding lime paste to study the evolution of portlandite, $Ca(OH)_2$, content that results from the hydration of the NHL compounds, mainly C_2S [8].

One of the most striking novelties of this research lies on the pioneering application of the EMM-ARM technique to NHL mortars. This test allows automatic and continuous evaluation of the elastic modulus immediately after casting without demoulding the specimen. EMM-ARM is based on the continuous evaluation of the resonance frequency of the tested specimen (simply supported composite beam), which can in turn allow direct evaluation of the tested material through application of the dynamic equation of motion of the system [81, 122–125]. For further comprehension of the early age behavior of NHL mortars, some relations were established among the results of the several conducted tests. In such way, EMM-ARM was compared with the results of CC on one reference mortar and penetration resistance tests on the three NHL mortars. Due to the nature of the EMM-ARM testing adopted, as well as its principles of operation, the test specimen is relatively slender (50.5 cm long cylinder), and the specimen needs to be kept within the mould during testing, in order to keep the same mechanical boundary conditions and avoid mass losses. These experimental requirements of EMM-ARM led to the need for application of vibration in the preparation of EMM-ARM samples (due to the long and thin mold), and the specimens were constantly sealed. These vibrated/sealed conditions do not match the fabrication/curing conditions required in the standards for NHL [31], which include compaction with 25 strokes of the tamper and unsealed curing conditions. Also, keeping the specimens sealed hinders the process of carbonation, that plays a role in the hardening of NHL mortars as well. For that reason, EMM-ARM, as performed herein, was limited to the maximum age of 7 days, during which the effects of carbonation would presumably still have been minor as in the case of unsealed curing. Anyhow, it was important to ascertain the impact of fabrication (compaction/vibration) and curing (sealed/unsealed) conditions in the studied NHL mortars so as to allow further conclusions to be drawn from the obtained results. Density, flexural and compressive strength tests were carried out on samples with different preparation and curing methods: the standard one (compacted with 25 strokes of the tamper and unsealed), the one followed in the preparation of EMM-ARM specimens (vibrated and sealed) and an additional one (compacted and sealed). In such a way, it was possible to relate the results of such tests implying stiffness and strength measurements. Furthermore, some relations were also established among the results of density, ultrasonic pulse velocity (UPV) and open porosity of the three mortars to better understand the interplay of these properties on the behavior of NHL mortars at early ages. Finally, the evolution of free portlandite content of one reference NHL paste was related to the compressive strength of the corresponding mortar through the performance of thermogravimetric analysis.

The organization of the chapter is as follows: Section 4.2 describes the materials and experimental procedure, whereas Section 4.3 pertains to the discussion of attained results, with conclusions being drawn in the last Section (4.4).

4.2. Experimental program

4.2.1. Raw materials

The three mortars were prepared with the same commercial natural hydraulic lime as the one used in the mortars of Chapter 2, which was of class NHL 3.5, according to EN 459-1 [12]. It was supplied by "Socli, Italcementi Group" (France) and had a density of 2580 kg/m^3 and an apparent density of 850 kg/m^3. Chemical and mineralogical analyses and laser particle size distribution curve of the natural hydraulic lime, NHL 3.5, are provided in Chapter 2, see Table 2.1 and Figures 2.1 and 2.2, respectively.

The sand used was commercial crushed limestone of maximum grain size of 4 mm and has a particle size distribution curve as the one presented in Chapter 2, see Figure 2.3 determined according to EN 1015-1 [84]. It had an apparent particle density of 2680 kg/m^3 according to EN 1097-6 [85] (Figure 2.4b) and an apparent density of 1820 kg/m^3 according to EN 1097-3 [86] (Figure 2.4c).

4.2.2. Mortar composition and preparation

Three mortar compositions were prepared with different water/lime ratios: 0.8, 0.9 and 1.1 by volume, corresponding to the mortars already presented in Chapter 2 as H08C04M, H09C04M and H11C04M, respectively. In this chapter, they will be named as H08, H09 and H11, respectively, for simplicity. The lime/aggregate ratio used for the three mortars was 1:3 by volume. Volume proportions of compounds were converted into weight so as to minimize effects of measurement imprecision in the mixing process, see Table 4.1. Depending on the water/lime ratio used, three values of consistency were obtained: 130-135 mm (H08 - dry), 150-155 mm (H09 - plastic) and 238-240 mm (H11 - fluid), determined by flow table test according to the standards EN 1015-3 [88] and EN 1015-6 [89]. As considered in Chapter 2, mortar M09 (in each of the three different compaction/sealing conditions, S, V and C, as explained as follows) has been regarded as the reference for all tests conducted and properties evaluated in this research work. The mixing process was performed according to EN 1015-2 [90] by following the procedure for small bowl mixers (in this case with a capacity of 5 dm^3). Different batches of the same mix were cast and repeatability was then checked for each test.

Table 4.1: Mortar compositions for each NHL mortar.

Mortar	Lime/aggregate ratio by volume	NHL (g)	Aggregate (g)	Water (cm^3)	Water/lime ratio by volume	Water/lime ratio by weight
H08	1:3	525.2	3367.3	494.3	0.8	0.94
H09	1:3	514.5	3298.6	544.7	0.9	1.06
H11	1:3	494.3	3169.2	639.7	1.1	1.29

Different sizes of specimens, compacting methods and curing conditions were used depending on the test to be applied (Table 4.2). The reason for the distinct fabrication methods employed has been given in the Introduction of this chapter. In this way, standard mortars were compacted with 25 strokes of the tamper and cured unsealed inside a humid chamber at RH 95% and 20°C. This humidity is recommended by EN 1015-11 [31] and is reported to favor the hydration of NHL mortars [25, 41, 52]. These mortars were tested to measure UPV, flexural and compressive strengths and open porosity. In the table, the column "Type of Mortar" includes the nomenclature H08, H09 and H11, with an additional suffix that clarifies the fabrication/curing conditions: suffix "S" for the standard situation that has just been described; suffix "V" for vibrated (with a vibration table) and sealed (inside the PVC tubes of the EMM-ARM samples or covered with two plastic bags in the case of the rest of the samples); suffix "C" for compacted (with 25 strokes of the tamper) and sealed (by following the same aforementioned procedure). All the mortars remained in humid chambers with corresponding curing conditions as indicated in Table 4.2. The days at which the different specimens were removed from their corresponding molds are also referred to in Table 4.2. Furthermore, a lime paste specimen has been prepared for TGA testing, with a single water to lime ratio of 0.9: P09.

4.2.3. Test procedures

Elastic Modulus Measurement through Ambient Response Method (EMM-ARM)

The EMM-ARM is a methodology proposed by Azenha *et al.* [81] for cement-based materials. It has been widely validated for cement pastes [123, 126–128], cement mortars [123], concrete [81, 129] and recently for aerial lime-cement mortars [82]. In this chapter, it was applied for the first time to the study of NHL mortars. This method allows the automatic and continuous evaluation of the elastic modulus immediately after casting and it has two fundamental differences compared to conventional resonant frequency methods (e.g. impact-resonance methods): (i) the

Table 4.2: Sizes of specimens, compacting methods and curing conditions of the NHL mortars.

Tests	Specimen shape and dimensions (mm)	Type of mortar	Curing conditions	Compacting method and sealing conditions	Day of demolding
EMM-ARM	Cylinder ⌀44 mm × 505 mm	H08V, H09V, H11V	20°C - sealed	Vibrated and sealed	No demolding
CC	Cylinder ⌀75 mm × 150 mm	H09S	20°C – RH 95%	Standard	At day 2
CC	Cylinder ⌀75 mm × 150 mm	H09V	20°C – RH 95%	Vibrated and sealed	Before testing
UPV (discrete measurements) – flexural and compression	Prisms 40 mm × 40 mm × 160 mm	H08S, H09S, H11S	20°C – RH 95%	Standard	At day 2
UPV (discrete measurements) – flexural and compression	Prisms 40 mm × 40 mm × 160 mm	H08V, H09V, H11V	20°C – RH 95%	Vibrated and sealed	At day 2
Flexural and compression	Prisms 40 mm × 40 mm × 160 mm	H08C, H09C, H11C	20°C – RH 95%	Compacted and sealed	At day 2
Open porosity	Prisms 40 mm × 40 mm × 160 mm	H08S, H09S, H11S	20°C – RH 95%	Standard	At day 2
Open porosity	Prisms 40 mm × 40 mm × 160 mm	H08V, H09V, H11V	20°C – RH 95%	Vibrated and sealed	At day 2
TGA	N/A (Sample sample of less than 20 mg)	P09	20°C – RH 95%	Sealed	Before testing

Figure 4.1: EMM-ARM setup.

resonant frequencies are much lower, well below 1kHz (thus more similar to quasi-static testing); (ii) the specimen is not demolded during testing [128]. The methodology is based on continuous modal identification of the first flexural resonant frequency of a composite beam that is placed horizontally, simply supported at both ends in the case of concrete and some mortars (in contrast with the cantilever beam configuration used for pastes). A typical setup adopted during the present experimental program is shown in Figure 4.1. At mid-span of the beam, vertical accelerations resulting from forced vibration with a non-contact magnetic actuator are measured. With this, it is possible to perform modal identification and evaluate the first flexural resonance frequency of the beam. This resonant frequency of the beam is related to the increasing elastic modulus of the tested material by applying the dynamic equation of motion of the system (all variables known except for the elastic modulus, which can be directly computed). In this way it is possible to obtain a real-time curve of elastic modulus against time [130].

The specimens used in this study were prepared with a PVC tube with inner/outer diameter of 44 mm/50 mm, 550 mm length and with a span of 500 mm between supports. Two specimens per mortar mix were cast and tested (Figure 4.1). The mortar was always vibrated as it was introduced in the tubes. After casting, the acceleration measurements could start within a period of less than 30 minutes since the mixing of lime and water. The samples remained sealed in the mold during the whole test for seven days.

Conventional compression (CC) tests on cylinders

Conventional compression (CC) tests were made on cylindrical specimens to measure the elastic modulus at ages of 2, 4 and 7 days on the reference mortars, H09S and H09V, and compared with the results obtained with EMM-ARM. The specimens had a diameter/height of 75 mm/150 mm. A hydraulic actuator with 25 kN capacity was used for load application, and three Linear Variable Differential Transducers (LVDTs), supported by 2 centered steel rings were attached to the specimens at 120° intervals, with a reference measuring span of 50 mm [128]. The test protocol was similar to the one followed in previous chapters and in [41, 80]. In order to obtain a stable value, five repeat monotonic tests were conducted up to 30% of the maximum load; the mean of the last three values measured were taken as the elastic modulus. The displacement rate of each test was 0.7 mm/min (in displacement control to better perform the test at such early ages). After each test, the specimens were broken in compression at 10 N/s to evaluate the compressive strength.

Penetration resistance tests

Penetration tests were applied on the three mortar compositions, H08V, H09V and H11V, according to standard ASTM C-403 [131] for concrete as a reference. A penetrometer by Controls,

model 54-C0145, was used. The purpose of this test was to obtain the initial setting time of the mixes and compare it with the early singularities of continuous monitoring provided by EMM-ARM. Cubic molds of 150 mm edge length were used. The time of initial setting is measured as the moment when the penetration resistance, measured by the shank of a needle, equals 3.5 MPa.

Ultrasound pulse velocity tests (UPV)

The UPV test is a method that consists in generating a pulse on one side of the sample, which is transmitted through the material and received on the opposite side of the sample. The time delay between the generated and received signals is recorded to obtain the wave travel time through the material. The velocity of the (P) wave, V_p, can be related to the elastic properties of the medium (the dynamic Poisson's ratio, υ_{dyn}, and the dynamic elastic modulus, E_{dyn}) and the density, ρ, through equation (4.1), which is applicable for homogeneous and isotropic media [128, 132].

$$V_P = \sqrt{\frac{(1-\upsilon_{dyn})\,E_{dyn}}{(1+\upsilon_{dyn})\,(1-2\upsilon_{dyn})\,\rho}} \tag{4.1}$$

UPV was measured in some specimens at discrete times in the transverse direction (Figure 4.2), particularly in the specimens used for flexural and compressive strength tests. UPV was measured just before the actual mechanical tests. The ultrasound probes had 25 mm diameter and operating frequency of 150 kHz. Probe of this diameter was considered adequate, as it was larger than the largest expected heterogeneity of the mortar. The spacing between the probes was set as 40 mm, longer than two wavelengths at the selected operating frequency [128].

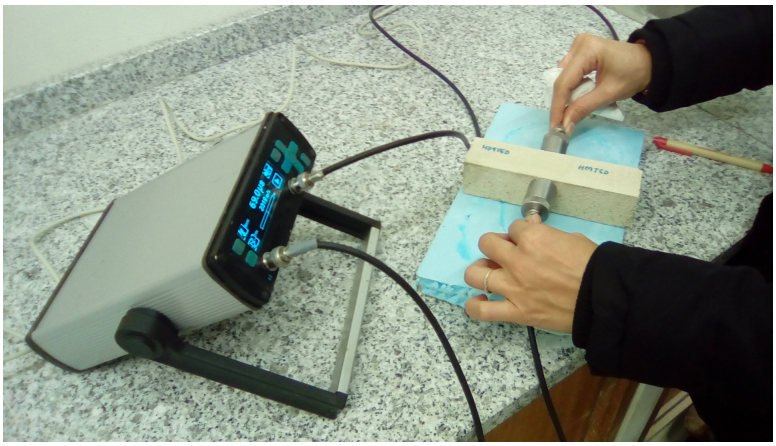

Figure 4.2: UPV setup. Discrete measurement in the lateral direction.

Flexural and compressive strength tests

Flexural and compressive strengths were measured at 2, 4 and 7 days. The standard EN 1015-11 [31] was observed. Flexural strength was measured by three-point bending on three 40 mm × 40 mm × 160 mm specimens applying a displacement rate of 0.2 mm/min. Compressive strength tests were conducted on six of the resulting remaining six half-prisms from the flexural strength tests, also in displacement control at 0.7 mm/min. These were the same displacement rates as the ones adopted in [25], instead of the ones set by the standard and the ones followed in the other chapters, to better control the tests at such early ages.

Open porosity

Open porosity was measured by the hydrostatic method on the three mortar mixes, particularly H08S, H09S and H11S and H08V, H09V and H11V, at day 7, according to UNE 83980 [109]. The

procedure is the same as the one explained in Chapter 2, see Section 2.2.5 and Eq. 2.7, with the exception that now m_3, which is the weight after water saturation, was obtained by using a vacuum pump instead of a boiling pan. Note that this standard allows both approaches depending on the device available.

Thermogravimetric analyses (TGA)

In thermogravimetric analysis (TGA), a material sample is submitted to a defined rate of temperature change until a maximum value is reached [133, 134]. The mass of the sample is monitored through the temperature range, and a resulting graph can be plotted with weight *vs.* temperature – TGA curve [133–135].

In this study, thermogravimetric analyses were performed on the lime paste of the corresponding reference mortar, P09, at day 0, 2, 4 and 7 to study the evolution of hydration by means of free portlandite, $Ca(OH)_2$, content, see Eq. (4.2).

$$2(2CaO \cdot SiO_2) + 4H_2O \rightarrow 3CaO \cdot 2SiO_2 \cdot 3H_2O + Ca(OH)_2 \tag{4.2}$$

For this purpose, the samples remained sealed until the moment of testing. Before testing, the technique of hydration stoppage with isopropanol according to [136] was applied. Then a sample of less than 20 mg was placed in an aluminum crucible. During the test, a heating rate of 10 °C/min from ambient temperature up to 1000°C was applied so as to allow direct measurement of hydroxide and carbonate compounds at hydroxylation and decarboxylation ranges, respectively [62, 134–136]. According to [64, 134], dehydroxylation, which is the process of decomposition of calcium hydroxide, $Ca(OH)_2$, typically occurs in the range 300-550°C, meanwhile the decomposition of calcium carbonate, $CaCO_3$, termed as decarboxylation, occurs in the range 650-950°C.

Once the test is finished, the quantity of calcium hydroxide that is decomposed can be obtained through Eq. (4.3) [136]:

$$\begin{aligned} M_{P,m} &= WL_P \frac{m_P}{m_w} \\ \text{Per 100 g paste} : M_{P,n} &= \frac{M_{P,m}}{W_{600}(1 + w/b)} \end{aligned} \tag{4.3}$$

where $M_{P,m}$ is the free portlandite measured, WL_P is the weight loss of the portlandite in the sample, m_P and m_w are the molecular masses of portlandite ($m_P = 74$ g/mol) and water ($m_w =$ 18g/mol), respectively, $M_{P,n}$ is the normalized free portlandite measured in the paste, W_{600} is the weight of the sample at 600°C and w/b the water/lime ratio.

4.3. Experimental results and analysis

4.3.1. Comparison between monitoring methods

First of all, the results of EMM-ARM are shown for the three mortars, H08V, H09V and H11V (Figure 4.3). For the reference mortar, M09, they were compared to the ones obtained through CC. Results from all three mortars were compared with the initial setting time measured through penetration resistance test.

EMM-ARM

EMM-ARM curves obtained for the three mortars tested, H08V, H09V and H11V, and comparison with CC for the reference mortars, H09V and H09S, are shown in Figure 4.3. It is worth mentioning that a wide range of elastic modulus was obtained throughout the curing process of the NHL mortars, ranging from ∼0 GPa to ∼4 GPa within the testing period. Furthermore, all elastic modulus evolution curves seem to be plausible, showing a short initial dormant period (with elastic modulus close to 0 GPa), after which elastic modulus evolved significantly for all tested mortars. Then, after around one day, the slope of elastic modulus evolution curves decreased with time

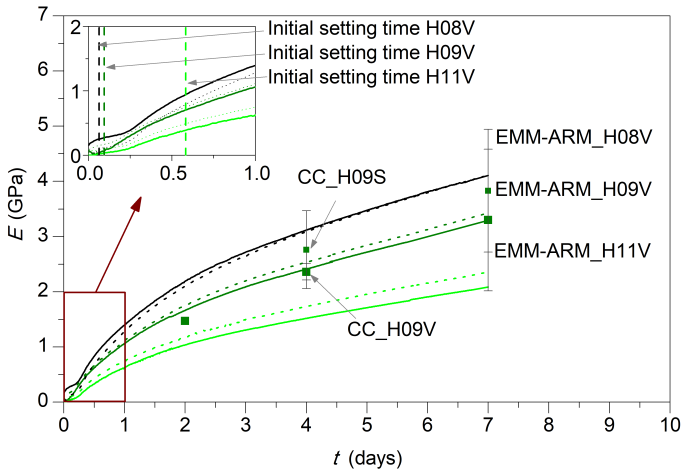

Figure 4.3: Results of EMM-ARM of the three mortars tested, comparison with CC for the reference mortar and initial setting time by means of penetration resistance test.

within the testing period. From the zoom of graph in Figure 4.3, it can be seen that mortar H08V (specimen 1) presented some initial stiffness in the early curing hours in comparison to mortars H09V and H11V. Such initial stiffness is likely to be due to the low viscosity of the mortar stemming from its low water/lime ratio and low value of consistency (130-135 mm). Mortars H09V and H11V, with higher water/lime ratios, did not present such initial stiffness as they were more fluid.

Two samples per mortar mix were tested as shown by the two curves of each mortar in Figure 4.3. It is possible to verify the good coherence of the two curves obtained for each mortar, demonstrating adequate repeatability of EMM-ARM. Mortar H08V presented especially good repeatability as its elastic modulus curves differed less than 0.17% at day 7. Furthermore, it is also possible to observe that the reduction of the water/lime ratio increases early hydration rates and leads to higher values of elastic modulus. For example, at day 7, the values of ∼4 GPa, ∼3 GPa and ∼2 GPa were obtained respectively, for H08V, H09V and H11V.

Table 4.3: Comparison of EMM-ARM and CC tests for the NHL mortars and corresponding initial setting times.

Mortar type	Curing days	Elastic modulus from CC (GPa)	Elastic modulus from EMM-ARM (GPa)			Initial setting time (h)		
		H09	H08	H09	H11	H08	H09	H11
	2	1.5 (-)						
S	4	2.8 (0.7)						
	7	3.8 (1.1)						
						1.50	2.25	14.00
	2	1.5 (-)	2.2	1.7	1.0			
			2.1	1.8	1.2			
V	4	2.4 (0.2)	3.1	2.4	1.5			
			3.1	2.5	1.7			
	7	3.3 (1.3)	4.1	3.3	2.1			
			4.1	3.4	2.4			

Note: values in parenthesis are standard deviations.

The comparison between the results of elastic modulus obtained by EMM-ARM and by CC for

the reference mortar H09V is also shown in Figure 4.3 and Table 4.3 (where the notation S refers to standard conditions [31] i.e. compacted and unsealed, the notation V refers to vibrated and sealed specimens (see Section 4.2.2) and the two values shown for EMM-ARM correspond to each sample). Additionally, results of CC tests of mortar H09S are included. It can be observed that the values obtained from EMM-ARM are similar to those obtained from CC tests in terms of magnitude and shape of the curve for the reference mortar vibrated and sealed, H09V. Results of both tests in the case of H09V only differ by only 1.5% at day 7 (comparing results from CC with the average of the two samples from EMM-ARM). For the standard mortar, H09S, the stiffness is higher from day 2, when the specimens were demolded, reaching a difference of 14% at day 7 . However, attention is paid to the standard deviation of the CC measurements (error bar in Figure 4.3 and values in parenthesis in Table 4.3), it can be observed that they are very high, especially at early ages when they can reach up to 40% (at day 2 only one specimen per mortar type was measured), in comparison to later testing when they normally reach 20% [41, 80]. Therefore, in spite of the fact of H09S seeming to be above H09V in a systematic manner, this might not be a meaningful difference as both measurements are within the margin of error. A possible reason for this relatively small difference (14% at day 7) can be due to carbonation reaction with CO_2 from the ambient exposure that is allowed to happen in H09S as opposed to the sealed condition of H09V, which would not allow carbonation. However, previous works [8, 61] have reported that carbonation does not play a significant role until later curing ages (e.g. 14 days onwards) and the main hardening mechanism in the early ages is actually hydration. Further research, therefore, is needed to study the cause of this difference. All things considered, it is therefore inferred that EMM-ARM can be used for very early age testing (e.g. before 2-3 days) for assessment of early kinetics. If longer periods of testing are intended, during which carbonation is expected to play a role, then the current set up of EMM-ARM would require adaptations that involve the actual demoldmolding of the specimen. This was not an objective of the present research and was thus not pursued further.

Moreover, initial setting times of the three mortars are shown in Figure 4.3 (vertical dash lines in the zoom). In view of the available data, a relation between elastic modulus as obtained by EMM-ARM and the setting time, as obtained by the penetration test was sought. For the reference mortar M0.9V, the initial setting happens at 2.25 hours after casting and the corresponding elastic modulus is 0.10 GPa. For the mortar M0.8V, the initial setting time is at 1.50 hours after casting (Table 4.3) and at that moment elastic modulus is around 0.46 GPa measured from the EMM-ARM curve. For mortar M1.1V, the initial setting time is recorded as 14.00 hours and the corresponding elastic modulus is 0.39 GPa. From previous studies, elastic modulus obtained for cement-based materials (pastes) at the moment of setting was found to range between 0.10 and 0.18 GPa [137]. This seems to be coherent with the value obtained for the reference mix M0.9V – 0.10 GPa. However, the values of 0.46 GPa and 0.39 GPa are relatively more dispersed, and the explanation proposed is as follows. The mortar M0.8V appears to have an inherent initial stiffness at time zero, possibly due to the its relatively low water/lime ratio, which increases the expected stiffness at the setting time measured. In the case of the mortar M1.1V, it is so fluid (238-240 mm) that the setting time is delayed quite a bit in addition to which it is also relatively weak. Therefore, in the time interval of 0-14 hours, the mortar had to gain some amount of stiffness before it could offer adequate resistance to penetration. More investigation is needed in order to better understand the range of elastic moduli that should be expected from NHL mortars at the instant of setting.

4.3.2. Influence of sample preparation and sealing conditions

In order to be able to relate elastic modulus measurements (through EMM-ARM and CC) of NHL mortars with density, flexural and compressive strength tests, and open porosity, the latter were performed on prismatic specimens prepared and cured according to standard procedures (compacted and unsealed) and according to the ones adopted for EMM-ARM (vibrated and sealed). Also, specimens compacted and sealed were tested to analyze better the influence of each preparation method. The following sub-sections describe the main findings in such concern.

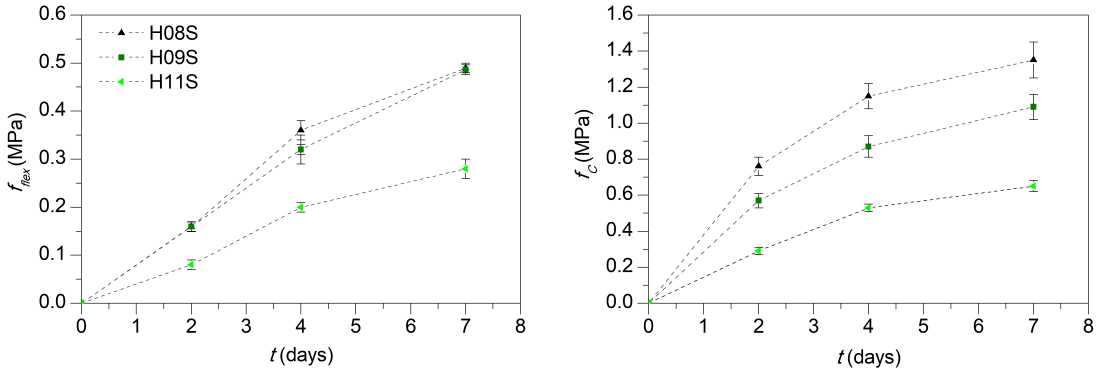

(a) (b)

Figure 4.4: Evolution of: (a) flexural, (b) compressive strengths with time.

Flexural and compressive strength tests

Flexural and compressive strength were assessed at 2, 4 and 7 days of age on the three mortar mixes with different preparation methods: standard (compacted with 25 strokes of the tamper and unsealed), vibrated and sealed, and compacted and sealed. In Figure 4.4, the results of the mixes prepared/cured with standard procedures (H08S, H09S and H11S), are plotted for the flexural strength (Figure 4.4a) and the compressive strength (Figure 4.4b). Each point represents the mean value of three specimens tested for the flexural strength and the one of the six resulting halves in the case of the compression strength. The error bars are the corresponding standard deviations. The results follow the expected path: mortars with lower water/lime ratios present higher flexural and compressive strengths. The flexural strengths of H08S and H09S are very similar to each other, in coherence with previous observations for the same mixes that had been studied at the age of 56 days [41].

Furthermore, the variability of results between mortars of different batches was checked for compression strength of the reference mortar, H09S: it was found to be less than 5% at day 7 among mortars of this chapter and the natural hydraulic lime one of Chapter 5, meaning that the results present good repeatability. Standard deviation of results, as shown in Figure 4.4, are also within acceptable ranges.

In addition, Table 4.4 shows a comparison between results of different preparation methods (values in brackets refer to the standard deviation). Here, $(f_s - f_v)/f_s(\%)$ and $(f_s - f_c)/f_s(\%)$ refer to the relative difference of the strength of the vibrated and sealed (V) and compacted and sealed (C) specimens, respectively, in relation to the corresponding standard (S) (beams). In general, mortars that are sealed provide lower flexural and compressive strengths compared to the standard ones. For example, for the reference mortar, H09 (at day 7), the flexural strength is 49% smaller for both mortars that are vibrated and sealed (V) and compacted and sealed (C), as compared to the standard situation (S). Furthermore, in comparison to the standard situation (S), the compressive strength is approximately 21% smaller in the mortars that are vibrated and sealed (V) and 29% in the ones that are compacted and sealed (C). This could be, at least partially, due to the fact that the sealed specimens (kept in the humid chamber inside two plastic bags) were still wet during testing as they could not be air dried in the humid chamber as the unsealed ones (just kept in the humid chamber in contact with the air). A similar phenomenon was observed in [138], where brick masonry prisms and its components (bricks and three types of cement mortars with different cement to sand ratios) were air cured at 30°C and RH 90% for 28 days. After this period, the specimens were divided into three groups and stored in oven-dry state (oven drying at 105°C), air dry (at 30°C and RH 90%) and wet state (water imnmersion) for 24 hours. Then, they were tested under compressive strength test, bond test and direct shear test. The results showed that the compressive strength of the weakest cement mortar could be 15.9% less for wet specimens in comparison to the air dried specimens (at 30°C and RH 90%). Popovcics [139] related

Table 4.4: Influence of the compacting method and curing conditions on the mechanical properties and comparison with the corresponding standard mortars at day 7.

	Flexural strength (MPa)			Compressive strength (MPa)		
	H08	H09	H11	H08	H09	H11
S	0.49 (0.01)	0.49 (0.01)	0.28 (0.02)	1.35 (0.10)	1.09 (0.07)	0.65 (0.03)
V	0.28 (0.06)	0.25 (0.01)	0.14 (0.01)	1.06 (0.04)	0.86 (0.03)	0.47 (0.01)
C	0.28 (0.01)	0.25 (0.02)	0.14 (0.01)	1.07 (0.06)	0.77 (0.06)	0.48 (0.02)
	Decrease on flexural strength (%)			Decrease on compressive strength (%)		
	H08	H09	H11	H08	H09	H11
$\frac{f_S - f_V}{f_S}$ (%)	43	49	50	22	21	27
$\frac{f_S - f_C}{f_S}$ (%)	44	49	49	21	29	26

Note: values in parenthesis are standard deviations.

this variation between wet and air cured specimens to the increase of the internal pressure in wet conditions due to a higher amount of water present in pores. Under this situation, the chance of cracking in a mortar with lesser external load increases and therefore the compressive strength is reduced. More detailed information on this phenomenon can be seen in [138].

Finally, it is worth remarking that the results of mortars that are vibrated and sealed and compacted and sealed are quite similar, meaning that the compaction method may not have much influence on the mechanical strength of NHL mortars at early stages.

In addition, the results of flexural and compressive strength of the mortars with the three different preparation methods were normalized with respect to their respective values at day 7 ($f_{flex}/f_{flex_{D7}}$ and $f_c/f_{c_{D7}}$, respectively). Then, non-dimensional evolution curves of flexural (Figure 4.5a) and compressive (Figure 4.5b) strengths with time were obtained as shown for the standard (S) mortar, as the kinetics of evolution was rather similar in all cases. Equations (4.4) and (4.5) and Table 4.5 show the corresponding non-dimensional laws for the three mortars with the three preparation methods (standards, S; vibrated and sealed, V; and compacted and sealed, C). These laws can be useful to obtain the flexural and compressive strengths of the different NHL mortars at early ages just by knowing their corresponding values at day 7, which can also be useful for numerical models with NHL mortars at early ages.

$$\frac{f_{flex}}{f_{flex_{D7}}} = k\left(\frac{t}{t_0}\right)^n \tag{4.4}$$

$$\frac{f_c}{f_{c_{D7}}} = o\left(\frac{t}{t_0}\right)^p \tag{4.5}$$

Where t_0 are 7 days.

To assess the impact of the three different variables used, namely - preparation method (S, V or C), the time of testing (2, 4 or 7 curing days) and the water/lime ratio (0.8, 0.9 or 1.1), a three-way ANOVA test was performed, using the software Matlab R2016 [140]. In Table 4.6, p values lower than 0.05 indicate significance of the corresponding factor. Observing the results, it may be concluded that both the preparation method as well as the water/lime ratio do not have a significant effect on the non-dimensional evolution curves of flexural and compressive strength (p value > 0.05), while, the time of testing does have an influence (p value < 0.05). In addition, from Table 4.6, it may also be observed that the interaction of the three factors does not have any statistical significance.

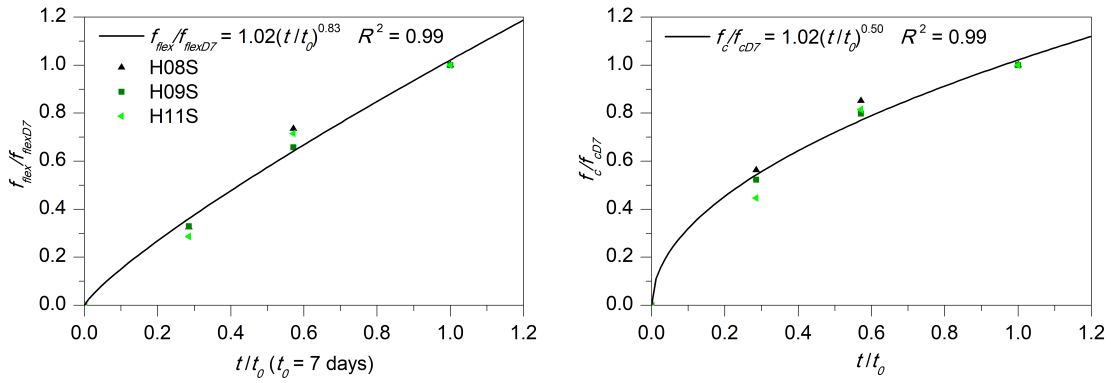

(a) (b)

Figure 4.5: Non-dimensional evolution curves of (a) flexural and (b) compressive strengths with time.

Table 4.5: Coefficients of equations (4.4) and (4.5).

		S	V	C	Mean (CV)
Flexural strength	k	1.02	1.01	1.00	1.01 (1%)
	n	0.83	0.71	0.80	0.78 (8%)
Compressive strength	o	1.02	1.02	1.00	1.01 (1%)
	p	0.50	0.54	0.52	0.52 (4%)

Table 4.6: Results of a three-way ANOVA of the influence of three factors on the non-dimensional flexural and compressive strengths.

Factors		Analysis on non-dimensional flexural strength	Analysis on non-dimensional compressive strength
		p value	p value
Preparation method (S, V and C)	g_1	0.13	0.24
Testing moment (2, 4 and 7 days)	g_2	0.00	0.00
Water/lime ratio (0.8, 0.9 and 1.1)	g_3	0.70	0.27
Interactions	$g_1 \times g_2$	0.09	0.20
	$g_1 \times g_3$	0.52	0.29
	$g_2 \times g_3$	0.92	0.21

We have proposed the use of a single value for each of the coefficients p, q, r and u. This is because the percentages of variation from the mean values were found to be low. Furthermore, from the results of ANOVA, it was found that the method of sample preparation did not have a statistically significant impact on the non-dimensional evolution of compressive and flexural. This implies that the two general equations with mean coefficients could be used to describe the non-dimensional evolution of flexural and compressive strengths up to 7 days of curing age, independent of the preparation method and the water/lime ratio.

Ultrasound pulse velocity (UPV)

Before performing flexural and compressive strengths, discrete measurements of UPV were taken in the transverse direction of the samples at day 2, 4 and 7. In this case, standard mortars (H08S, H09S and H11S) were compared with mortars that are vibrated and sealed (H08V, H09V and H11V) (see Table 4.7, where the values in brackets indicate the standard deviation). Results from Table 4.7 show a similar trend as the one observed for the mechanical properties: mortars with lower water/lime ratios present higher velocities than the ones with higher water/lime ratios. For example, pulse velocity measured on average was 1750 m/s, 1530 m/s and 1300 m/s for H08S, H09S and H11S, respectively, at day 7. Variability of results among mortars of different batches was also checked for the reference mortar, H09S, and found to be less than 5% at day 7, confirming good repeatability of the tests. On the other hand, comparison of results between vibrated and sealed counterparts of the standard mortar shows that the latter presents higher values of transverse velocity than compared to the standard ones. For example, it was 2070 m/s in the reference mortar vibrated and sealed, H09V,while for the standard reference mortar, H09S, it was 1530 m/s. It is noted that this trend is opposite to the one described for compressive/flexural strength (and even elastic modulus) described in the previous sections, where the "S" mixes were systematically presenting higher values for mechanical properties than "V" mixes. This fact can be interpreted by the influence of water present in the porous network of the specimens during testing, which can play a role in the measured UPV. According to Lencis *et al.* [141] and Lafhaj *et al.* [142], UPV measurements increase with the material's degree of saturation. For example, for concrete, UPV can be 19% higher in fully saturated specimens in comparison to the completely dry ones [141]. Also Bungey [143] showed that UPV in wet concrete specimens was higher than in the corresponding dry ones. Considering this, it is reasonable that UPV values may be higher in the sealed specimens as they were still wet in the moment of testing, in comparison to the standard ones that were air dried in the humid chamber.

Table 4.7: Results of UPV in the lateral and longitudinal directions for the standard (S) and vibrated and sealed (V) mortars.

		Transverse wave velocity (m/s)		
	Curing days	H08	H09	H11
S	2	1430 (40)	1230 (80)	-
	4	1530 (20)	1300 (20)	1030 (40)
	7	1750 (50)	1530 (10)	1300 (20)
V	2	1790 (20)	1800 (30)	1500 (60)
	4	1970 (60)	2020 (60)	1550 (200)
	7	2110 (50)	2070 (20)	1630 (80)

Note: values in parenthesis are standard deviations.

Density and open porosity

Relationships were also established among the physical properties measured on the NHL mortars, such as wave propagation velocity from UPV, density and open porosity. Density was measured for all mortars at day 2, 4 and 7 just before performing flexural and compressive strengths (the weight of each sample was divided by their corresponding volume). In general, the results of density follow the same trend as that of mechanical properties and UPV (see Table 4.8 where the values in brackets are the standard deviation): mortars with lower water/lime ratios present higher values of density. For example, it is 2080 kg/m^3, 2030 kg/m^3 and 1940 kg/m^3, respectively for standard mortars H08S, H09S and H11S. On the other hand, for all mortar compositions, density tends to decrease with time in the first seven curing days, probably, due to the evaporation of water present inside the mortars. For instance, it is 2210 kg/m^3 at day 2 and 2030 kg/m^3 at day 7 for reference mortar H09S. Furthermore, comparing mortars that are sealed with the standard ones, it is observed that the former have higher values of density as their water content is higher due to the sealed conditions. For example it changed from 2240 kg/m^3 to 2030 kg/m^3 when comparing H09V with H09S.

Table 4.8: Results of bulk density at different curing days for the standard (S), vibrated and sealed (V) and compacted and sealed (C) mortars.

	Curing days	H08 (kg/m^3)	H09 (kg/m^3)	H11 (kg/m^3)
S	2	2250 (8)	2210 (4)	2170 (10)
	4	2180 (10)	2120 (5)	2060 (4)
	7	2090 (7)	2030 (6)	1940 (7)
V	2	2250 (8)	2250 (4)	2200 (14)
	4	2240 (10)	2250 (5)	2180 (4)
	7	2230 (7)	2240 (6)	2170 (7)
C	2	2310 (6)	2280 (9)	2200 (14)
	4	2290 (7)	2280 (1)	2200 (10)
	7	2270 (10)	2270 (7)	2200 (10)

Note: values in parenthesis are standard deviations.

As for open porosity, standard mortars were compared with the vibrated and sealed ones at day 7, see Table 4.9 (again values in brackets are standard deviation). In general, as the water/lime ratio increases, the porosity also does, measuring 26.1%, 27.2% and 29.9%, respectively for mortars H08S, H09S and H11S. Comparing both preparation methods, it was checked that open porosity was slightly higher for the mortars that are vibrated and sealed in comparison with the standard ones, but in fact this difference is very low and in most cases it is within the margin of error, so no clear conclusions can be extracted from this.

Table 4.9: Results of open porosity at day 7 for the standard (S) and vibrated and sealed (V) mortars.

	Curing days	H08 (%)	H09 (%)	H11 (%)
S	7	26.1 (0.3)	27.2 (0.2)	29.9 (0.4)
V	7	26.5 (0.2)	28.0 (0.3)	30.9 (0.2)

Note: values in parenthesis are standard deviations.

Figure 4.6 shows some of these tendencies in relation to results of UPV for the standard mortars

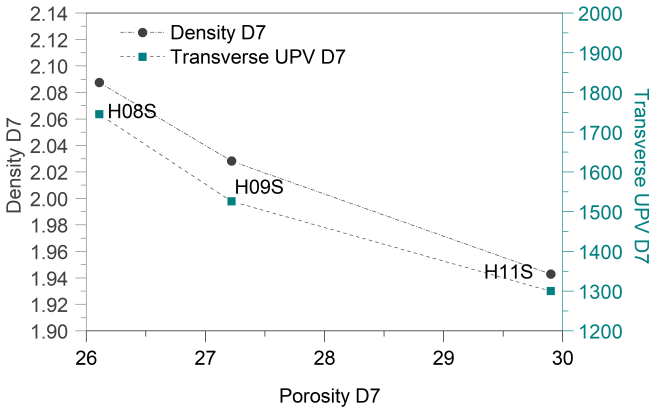

Figure 4.6: Relationship between open porosity, density and UPV at day 7 for H09S.

(H08S, H09S and H11S) at day 7. In general, it can be observed that, as open porosity increases, density and lateral velocity of UPV decrease. It is logical that density decreases as the number of pores increases and therefore open porosity also increases with a consequent decrease of the wave propagation velocity. Similar trends of pulse velocity decreasing with porosity, were also observed by Lafhaj *et al.* [142] for cement mortars.

4.3.3. Thermogravimetric analyses

The material was also characterized by means of free portlandite content through thermogravimetric analysis (TGA). For this purpose, tests were performed at day 0, 2, 4 and 7 on the corresponding lime paste, P09, of the reference mortar. The samples were sealed until the moment of testing in order to study the evolution of hydration by measurement of free portlandite content and to avoid carbonation reaction. Figure 4.7 shows the relation between free portlandite content of P09 and the compressive strength of mortar H09V at the same curing age. It can be observed that portlandite content increases as a function of the compressive strength. A similar trend was also observed by Boualleg *et al.* [144] for cement pastes and mortars. They obtained a linear fitting for different cement samples while we obtain a similar linear adjustment for the same sample at different curing days. Lanas *et al.* [8] also studied the evolution of free portlandite content on NHL type 5 mortars and they observed that it increased up to 28 or 91 days depending on the lime/aggregate ratio.

In Figure 4.7, it may be remarked that the presence of free portlandite at day 0, is typical of the nature of raw material itself. For example, in the work by Arizzi *et al.* [13], the raw NHL 3.5 presented a content of portlandite between 40% and 50%. This amount is coherent with results of XRD of the NHL 3.5 of the present study (see Table 2.1 and Figure 2.1 of Chapter 2), where a range between 40% and 45% of portlandite is obtained.

4.4. Conclusions

In this research, properties of three NHL type 3.5 mortars with different water/lime ratios and same lime/aggregate ratio are studied at early ages, such as density, flexural and compressive strengths, stiffness evolution through EMM-ARM and CC, and the evolution of free portlandite content with time. An exhaustive physical and mechanical characterization was performed on the material under different fabrication and curing methods: standard procedures (compacting and unsealing), vibration and sealing, and compacting and sealing. The results show good repeatability in the tests, especially in EMM-ARM, flexural and compressive strength tests. The following main conclusions can be extracted from this research:

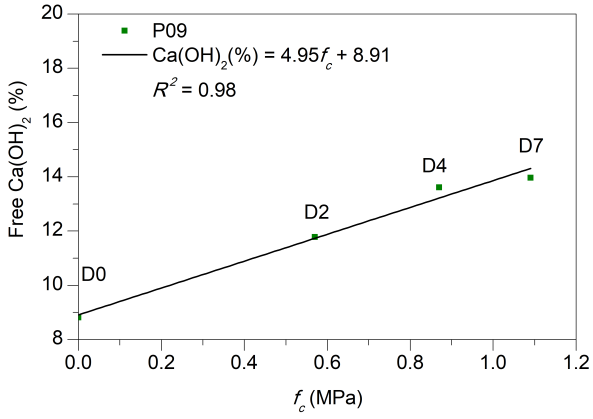

Figure 4.7: Free portlandite content as a function of compressive strength on the reference sealed paste samples.

1. The EMM-ARM method has shown feasible potential of application to the study of NHL mortars at early ages (< 3-7 days), with a very good repeatability and good comparability with results obtained from CC testing (with both standard compaction/curing and non-standard curing involving vibration and sealing). The initial dormant period was well captured, as well as the entire kinetics of stiffness increase, which was clearly different amongst the three studied mortars. As time passes, and the standard curing condition allows specimens to harden further, the results attained by EMM-ARM (in sealed conditions) start to deviate from the CC results with standard curing (less stiffness assessed by EMM-ARM). Therefore, if EMM-ARM is to be applied for longer durations, more than a mere couple of days, adaptations to the test setup are necessary, so as to allow carbonation. These adaptations will bring new challenges due to mass variations of the specimen during testing, which will need to be monitored, so as to provide adequate estimates of elastic modulus (obtained through the dynamic equation of motion).

2. Flexural and compressive strength behave as expected: mortars with lower water/lime ratios presenting higher strengths. Comparing standard cured specimens (S) with the ones that are sealed (V and C), it is observed that the latter have lower strength. These results were unexpected since the sealed specimens were subjected to more humid moisture curing conditions and therefore higher degrees of hydration. One possible explanation for this may be that the sealed specimens were wetter at the moment of testing compared to the unsealed specimens (subjected to air curing inside the humid chamber) and therefore exhibited lower values of mechanical strength as discussed by other researchers [138, 139]. Further research would be needed to study the effect of wetting conditions on NHL mortars.

3. Furthermore, the evolution tendencies of normalized flexural and compressive strength with respect to their corresponding values at day 7 were obtained. These formulas could be useful for numerical models with NHL mortars at early ages. It must be noted though, that these evolution trends have been presented specifically with regard to mixes having lime/aggregates ratio of 1:3 (by volume) and employing limestone aggregates.

4. Discrete measurements of UPV were also taken in the transverse direction of the prismatic specimens just before performing flexural and compressive strength tests. The results showed that pulse velocity increased with lower water/lime ratios. Furthermore, velocity also increased in specimens that were more humid, such as the sealed ones. This is possibly related to longitudinal waves propagating faster through pores filled with water than through the ones filled with air [145]. Such tendencies appear to be similar to the ones found by Lencis *et al.* [141], Lafhaj *et al.* [142] and Bungey [143]. This caused the sealed specimens to exhibit higher UPV than the standard cured specimens, which is a different trend to the one found

in other mechanical tested properties (strength and stiffness). A word of caution is thereby issued on potentially misleading observations that might be taken when comparing UPV test results of specimens cured under different conditions.

5. Density follows the same trend as flexural and compressive strength and UPV: it is higher for mortars with lower water/lime ratios. Comparing specimens that are sealed with the standard ones, it was observed that the former has higher values of density as they are more humid.

6. Open porosity was measured at day 7 and, as expected, it increases with higher water/lime ratios. In general, it was observed that density and pulse velocity decreased as open porosity increased.

7. Finally, the evolution of free portlandite content was measured in the reference lime paste at days 0, 2, 4 and 7. It was related to the compressive strength of the mortar with the same composition at corresponding ages. This relation was adjusted with a linear fitting up to day 7. Other authors [8] also observed that free portlandite content increased up to day 28 or 91 depending on the lime/aggregate ratio of NHL mortars.

Chapter 5

Time effect on the physical and mechanical properties of a natural hydraulic and an aerial lime mortars in the long-term

Article title: Age effect on the physical and mechanical properties of a natural hydraulic and an aerial lime mortars
Authors: Lucía Garijo, Xiaoxin Zhang, Gonzalo Ruiz, José J. Ortega
Journal: Construction and Building Materials
Submitted: 29/04/2019

This chapter focuses on the advanced mechanical characterization of a natural hydraulic and an aerial lime mortars. Seven properties, such as density, flexural, compressive and splitting tensile strengths, fracture energy, elastic modulus from prisms and carbonation depth by means of the phenolphthalein method, were measured at different instants. The results show that there is a faster increase of the mechanical properties in both mortars up to 56 days, which ranges between 60% and 90% of their corresponding values at an age of 448 days depending on the mechanical property and type of mortar. After this age, there is a more moderate but progressive evolution up to 224 days. However, from this age to 448 days, the evolution of the mechanical properties is very slow for the aerial lime mortar and shows a slight increase for the natural hydraulic one. Furthermore, some empirical equations of such behaviors with time are proposed for both mortars.

Keywords: Natural hydraulic lime mortar, Aerial lime mortar, Long-term behavior, Mechanical characterization, Fracture energy, Empirical equations.

5.1. Introduction

Natural hydraulic and aerial lime mortars are mostly present in historical masonry structures for long periods of time. It is well known that the carbonation process of both lime mortars can be long lasting [9, 58, 64] and it is therefore frequent that their strengths at early ages is lower than the corresponding ones in the long term. Thus, there is an urgent need for quantifying the corresponding increase of mechanical properties.

Up to present, most researchers have concentrated on the evolution of compressive and flexural strengths or dynamic modulus of elasticity [6, 8, 9, 17, 21, 47, 65]. However, regarding the evolution of fracture energy, which is an important parameter to characterize the ductility and fracture behavior of mortars, it is still unknown. Thus, in the chapter, an advance mechanical characterization of a natural hydraulic and an aerial lime mortars is performed in the long-term up to 448 days. For this purpose, density, carbonation depth, flexural, compressive and splitting tensile strengths, fracture energy and elastic modulus were measured at different ages and the evolution of these properties were studied as well. Furthermore, some non-dimensional laws are provided for all these mechanical properties with respect to their corresponding values at 28 days,

which could be useful for numerical simulations of masonry structures with these materials in the long-term.

The rest of the chapter is organized as follows. The next section describes the experimental procedure. Section 5.3 presents the results and some analysis. Finally, some conclusions are extracted in Section 5.4.

5.2. Experimental procedure

5.2.1. Raw materials

According to EN 459-1 [12], the limes used were a natural hydraulic one, NHL 3.5, and an aerial one of class CL 90-S, the same ones as those used in Chapters 2, 3 and 4. The former was supplied by "Socli, Italcementi Group" (France) and had an apparent density of 850 kg/m^3; the latter was provided by "Calcasa Calcinor" (Spain) and had an apparent density of 490 kg/m^3. Chemical and mineralogical analyses and particle size distribution of each lime are presented in Chapters 2 (Table 2.1, Figures 2.1 and 2.2) and 3 (Table 3.1, Figures 3.1 and 3.2), respectively.

A commercial crushed limestone was used as aggregate. It had particle size distribution curve as presented in Chapter 2, see Figure 2.3, determined according to EN 1015-1 [84]. Its apparent particle density was 2680 kg/m^3 in accordance with EN 1097-6 [85] (Figure 2.4b) and its apparent density was 1820 kg/m^3 according to EN 1097-3 [86] (Figure 2.4c).

5.2.2. Fabrication of the natural hydraulic and aerial lime mortars

Both mortars were fabricated with a lime/aggregate ratio of 1:3 by volume according to the traditional historic mortars [26, 40, 146]. The water/lime ratio was 0.9 by volume as well, which provided plastic consistencies according to EN 1015-3 [88] and EN 1015-6 [89]. That is to say, the consistency of the natural hydraulic lime mortar was 150-155 mm and the one of aerial lime mortar was 140-150 mm. For obtaining a convenient measurement during the fabrication process, volume proportions of compounds were converted to weight by using their corresponding apparent density.

The specimens were prepared according to EN 1015-11 [31]. They were cast in prismatic molds measuring 40 mm × 40 mm × 160 mm. Natural hydraulic lime mortar specimens were just cured since fabrication in the humid chamber (RH 97 ± 0.5% and 20 ± 0.5°C) with the first two days in the molds, while aerial lime mortar beams were cured initially five days with molds, then two days without molds in the humid chamber and finally in the ambient laboratory conditions (RH 51 ± 10% and 17 ± 3°C).

It must be remarked that this aerial lime mortar and those of Chapters 3 and 6 are not the same materials as they were not cured under exactly the same conditions. All of them were fabricated by following the same procedure: they were cured in the humid chamber for the first seven days and then the rest under ambient laboratory conditions. The small variations on the latter conditions should have an impact on the resulting mechanical properties. In fact, the initial 14 days of curing in the laboratory were especially favorable for the carbonation process of the aerial lime mortars of this chapter (RH 60 ± 6% and 16.6 ± 0.5°C) [54, 57, 59–61, 147]. In this sense, several authors have already highlighted the influence that the curing conditions have on the mechanical properties of aerial lime mortars [54, 59–61, 147], as explained in Chapter 3. Among them, Faria *et al.* [59, 60] found that curing aerial lime mortars under 20°C and 50% or under 20°C and 65% provided corresponding compressive strengths at the age of 60 days 20% higher for the latter.

The natural hydraulic lime mortars, instead, were all cured inside the humid chamber under the same curing conditions (RH 97 ± 0.5% and 20 ± 0.5°C) so as to favor the hydration process [25, 61].

5.2.3. Mechanical and physical tests on lime mortars

Seven physical and mechanical properties were measured on both lime mortars, such as, density, carbonation depth, flexural and compressive strengths at ages of 7, 14, 28, 56, 112, 224 and 448 days; splitting tensile strength (the specimens were obtained from the remaining prisms of the three-point bending test to obtain the fracture energy), fracture energy and elastic modulus from prisms were obtained at the same ages but starting at 28 days due to the fact that the prismatic notch specimens could be damaged during the installation process for the test before that age. Aerial lime mortar was not tested at 7 days as the specimens were not hard enough. The mechanical tests were performed according to the procedures indicated in Chapter 2. The carbonation test method is explained as follows.

Carbonation test method

As for the carbonation test method, there is no standard for lime mortars. The aim of performing such a test is to analyze the evolution of the carbonation state on the specimen surfaces. Carbonation in concrete is not a desired chemical reaction because it reduces the pH value of the material causing cracking and carbonation-induced steel corrosion [148]. However, in the case of lime mortars, carbonation is one of the hardening mechanisms [9, 58]. In fact, the increase of the carbonation depth is linked to the evolution of the mechanical properties [8, 17]. For this reason, in order to understand better the hardening mechanisms of both lime mortars and their evolution, carbonation depth was determined by the phenolphthalein method. This consists in spraying this substance on a broken surface of the mortar sample [144], in our case, on the prismatic ones after performing compressive tests. The phenolphthalein makes some central part of the broken surface turn a purple color, meaning that this part remains uncarbonated. The part with no change of color (usually on the borders) reflects that it has been carbonated. Carbonation depth is the length between the external surface of the mortar and the end of the colored region [144]. The tests were performed on the natural hydraulic and aerial lime mortars from 14 up to 448 days, on the remaining parts of the prismatic specimens tested under compression.

5.3. Results and discussion

In this section, the results of the experimental campaign described in Section 5.2 for the natural hydraulic and the aerial lime mortars are presented.

5.3.1. Evolution of density and mechanical properties

The evolution of density and some mechanical properties for both natural hydraulic and aerial lime mortars can be observed in Table 5.1 and Figure 5.1. In Table 5.1, ρ, f_{flex}, f_{cpr}, f_t, G_F and E_{pr} are, respectively, the apparent density, flexural strength, compressive strength from prisms, splitting tensile strength, fracture energy and elastic modulus measured through prisms. Furthermore, Std. Dev. and CV stand for the standard deviation and the coefficient of variation, respectively. In Figure 5.1, the error bars are the standard deviation. It is observed that the density and mechanical properties of the natural hydraulic lime mortar are higher than that of the corresponding aerial lime mortar. This is mainly due to the different mineralogical composition of both binders and different hardening process of both mortars. As explained in the Introduction, aerial lime is mainly composed of portlandite, while natural hydraulic lime has calcium silicates (mainly dicalcium silicates, C_2S) besides portlandite (Table 2.1 and Figure 2.1) [13–16]. The former hardens by carbonation (Eq. 5.1), while the latter also hardens due to the hydration of its mineralogical compounds (Eq. 5.2) [17, 61].

$$Ca(OH)_2 + CO_2 \rightarrow CaCO_3 + H_2O \tag{5.1}$$

$$2(2CaO \cdot SiO_2) + 4H_2O \rightarrow 3CaO \cdot 2SiO_2 \cdot 3H_2O + Ca(OH)_2 \tag{5.2}$$

Table 5.1 and Figure 5.1a show that for both mortars the density decreases considerably since the fabrication moment (apparent density of fresh mortar was obtained according to EN 1015-6 [80, 89]) up to 56 days. This decrease on density is due to the water evaporation of the mortars during samples air drying process [55, 58]. At this age, the hydraulic lime mortar loses 8.88% of its density compared with the value at the fabrication moment, while the loss is 9.76% for the aerial one. This water loss is logically more pronounced for the aerial lime mortar than for the natural hydraulic one, as the former is cured in the ambient laboratory conditions after seven days instead of being the entire time in the humid chamber at higher RH conditions for the latter. After 56 days, the density of the hydraulic lime mortar remains almost constant, in the reference [8], the similar tendency was also found for mortars fabricated with NHL 5 and low lime/aggregate ratios. For the aerial lime mortar, instead, the density increases slightly after 56 days. This is due to the transformation of portlandite into calcite that causes a weight increase as the larger pores are filled with the expanding calcium carbonate without any appreciable change of the volume [54, 55, 58].

Regarding the evolution of mechanical properties (see Figure 5.1b-f), the results show that there is a sharp increase up to 56 days for both lime mortars. In the case of the natural hydraulic lime mortar, taking the mechanical properties at 448 days as references, the flexural strength (Figure 5.1b), compressive strength (Figure 5.1c), splitting tensile strength (Figure 5.1d), fracture energy (Figure 5.1e) and elastic modulus (Figure 5.1f), gain 89%, 73%, 61%, 88%, 69%, respectively. This increase of the mechanical properties is attributed to the hydration of several hydraulic compounds that form hydrated calcium silicates (C-S-H phases) [8, 149]. They can be mainly tricalcium silicates, C_3S, that can be present in small amounts in NHL mortars and have an influence at very early ages up to 28 days [8, 17] and also dicalcium silicates, C_2S, that start to contribute to the hardening process after 28 days as explained in [8, 17] (Eq. (5.2)). Also, within 14 or 28 days, the beginning of the carbonation process can play a role (Figure 5.3a-b) [8, 17, 46, 61]. In the case of the aerial lime mortars, also taking the mechanical properties at 448 days as references, the flexural strength (Figure 5.1b), compressive strength (Figure 5.1c), splitting tensile strength (Figure 5.1d), fracture energy (Figure 5.1e) and elastic modulus (Figure 5.1f) gain 83%, 88%, 75%, 75%, 89%, respectively, at 56 days. The aerial lime mortars start to set and then harden by loss of water, once their pores have reached an optimum moisture content (for Portland cement with hydrated lime it is around 50% of its pore volume [54]), the carbonation process is maximized [55, 58, 148]. If the pores are saturated with water, carbonation is not developed as the diffusion of CO_2 is not allowed; only when the specimens start to dry, the carbonation begins to play a role [55, 58, 61, 64, 148]. As mentioned previously, this process usually starts within 14 or 28 days, see Figure 5.4a-b [9, 17, 61] (Eq. 5.1). Then, carbonation increases considerably up to around 2 months of curing after which it increases more moderately [46]. This increase on the carbonation process of aerial lime mortars is reflected on its mechanical properties.

After 56 days, the mechanical properties of both lime mortars present a more moderate increase up to 224 days. From this moment and up to 448 days the evolution of the mechanical properties is more or less constant for the aerial lime mortars and with a slight increase for the natural hydraulic one. For example, at 448 days for the natural hydraulic lime mortar the flexural strength reached 1.45 MPa, compressive strength 4.45 MPa, splitting tensile strength 0.64 MPa, fracture energy 13.6 N/m and elastic modulus from prisms 8.3 GPa. In this mortar, this moderate increase is mainly due to the fact that the remaining C_2S continues reacting in the long-term [8, 17, 150]. The own carbonation process, as evidenced by Figure 5.3d-f and observed in [8, 146], can also have an influence on the development of mechanical properties. The evolution of flexural strength of the natural hydraulic lime mortar at 448 days is irregular. At this age, the flexural strength tests performed on three specimens according to EN 1015-11 [31] provided quite inclined crack paths in the three cases, which could cause a reduction on the flexural strength at this age as observed in Figure 5.1b. For the aerial lime mortar, at 448 days the flexural strength is 0.75 MPa, compressive strength 2.03 MPa, splitting tensile strength 0.20 MPa, fracture energy 5.2 N/m and elastic modulus from prisms 3.5 GPa. In the case of this mortar, the increase on the mechanical properties is much less pronounced as it is only due to the own carbonation process [17, 61].

Table 5.1: Physical and mechanical properties of both natural hydraulic and aerial lime mortars at various ages.

Type of mortar	Age (Days)		ρ (kg/m^3)	f_{flex} (MPa)	f_{cpr} (MPa)	f_t (MPa)	G_F (N/m)	E_{pr} (GPa)
Natural hydraulic lime	7	Mean	**2160**	**0.37**	**1.10**	-	-	-
		Std. Dev.	10	0.03	0.07			
		CV (%)	0.5	8	6			
	14	Mean	**2140**	**0.51**	**1.53**	-	-	-
		Std. Dev.	20	0.01	0.02			
		CV (%)	0.9	2	1			
	28	Mean	**2060**	**0.89**	**2.41**	**0.30**	**7.6**	**4.7**
		Std. Dev.	20	0.20	0.15	0.01	0.8	0.8
		CV (%)	1	22	6	3	11	17
	56	Mean	**2050**	**1.28**	**3.24**	**0.39**	**11.9**	**5.7**
		Std. Dev.	20	0.10	0.10	0.02	2.0	1.0
		CV (%)	1	8	3	5	17	18
	112	Mean	**2060**	**1.52**	**3.36**	**0.49**	**12.5**	**6.7**
		Std. Dev.	10	0.05	0.16	0.04	2.0	0.5
		CV (%)	0.5	3	5	8	16	8
	224	Mean	**2040**	**1.75**	**4.35**	**0.53**	**12.5**	**7.3**
		Std. Dev.	10	0.03	0.50	0.04	1.0	1.0
		CV (%)	0.5	2	12	8	8	14
	448	Mean	**2040**	**1.45**	**4.45**	**0.64**	**13.6**	**8.3**
		Std. Dev.	10	0.10	0.13	0.04	2.0	0.9
		CV (%)	0.5	7	3	6	15	11
Aerial lime	14	Mean	**2050**	**0.27**	**0.69**	-	-	-
		Std. Dev.	10	0.01	0.05			
		CV (%)	0.5	4	7			
	28	Mean	**2010**	**0.57**	**1.27**	**0.13**	**3.7**	**2.5**
		Std. Dev.	20	0.07	0.08	0.02	0.4	0.3
		CV (%)	1	12	6	15	11	12
	56	Mean	**2010**	**0.62**	**1.79**	**0.15**	**3.9**	**3.1**
		Std. Dev.	10	0.04	0.15	0.02	0.5	0.2
		CV (%)	0.5	7	8	13	13	7
	112	Mean	**2020**	**0.73**	**1.88**	**0.18**	**5.3**	**3.4**
		Std. Dev.	20	0.03	0.10	0.01	0.8	0.2
		CV (%)	1	4	5	6	15	6
	224	Mean	**2030**	**0.76**	**2.02**	**0.18**	**5.6**	**3.5**
		Std. Dev.	20	0.05	0.09	0.01	1.5	0.1
		CV (%)	1	7	5	6	27	3
	448	Mean	**2040**	**0.75**	**2.03**	**0.20**	**5.2**	**3.5**
		Std. Dev.	10	0.05	0.12	0.01	2.4	0.1
		CV (%)	0.5	7	6	5	46	3

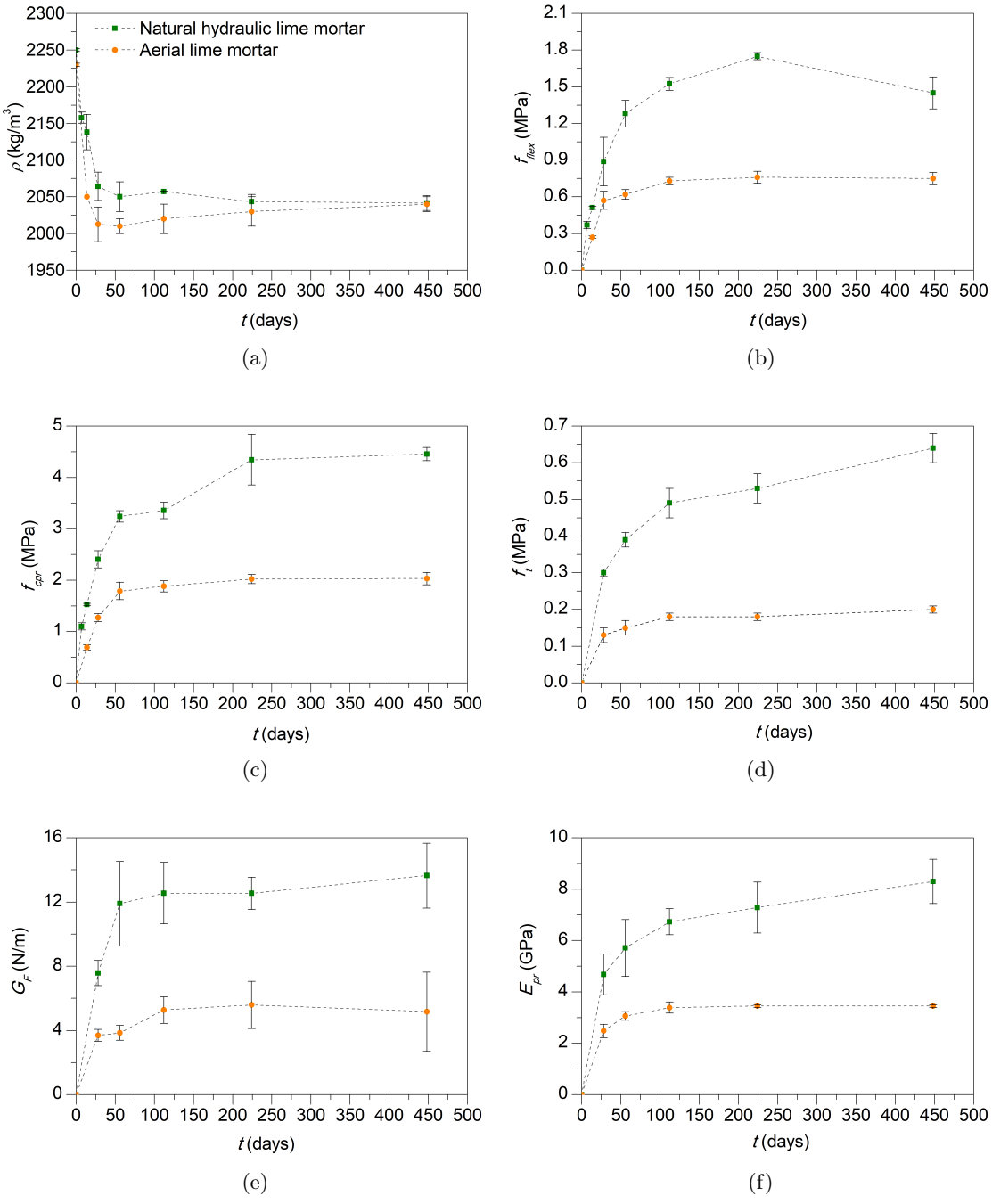

Figure 5.1: Evolution of the physical and mechanical properties of both natural hydraulic and aerial lime mortars: (a) density, (b) flexural strength, (c) compressive strength from prisms, (d) splitting tensile strength, (e) fracture energy, (f) elastic modulus from prisms.

5.3.2. Non-dimensional evolution of density and mechanical properties

Non-dimensional tendencies of the evolution of the mechanical properties of both lime mortars with respect to their corresponding values at 28 days were obtained by the least square method, see Figure 5.2. Moreover, empirical equations are also proposed, as shown in Eq. 5.3 and Table 5.2. The mechanical properties at 28 days were selected as references, due to the fact that they are measured in general according to the standard [31]. It is worth noting that the natural hydraulic and aerial lime mortars of this research have only reached at this age 54% and 62%, respectively, of their corresponding compressive strengths at 448 days.

From Figure 5.2, it is observed that the relative increase of all mechanical properties tested is higher for the natural hydraulic lime mortar than that for the aerial one, especially, after 28 days. For example, at 448 days, the non-dimensional compressive strength is around 14% higher for the natural hydraulic lime mortar than the aerial one, while the splitting tensile strength is 26% higher for the former. This is mainly due to the hydration of dicalcium silicates, C_2S, that contributes to the strength of natural hydraulic lime mortars after 28 days [8, 17]. The tendency of the flexural strength for the natural hydraulic lime mortar is obtained up to 224 days. As explained in Section 5.3.1, the corresponding results at 448 days were irregular, so they were not included in the fitting to obtain the empirical formula. For such a reason, the tendency is estimated according to the expected regular behavior after 224 days (green dashed line in Figure 5.2b). It is obvious that these empirical equations would be useful for the numerical simulations of the long-term behavior of masonry structures built with aerial or natural hydraulic lime mortars presenting a lime/aggregate ratio of 1:3 and limestone aggregates.

$$\frac{Y}{Y_{28}} = q\left(\frac{t}{t_0}\right)^r \tag{5.3}$$

t_0= 28 days.

Table 5.2: Coefficients for Equation (5.3).

	Natural hydraulic lime mortar		Aerial lime mortar	
Y	q	r	q	r
f_{flex}	0.99	0.27	0.88	0.19
f_{pr}	0.94	0.28	1.00	0.21
f_t	1.08	0.25	1.05	0.15
G_F	1.18	0.18	1.05	0.11
E_{pr}	1.05	0.19	1.10	0.10

5.3.3. Evolution of the carbonation depth

The evolution of the carbonation depth on the natural hydraulic and aerial lime mortar samples by means of the phenolphthalein method can be observed in Figures 5.3 and 5.4, respectively. The results of this method must be treated with care because the carbonation front is not sharply defined as the reaction tends to proceed along cracks and voids beyond the front; however, it is still a suitable method to study the progress of carbonation [61, 146, 151]. For the natural hydraulic lime mortar, the carbonation depth was also measured at 7 days but it is not included in the thesis as almost the whole surface turned a purple color meaning that the specimens were not carbonated at such early age. From Figures 5.3 and 5.4, it is observed that the carbonation process does not start until 14 or 28 days (shown by a narrow unstained area in the sample borders). Due to the fact that the carbonation process only begins once excess pore blocking water is evaporated [55, 58, 61, 64, 148]. Thus, little carbonation can occur before 14 days. For the natural hydraulic lime mortar, the carbonation process continues progressively from the outside to inward [54] up to 448 days, as shown by the increase of the unstained depth in Figure 5.3. It shows that the

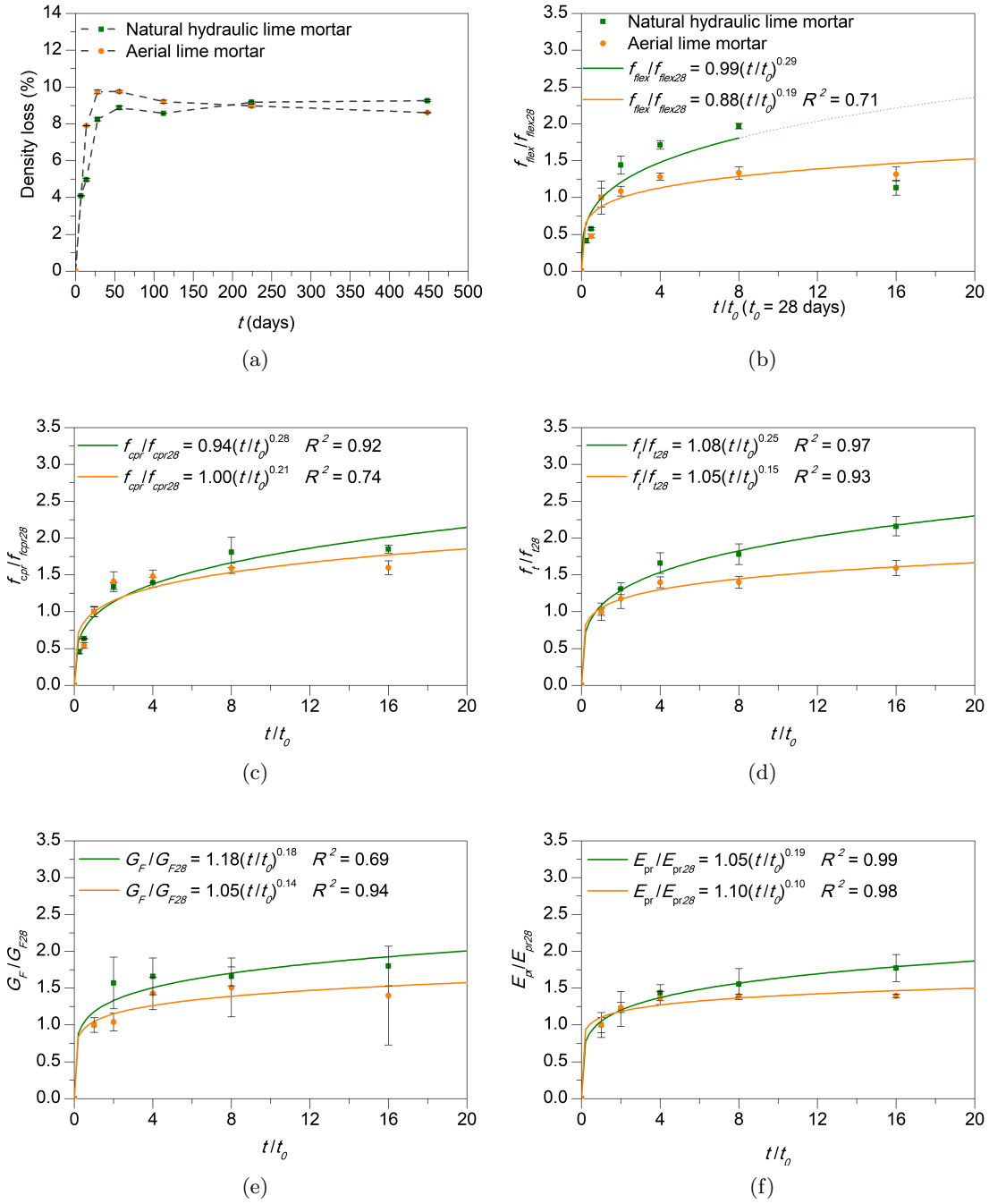

Figure 5.2: (a) Density loss of both natural hydraulic and aerial lime mortars with time. (b-f) Non-dimensional graphs of the evolution of the mechanical properties of the mortars with respect to their corresponding values at 28 days: (b) flexural strength, (c) compressive strength from prisms, (d) splitting tensile strength, (e) fracture energy, (f) elastic modulus from prisms.

shape of the carbonation front can be irregular, especially as the time passes and it usually gets wider at the surface where the specimen is laid as the atmospheric CO_2 is prevented from getting inside [146]. For the aerial lime mortar, instead, it can be observed a configuration similar to the Liesegang pattern from 112 to 448 days (Figure 5.4).

(a) 14 Days (b) 28 Days (c) 56 Days

(d) 112 Days (e) 224 Days (f) 448 Days

Figure 5.3: Carbonation degree of natural hydraulic lime mortar at different days.

(a) 14 Days (b) 28 Days (c) 56 Days

(d) 112 Days (e) 224 Days (f) 448 Days

Figure 5.4: Carbonation degree of the aerial lime mortar at different days.

This phenomenon is a "quasi-periodic self-organised precipitation of a sparingly soluble product in the wake of a moving reaction front" [64, 152, 153]. This pattern consists in concentric rings of stained and unstained material. The pale rings represent areas with a higher level of carbonation

than the purple ones [64]. This phenomenon is more typical of calcium lime in the putty form, specially the aged one that is stored for long time under water, but it can also happen, more rarely and not so clear, in calcium lime in the form of powder at long curing days [134, 146] as in the case of this research. More information about Liesegang pattern can be found in [64, 146, 152, 153]. At 448 days, it is observed that there are still purple areas in both mortars, in the core of the sample of the natural hydraulic lime mortar and in the form of Liesengang pattern, as explained, for the aerial lime one. This shows that there is still some remaining portlandite in the mortars and therefore the carbonation process could continue beyond 448 days [58, 64].

5.4. Conclusions

This chapter studies the evolution of some physical and mechanical properties of a natural hydraulic and an aerial lime mortars, with a lime/aggregate ratio of 1:3, up to 448 days. Seven properties, such as, density, flexural, compressive and splitting tensile strengths, fracture energy, elastic modulus from prisms and carbonation depth by means of the phenolphthalein method were assessed at different instants. The results show that for both mortars there is a faster increase of their mechanical properties up to 56 days. Then, the increase of their mechanical properties is more moderate but progressive up to 224 days. From this age to 448 days, the evolution of the mechanical properties is very slow for the aerial lime mortar while it shows a slight increase for the natural hydraulic one. At this age, still some portlandite remains as shown by the phenolphthalein method. Furthermore, some empirical equations were obtained to describe the evolution of the mechanical properties, which could be useful for numerical simulations with natural hydraulic and aerial lime mortars presenting a lime/aggregate ratio of 1:3, as they are the most common in historical masonry constructions.

Chapter 6

Loading rate effect on the fracture properties of a natural hydraulic and an aerial lime mortars

Article title: Loading rate effect on the fracture response of natural hydraulic and aerial lime mortars
Authors: Xiaoxin Zhang, Lucía Garijo, Gonzalo Ruiz, José J. Ortega
Journal: Journal of Materials in Civil Engineering
Submitted: 09/07/2019

Loading rate effect on properties of steels and concretes has been studied extensively, but for lime mortars such information is scant. This chapter presents the rate effect on the fracture behaviors of a natural hydraulic lime mortar and an aerial one, under three different loading rates (loading-point displacement rates, 5.0×10^{-4} mm/s, 5.0×10^{-1} mm/s and 1.6×10^{1} mm/s). The results show that the peak load and fracture energy are rate sensitive. The maximum dynamic increase factors of the peak load are 1.4 and 1.6 for the natural hydraulic and the aerial lime mortars, respectively, whereas it is 1.9 for the fracture energy for both mortars. Moreover, the increase in the peak load and fracture energy of the natural hydraulic lime mortar is mainly due to the viscous effect of free water in the mortar. However, for the aerial lime mortar, the rate effect is related chiefly to the crack growth and velocity.

Keywords: Lime mortars, Fracture energy, Loading rate, Dynamic Increase Factor (DIF).

6.1. Introduction

The studies on the dynamic mechanical behavior of lime mortars are scant, especially for fracture energy, though it is an important parameter to characterize ductility and fracture behavior of the material. Thus, in order to disclose the rate effect on the fracture energy, in the chapter, a natural hydraulic and an aerial lime mortar beams were tested at various loading rates by using a servo-hydraulic testing machine, from the quasi-static one, 5.0×10^{-4} mm/s, to rate sensitive ones, 5.0×10^{-1} mm/s and 1.6×10^{1} mm/s. The results show that the peak load and fracture energy of both lime mortars are rate sensitive. Moreover, the morphology of fracture surfaces was analyzed by Scanning Electron Microscope (SEM) analysis, and the intergranular failure was observed at low and fast loading rates. Furthermore, in order to check the mechanism of rate effect, some specimens were dried at 105°C and tested at 5.0×10^{-4} mm/s and 1.6×10^{1} mm/s.

The rest of the chapter is organized as follows. The next section describes the experimental procedure. Experimental results are presented and analyzed in Section 6.3, in Section 6.4 some conclusions are extracted.

6.2. Experimental procedure

6.2.1. Raw materials

The same natural hydraulic and aerial limes as those presented in previous chapters were used according to EN 459-1 [12]. The natural hydraulic lime was a commercial one of class NHL 3.5, and was provided by "Socli, Italcementi Group" (France). It had an apparent density of 850 kg/m^3. The aerial one was of class CL 90-S, and was supplied by "Calcasa Calcinor" (Spain). It had an apparent density of 490 kg/m^3. Their chemical and mineralogical analyses and laser particle size distribution curves can be seen in Chapters 2 (Table 2.1, Figures 2.1 and 2.2) and 3 (Table 3.1, Figures 3.1 and 3.2), respectively.

The aggregate used was a common commercial crushed limestone with particle size distribution curve as presented in Figure 2.3 , determined in accordance with EN 1015-1 [84]. It had an apparent particle density of 2680 kg/m^3 according to EN 1097-6 [85] (Figure 2.4b) and an apparent density of 1820 kg/m^3 according to EN 1097-3 [86] (Figure 2.4c).

6.2.2. Fabrication of the natural hydraulic and aerial lime mortars

For both mortars, the lime/aggregate ratio was 1:3 by volume, following the traditional treatises, and the water/lime ratio of 0.9 by volume was selected to obtain a plastic consistency from 140 mm to 200 mm, determined by the flow table test, according to the standards EN 1015-3 [88] and EN 1015-6 [89]. That is to say, the consistency was 150-155 mm for the natural hydraulic lime mortar and 140-150 mm for the aerial one. It is worth noting that the volume proportions of compounds were converted to weight for obtaining a convenient measurement during the fabrication process, as shown in Table 6.1.

Table 6.1: Composition of mortars.

Type of lime mortar	Lime/aggregate ratio (by volume)	Lime/aggregate ratio (by weight)	Water/lime ratio (by volume)	Water/lime ratio (by weight)	Curing conditions
Hydraulic	1:3	0.16	0.9	1.05	56 days in HC
Aerial	1:3	0.09	0.9	1.84	7 days in HC and 49 days in AC

Note. HC: Humid chamber (RH 97 ± 0.5%, 20 ± 0.5°C), AC*: Ambient laboratory conditions (RH 50 ± 10%, 23 ± 2°C).

Prismatic specimens (40 mm × 40 mm × 160 mm) were cast and cured following the standard EN 1015-11 [31] for the tests. For the purpose, a vertical axis mortar mixer with sufficient capacity was used so as to cast one batch per mortar type within this chapter. Natural hydraulic lime mortar specimens were just cured 56 days in the humid chamber (RH 97 ± 0.5% and 20 ± 0.5°C) with the first two days in the molds, while aerial lime mortar beams were cured initially five days with molds, then two days without molds in the humid chamber and finally in the ambient laboratory conditions (RH 50 ± 10% and 23 ± 2°C) until reaching 56 days for the tests (see Table 6.1).

6.2.3. Mechanical tests on lime mortars

Flexural and compressive strengths

As explained in Chapter 2, the flexural and compressive strengths were measured according to the standard EN 1015-11 [31] at the quasi-static loading conditions by using an Instron 1011 testing machine. The loading rates were 10 N/s and 50 N/s for the flexural and compressive tests, respectively [41, 80]. Moreover, they are also the minimum ones specified by the standard. Initially, three beams without notch were tested for obtaining the flexural strength, and then, six remaining

Table 6.2: Various types of tests for mechanical properties of each lime mortar.

Type of test	Mechanical property	Specimen size	Notch/ depth	Loading rate	Type of specimen	No. of test
Three-point bending test	Flexural strength	40 mm × 40 mm × 160 mm	-	10 N/s	Normal*	3
Compressive test	Compressive strength	Remaining half–prisms	-	50 N/s	Normal	6
Three-point bending test	Fracture energy	40 mm × 40 mm × 160 mm	0.5	5.0×10^{-4} mm/s	Normal	3
					Dry**	3
				5.0×10^{-1} mm/s	Normal	3
				1.6×10^{1} mm/s	Normal	3
					Dry	3

*Normal specimens: cured in the humid chamber (RH 97 ± 0.5%, 20 ± 0.5°C) for 56 days in the case of the natural hydraulic lime mortar, and for 7 initial days in the humid chamber and 49 days in the ambient laboratory conditions (RH 50 ± 10%, 23 ± 2°C) in the case of the aerial lime mortars.

**Dry specimens: specimens cured for 56 days as the corresponding normal ones and then dried in an oven for two days at 105°C.

half–prisms were used to perform compressive tests to determine the compressive strength at the age of 56 days.

Fracture energy

Fracture energy is defined as the energy required to open an unit area of crack surface. It was measured by a three-point bending following the RILEM recommendations [93] and the improvements proposed by Planas, Guinea and Elices [94–96]. A pre-cast notch in the middle of the beam was made by using a cardboard piece (2 mm in thickness and 20 mm in depth) during the fabrication. That is to say, the notch-depth ratio was 0.5. More detailed information on how to determine the fracture energy can be found in Chapter 2 and in the references [41, 80].

The tests were performed in the displacement control. In order to study the rate effect on the fracture energy, three various loading rates were applied during the test from a quasi-static level (5.0×10^{-4} mm/s) to rate dependent (dynamic) levels (5.0×10^{-1} mm/s and 1.6×10^{1} mm/s). In such a way, it took around 30 minutes and 0.3 second to finish the tests for the lowest and fastest loading rates, respectively. Three beams were tested at each loading rate, as shown in Table 6.2. The corresponding strain rate, $\dot{\varepsilon}$, can be calculated approximately according to the Eq. (6.1) [154].

$$\dot{\varepsilon} = \frac{6(D-a)\dot{\delta}}{S^2} \tag{6.1}$$

where $\dot{\delta}$ stands for the loading rate, D and S are the beam depth and span, respectively. a is the notch depth.

Moreover, six dried beams for each type of lime mortar were tested at the lowest and highest loading rates, so as to check if the movement of free water (viscous effect) would influence the mechanical properties due to the fact that it is the mechanism of rate sensitivity of concrete under such loading rate range [72, 98, 119, 154].

6.3. Results and discussion

6.3.1. Quasi-static flexural and compressive strengths

The properties measured for both natural hydraulic and aerial lime mortars are shown in Table 6.3, where f_{flex} and f_c are the flexural and compressive strengths, respectively. It is obvious that the mechanical properties of the natural hydraulic lime mortar are more than two times of the aerial lime mortar. This is mainly due to the different chemical composition and hardening way as mentioned in the Introduction. That is to say, hydraulic lime mortars harden by carbonation and hydration, while aerial lime mortars only harden due to carbonation. Moreover, the water content in percentage of the specimens was obtained comparing their corresponding normal and dry weights.

Table 6.3: Properties of the lime mortars.

Type of lime mortar	f_{flex} (MPa)	f_c (MPa)	Water content (%)
Natural hydraulic	1.1 (0.1)	3.1 (0.2)	2.52 (0.24)
Aerial	0.54 (0.01)	1.30 (0.03)	0.32 (0.08)

Note: values in parenthesis are standard deviations.

6.3.2. Loading rate effect on the fracture behavior of the lime mortars

Figure 6.1 shows the comparison of the load-displacement (deflection) curves at different loading rates for each lime mortar. From the figure, it is observed that the peak load increases with the increase in the loading rate. The stiffness presents the similar tendency as well. It is worth noting that each curve represents the average of three ones corresponding to the tests.

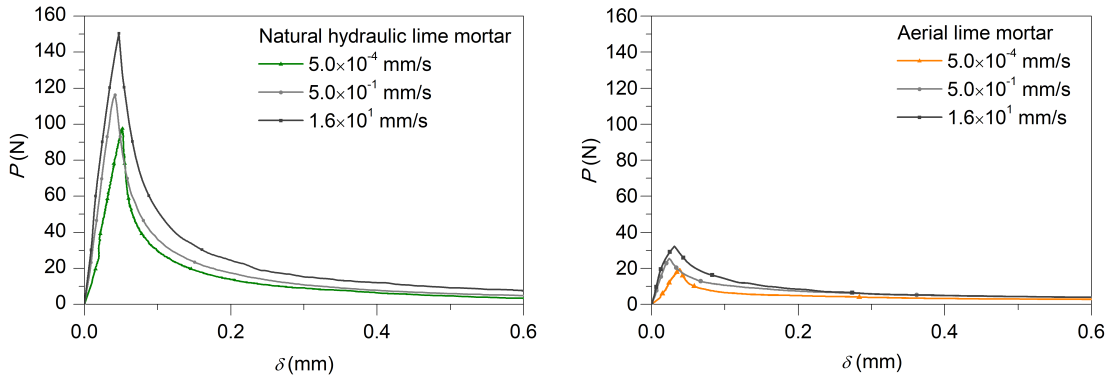

(a) (b)

Figure 6.1: Load-displacement curves at various loading rates (a) natural hydraulic lime (b) aerial lime mortars.

Table 6.4 provides detailed information about the experimental results of the natural hydraulic and aerial lime mortars at various loading rates. The DIF is defined by the ratios of peak load (P_{max}) and fracture energy (G_F) to their corresponding quasi-static values. Herein, the lowest loading rate ($\dot{\delta} = 5.0 \times 10^{-4}$ mm/s) is set as the quasi-static condition. Moreover, an estimation of the corresponding strain rates ($\dot{\varepsilon}$) for various loading rates is also listed in the table, which would be helpful for the comparison with experimental results in the literature under different loading methods. Figure 6.2 shows the peak load and fracture energy at three loading rates for the natural

hydraulic lime and aerial lime mortars. From Table 6.4 and Figure 6.2, it is obvious that the peak load and fracture energy increase with an increase in loading rates for both mortars. The values of DIF are quite similar though the natural hydraulic lime mortar has much higher mechanical properties than that of the aerial lime mortar. For example, at the loading rate 1.6×10^{1} mm/s, for the peak load, they are 1.4 and 1.6, respectively for the natural hydraulic and the aerial lime mortars. However, they are 1.9, the same for the fracture energy.

Table 6.4: Experimental results at different loading rates.

Type of lime mortar	$\dot{\delta}$ (mm/s)	P_{max} (N)	DIF for P_{max}	G_F (N/m)	DIF for G_F	$\dot{\varepsilon}$ (s^{-1})
Natural Hydraulic	5.0×10^{-4}	99 (10)	1.0	12.2 (1)	1.0	6×10^{-6}
	5.0×10^{-1}	120 (10)	1.2	17.3 (1)	1.4	6×10^{-3}
	1.6×10^{1}	140 (15)	1.4	22.8 (6)	1.9	2×10^{-1}
Aerial	5.0×10^{-4}	21 (4)	1.0	3.0 (1)	1.0	6×10^{-6}
	5.0×10^{-1}	26 (3)	1.2	4.0 (1)	1.3	6×10^{-3}
	1.6×10^{1}	32 (2)	1.6	5.7 (1)	1.9	2×10^{-1}

Note: values in parenthesis are standard deviations.

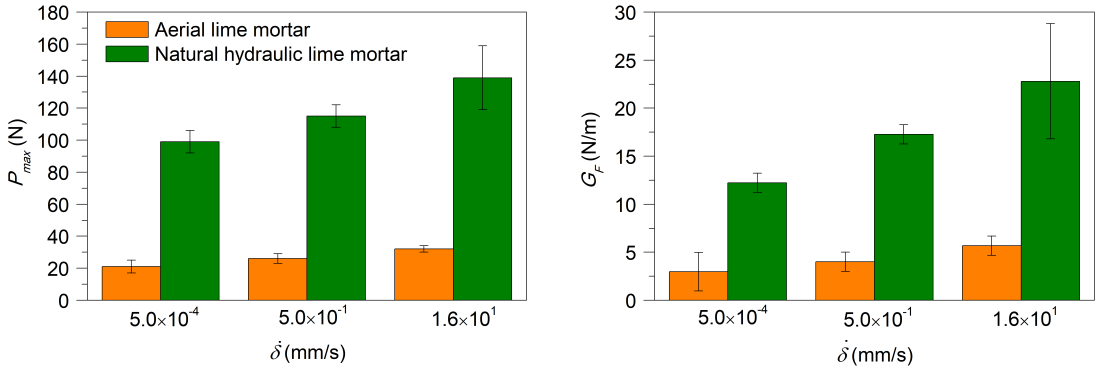

Figure 6.2: (a) Peak load and (b) fracture energy of the lime mortars at different loading rates.

The tendency of the rate effect on the peak load and fracture energy is also presented in Figure 6.3. Moreover, a curve fitting of the DIF for each lime mortar in regard to the peak load and fracture energy is derived from the experimental results as shown in Eqs.(6.2, 6.3) by using the least-squares method. The correlation coefficient is over 95%. Though the format of such equation was original for plain and steel fiber-reinforced concretes considering rate effect on mechanical properties [72, 98, 119, 154], it is still useful for lime mortars.

$$DIF_P = 1 + s\left(\frac{\dot{\delta}}{\dot{\delta}_0}\right)^u \tag{6.2}$$

$$DIF_{G_F} = 1 + v\left(\frac{\dot{\delta}}{\dot{\delta}_0}\right)^w \tag{6.3}$$

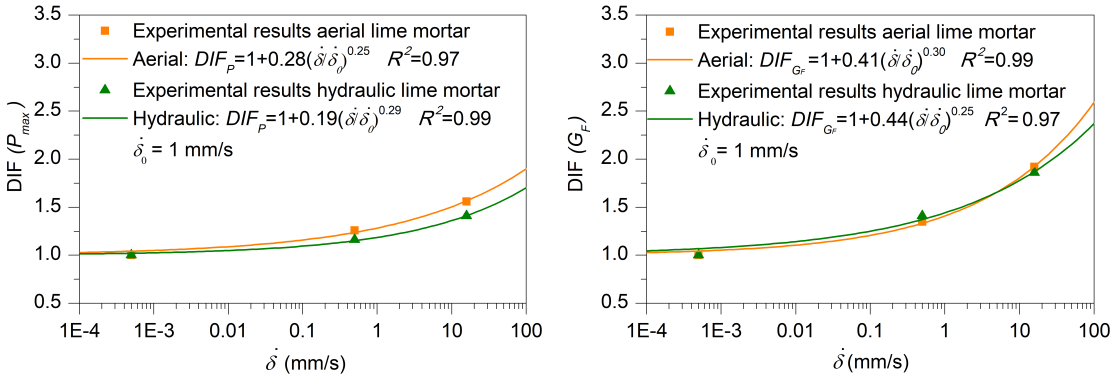

(a) (b)

Figure 6.3: Loading rate effect (a) on the peak load and (b) on fracture energy of the mortars.

where $\dot{\delta}$ is the loading rate in mm/s, $\dot{\delta}_0$ is set as 1 mm/s. Thus, the adjustment parameters s, u, v and w do not have units. The adjusting values of the parameters are listed in Table 6.5. Such equations may be used to predict the rate effect on peak load and may also be helpful in performing numerical simulations involving fracture of these mortars.

Table 6.5: Values of adjustment parameters of equations.

Type of lime mortar	Peak load		Fracture energy	
	s	u	v	w
Natural hydraulic	0.19	0.29	0.44	0.25
Aerial	0.28	0.25	0.41	0.30

6.3.3. Failure pattern and morphology of fracture surfaces

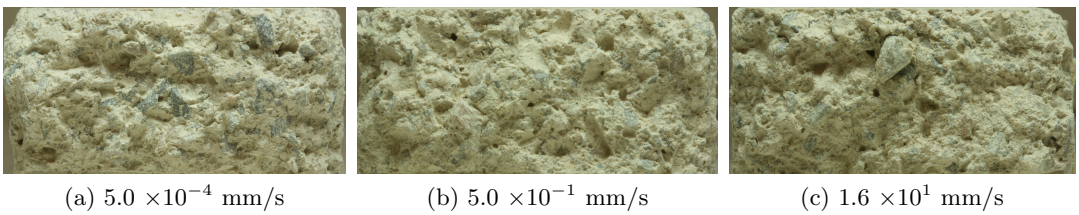

(a) 5.0 $\times 10^{-4}$ mm/s (b) 5.0 $\times 10^{-1}$ mm/s (c) 1.6 $\times 10^{1}$ mm/s

(d) 5.0 $\times 10^{-4}$ mm/s (e) 5.0 $\times 10^{-1}$ mm/s (f) 1.6 $\times 10^{1}$ mm/s

Figure 6.4: Morphology of fracture surfaces of the natural hydraulic and aerial lime mortars under various loading rates. (a-c) natural hydraulic lime mortar (d-f) aerial lime mortar.

All beams tested present flexural failure pattern. Figure 6.4 shows the morphology of fracture surfaces of both lime mortars at various loading rates. All surfaces are similar in spite of the fact that there is a difference of five orders of magnitudes in the loading rates. Moreover, no broken aggregates are found by naked eyes. That is to say, the crack path passes around the aggregate (intergranular fracture), not through it (transgranular fracture). In order to confirm this phenomenon, SEM analysis was performed by using a microscope Quantta 250 on two samples of the natural hydraulic lime mortar, corresponding to the lowest and highest loading rates, due to the fact that the natural hydraulic lime mortar has better mechanical properties than the aerial lime mortar. Figure 6.5 presents such photos at the loading rates 5.0×10^{-4} mm/s and 1.6×10^{1} mm/s. It is clear that the intergranular failure is detected for both cases.

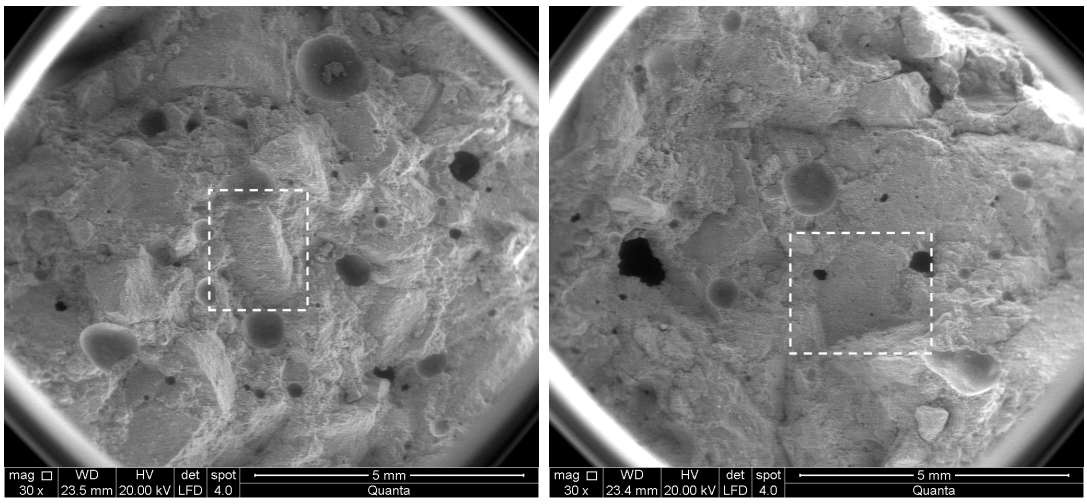

(a) 5.0 $\times10^{-4}$ mm/s (b) 1.6 $\times10^{1}$ mm/s

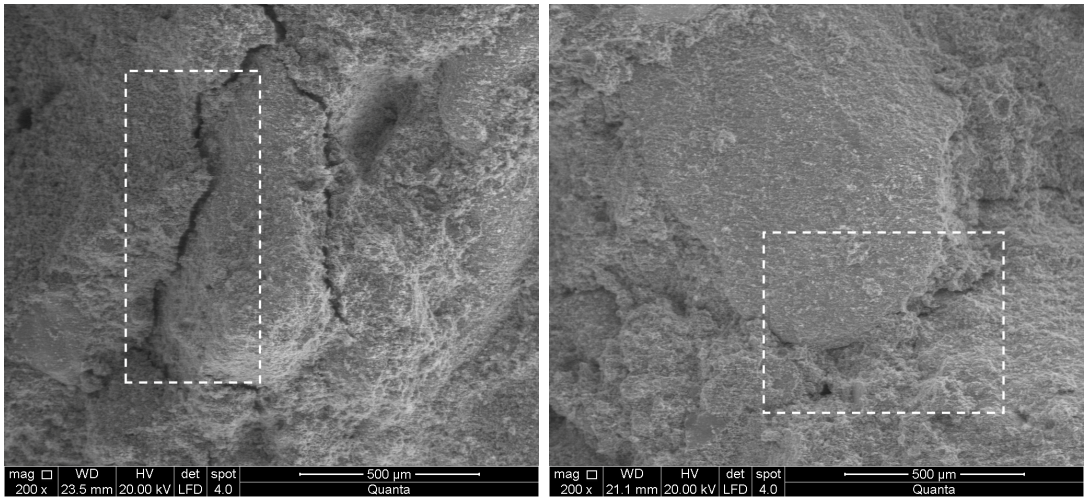

(c) 5 $\times10^{-4}$ mm/s (d) 1.6 $\times10^{1}$ mm/s

Figure 6.5: SEM photos on the hydraulic lime mortar: (a) and (c) specimen broken at 5.0×10^{-4} mm/s, (b) and (d) specimen broken at 1.6×10^{1} mm/s. White squares show evidences of intergranularity.

6.3.4. Mechanisms of the rate sensitivity

In general, at low loading rates, not impact condition, the rate sensitivity of concrete is usually ascribed to two causes. One is the viscous time-dependent movement of free water through voids

and pores, the other is the time-dependent nature of crack growth relative to loading rate [117]. However, for lime mortars, the mechanism of the rate effect on mechanical properties has not been studied yet. Thus, in order to check the influence of the movement of free water on the rate effect, six beams for each lime mortar were dried for 48 hours at 105°C in an oven, then, tested at quasi-static loading rate 5.0×10^{-4} mm/s and the highest one 1.6×10^{1} mm/s, respectively. Three tests were performed at each loading rate.

The detailed experimental results at two loading rates are presented in Table 6.6. Moreover, the comparison of the maximum DIF between normal and dry lime mortars is shown in Figure 6.6. It is obvious that the rate effect of the natural hydraulic lime mortar is mainly related with the movement of free water in pores. For example, for the dry natural hydraulic lime mortar, the peak load is almost constant at different loading rates, a 30% increase in fracture energy. However, for the normal hydraulic lime mortar, the DIFs of the peak load and fracture energy are 1.4 and 1.9, respectively.

In Figure 6.6 and Table 6.6., the DIFs of the peak load between the normal and dry aerial lime mortars are the same as 1.6. Thus, it is clear that the movement of free water in pores does not influence the rate sensitivity of the aerial lime mortar, it would be related with the crack growth and velocity. That is to say, the crack path is altered with higher resistance under high loading rates. It is also worth noting that the free water content of the hydraulic lime mortar, 2.52%, is much greater than that of the aerial lime mortar, 0.32%.

Table 6.6: Mechanical properties of the dry natural hydraulic and aerial lime mortars at quasi-static (5.0×10^{-4} mm/s) and the highest loading rates (1.6×10^{1} mm/s).

Type of lime mortar	$\dot{\delta}$ (mm/s)	P_{max} (N)	DIF for P_{max}	G_F (N/m)	DIF for G_F
Natural hydraulic	5.0×10^{-4}	110 (20)	1.0	17.9 (2)	1.0
	1.6×10^{1}	110 (10)	1.0	22.5 (7)	1.3
Aerial	5.0×10^{-4}	19 (1)	1.0	3.3 (1)	1.0
	1.6×10^{1}	30 (4)	1.6	3.7 (1)	1.1

Note: values in parenthesis are standard deviations.

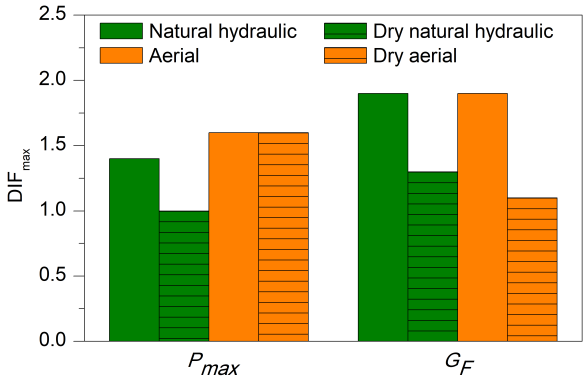

Figure 6.6: Comparison of the DIF obtained for the different lime mortars.

Furthermore, comparing Tables 6.4 and 6.6 (rate effects on normal and dry specimens, respectively), it is observed that the peak load of the natural hydraulic lime mortar at quasi-static loading rate increases from the normal to the dry specimens, that is to say, from 99 N to 110 N. This tendency is similar with observations in brick masonry and concrete ([138, 139]), due to the

fact the internal pressure in pores decreases with the reduction in water content during the drying process. For the aerial lime mortar, instead, this phenomenon is not appreciable as the water content in the normal situation was already very low (0.32%) compared with 2.52% of the natural hydraulic lime mortar.

6.4. Conclusions

This chapter focuses on the fracture behavior of a natural hydraulic and aerial lime mortars with a lime/aggregate ratio of 1:3, under three various loading rates, 5.0×10^{-4} mm/s, 5.0×10^{-1} mm/s and 1.6×10^{1} mm/s. The results show that both lime mortars are rate sensitive, that is to say, their peak load and fracture energy increase with an increase in loading rates. The DIFs on the peak load and fracture energy of both mortars are quite similar although the mechanical properties of the natural hydraulic lime mortar are much higher than the ones of the aerial one. The DIFs of the peak load are 1.4 and 1.6 for the natural hydraulic and aerial lime mortars at the highest loading rate, respectively, while it is 1.9 on the fracture energy for both mortars. Moreover, according to SEM analysis on the fracture surfaces of both lime mortars at 5.0×10^{-4} mm/s and 1.6×10^{1} mm/s, the crack advances around the aggregates due to the fact that the strength of the matrix and the bond zone are much lower than that of the aggregates. Namely, the crack path is intergranular regardless of the loading rate.

Two empirical equations for the rate sensitivity of the peak load and fracture energy are provided for each lime mortar. They would be helpful in numerical simulations that evaluate the loading rate effect on the fracture behavior of these mortars.

Regarding the mechanism of the rate effect, through the comparison of experimental results on the dry and normal beams at loading rates 5.0×10^{-4} mm/s and 1.6×10^{1} mm/s for both lime mortars, it is inferred that the rate sensitivity of the natural hydraulic lime mortar is mainly because of the viscous effects caused by the presence of free water in the porous structure. However, it is primarily due to the crack growth and velocity for the aerial lime mortar.

Chapter 7

Geometry and size effects on the compressive strength of natural hydraulic lime mortars; cohesive simulation of their failure behavior

Article title: Advanced mechanical characterization of NHL mortars and cohesive simulation of their failure behavior
Authors: Lucía Garijo, Xiaoxin Zhang, Gonzalo Ruiz, José J. Ortega, Rena C. Yu
Journal: Construction and Building Materials
Submitted: 11/11/2016
Accepted: 13/07/2017
DOI: 10.1016/j.conbuildmat.2017.07.127
Available at: http://dx.doi.org/10.1016/j.conbuildmat.2017.07.127

In view of the difference obtained in the compressive strengths of prisms and cylinders for the natural hydraulic lime mortars, an advanced mechanical characterization of two NHL mortars, with water/lime ratios of 0.8 and 1.1, is reported, including direct measurement of the compressive strength on both types of specimens. The results are significantly lower for the higher water/lime ratio. Besides, the compressive strength depends very much on the type of specimen used. A cohesive simulation is performed to prove that such variations in the compressive strength are due to the effect of the shape and size of the specimen. Furthermore, a numerical simulation of the three-point bending test (TPB) on such mortars show that they behave as cohesive materials. Their corresponding softening laws are adjusted to a bilinear model.

Keywords: Natural Hydraulic lime (NHL) mortar, Water/lime ratio, Mechanical characterization, Fracture energy, Size effect, Cohesive simulation

7.1. Introduction

Once the mechanical properties of the natural hydraulic lime mortars presented in Chapter 2 are obtained, the aim of this chapter is to model the mortar's failure behavior using cohesive models. In particular, we focused on the two mortars with extreme water/lime ratios, such as the ones with 0.8 and 1.1, respectively. Then, we numerically reproduced the load vs crack mouth-opening curves of the fracture tests, simulated the compressive tests on prisms and performed a size-effect study. It shows that the differences in the values of the compressive strength from the two types of test stem from the effects of the size and shape of the specimen. The numerical model is also used to obtain a reference value for the compressive strength that can be considered a true material property. It roughly coincides with the value obtained from cylinders. Furthermore, the numerical simulation of the TPB test show that the material presents a cohesive behavior.

The rest of the chapter is organized as follows. Next section describes the experimental procedure. Experimental results are presented and analyzed in Section 7.3. In Section 7.4 a thorough numerical analysis and discussion are provided. Finally, some conclusions are extracted in Section 7.5.

7.2. Experimental procedure

7.2.1. Raw materials

The natural hydraulic lime used is the same one as in previous chapters, a commercial lime of class NHL 3.5, according to EN 459-1 [12]. It has a density of 2580 kg/m^3 and an apparent density of 850 kg/m^3. Its laser particle size distribution curve, chemical and mineralogical analyses are shown in Chapter 2 (see Figure 2.2, Table 2.1 and Figure 2.1, respectively).

The sand used was the same one as presented in previous chapters, a commercial crushed limestone common sand. The particle size distribution curve, determined according to EN 1015-1 [84] is presented in Figure 2.3. The sand has an apparent particle density of 2680 kg/m^3 according to EN 1097-6 [85] (Figure 2.4b) and an apparent density of 1820 kg/m^3 according to EN 1097-3 [86] (Figure 2.4c).

7.2.2. Mortar composition and preparation

Table 7.1: Mortars compositions

Mortar	Lime/aggregate ratio by volume	NHL (kg)	Aggregate (kg)	Water (m^3)	Water/lime ratio by volume	Water/lime ratio by weight
H08C04M	1/3	3.40	21.80	3.20	0.8	0.94
H11C04M	1/3	3.40	21.80	4.40	1.1	1.29

Two mortar compositions were studied by using two water/lime ratios: 0.8 and 1.1 by volume. They were the same as those introduced in Chapter 2 as H08C04M and H11C04M, respectively. The lime/aggregate ratio used for both of them was the traditional one, 1:3 by volume. Volume proportions of compounds were converted in weight to avoid measurement imprecision on mixing process (see Table 7.1). The mortars were made with consistence of the flow table test of 130-135 mm and 238-340 mm, dried and fluid, respectively, according to standard EN 1015-3 [88] (see Figure 2.6 c).

The mixture was performed according to standard EN 1015-2 [90]. We made 40 mm $\times$ 40 mm $\times$ 160 mm prisms and 75 mm in diameter and 150 mm in height cylinders using steel molds, which were lubricated with mineral oil to prevent adhesion of the mortar to the mold walls. The mortar was poured in two layers when using the prismatic moulds and in three layers when using the cylindrical ones, each compacted with 25 strokes of the tamper. In total, 18 prismatic and 6 cylindrical samples were prepared for each type of mortar. They were demolded two days later according to standard EN 1015-1 [84]. Curing was executed in the humidity chamber until the day of testing (RH 97 $\pm$ 0.5% and 20 $\pm$ 0.5 °C) so as to favor the hydration process of such hydraulic mortars [15, 57, 61].

7.2.3. Test procedures

The characteristics of the mortars were evaluated by laboratory tests. For fresh state the consistence was measured. For hardened state the flexural, compressive and splitting tensile strengths, elastic modulus, fracture energy and characteristic length were evaluated at 56 days as well as the open porosity. Carbonation depth by means of the phenolphthalein method were assessed in the

long term (at 614 curing days) in order to study the possible different carbonation process of prisms and cylinders.

The flexural and compressive strengths were determined according to EN 1015-11 [31]. Splitting tensile strength (f_t) was measured through quasi-static splitting tests (Brazilian tests) on four 40 mm × 40 mm × 80 mm prismatic halves resulting from the preceding bending test to measure the fracture energy and adapting the procedures recommended by EN 12390-6 [102] to lime mortar. The details of the observed fracture mechanisms are indicative of the test validity and they can be studied through the crack pattern, which is a single crack [106] (Figure 7.1). The elastic modulus was measured from the stress-strain diagrams of the compressive tests carried out on four cylinders which were 75 mm in diameter and 150 mm in height by adapting the recommendations of EN 12390-13 [92], which is intended for concrete. The fracture energy, G_F, was measured through three-point bending tests adapting the procedure recommended by RILEM [93] and the improvements proposed by Planas, Guinea and Elices [94–96]. Finally, the characteristic length of lime-based mortars was also calculated in this research as already explained, Eq. 2.6 [107]. More detail information on the experimental procedure to obtain such mechanical properties is provided in Chapter 2 and references [41, 80].

Figure 7.1: Example of crack pattern in the Brazilian test.

Furthermore, open porosity measurements were carried out according to standard UNE 83980 [109] for concrete as a reference, determined by the water saturation test with a hydrostatic balance. Carbonation depth method was measured at an age of 614 days by means of the phenolphthalein method following procedures explained in Chapter 5. The purpose of such a test was to check possible differences in the carbonation process between prisms and cylinders.

7.3. Experimental results

7.3.1. Flexural and compressive strengths

The obtained results are presented in Table 7.2, where CV is the coefficient of variation and f_{flex}, f_{cpr} and f_{ccy} are, respectively, the average flexural and compressive strengths from prisms and from cylinders. Similar results of flexural and compressive strengths were obtained by other authors [8, 21, 25].

The results disclose how the water/lime ratio affects the mechanical response. Comparing the results for a water/lime ratio of 0.8 and for 1.1, it can be seen that the flexural strength decreases by 33%, the compressive strength from prisms by 61% and the one from cylinders by 48%. This can be attributed to the fact that both the carbonation rate of calcium hydroxide and calcium silicate hydrates in NHL paste present a downward trend with an increase in the water/lime ratio [48]. Comparing with the obtained results of open porosity, it can be observed that as the water/lime ratio increases, the open porosity also increases with a decrease of the mechanical properties of the material.

As observed in Table 7.2, a significant difference has been found in the compressive strength from prisms (f_{cpr}) and cylinders (f_{ccy}). Their ratio can be as high as 1.6. Considering that the

Table 7.2: Mechanical properties of two different NHL mortars.

Mechanical properties	H08C04M		H11C04M		$\frac{(1)-(2)}{(1)}$(%)
	Mean (1)	CV(%)	Mean (2)	CV(%)	
Flexural strength, f_{flex} (MPa)	1.33	7	0.89	5	33
Compressive strength of prisms, f_{cpr} (MPa)	4.2	6	1.7	4	61
Compressive strength of cylinders, f_{ccy} (MPa)	2.7	12	1.4	8	48
Splitting tensile strength, f_t (MPa)	0.51	1	0.24	12	54
Elastic modulus, E (GPa)	5.4	10	2.8	25	49
Fracture energy, G_F (N/m)	12.7	9	4.9	16	61
Characteristic length, ℓ_{ch} (mm)	260	$24^{(*)}$	240	$50^{(*)}$	10

$^{(*)}$ Calculated from its error as a derived magnitude.

variations of density and open porosity of both specimens are around 1% and 0.4%, respectively (see Table 2.6 of Chapter 2), the fabrication process should not result in a such large difference. Our hypothesis is that this difference is mainly due to geometry and size effects [78, 80]. This assumption will be verified through a numerical analysis in Section 7.4.

7.3.2. Splitting tensile strength, elastic modulus and fracture energy

The obtained results are presented in Table 7.2, where f_t is the splitting tensile strength, E is the elastic modulus obtained from the compressive test on cylinders and G_F is the fracture energy. Also in this case, the influence of the water/lime ratio can be observed. Comparing the results for a water/lime ratio of 0.8 and for 1.1, it can be seen that the splitting tensile strength decreases by 54%, the elastic modulus by 49% and the fracture energy by 61%.

7.3.3. Characteristic length

The characteristic length was derived from Eq. 2.6 and the results are presented in Table 7.2. The CV of this parameter was calculated from its error as a derived magnitude. The results were 24% for H08C04M and 50% for H11C04M. These values are reasonable as the characteristic length is an indirect magnitude.

7.3.4. Open porosity

The obtained open porosity for the two NHL mortars of water/lime ratios of 0.8 and 1.1 at 56 days was 25% and 30% respectively. It can be observed, how as the water/lime ratio increases, the porosity also increases and the mechanical properties decreases due to a weakening of the structure of the material, as already explained in Chapter 2.

7.3.5. Carbonation depth

As observed in Figure 7.2, no significant differences can be observed in the carbonation depth between prisms and cylinders in the long-term. Considering that both specimens are cured under high humid conditions (RH 97 $\pm$0.5% and 20 $\pm$0.5 °C) for the entire time, hydration has presumably been favored [57, 61]. Under such conditions, a possible different carbonation process between prisms and cylinders it not expected to have such a significant role so as to cause such a large difference in the compressive strengths of both specimens. Therefore, as mentioned in Section 7.3.1, our hypothesis is that the difference found in the compressive strengths of prisms and

cylinders is due to a possible size and geometry effect. Anyhow, further research concerning the performance of thermogravimetric analysis (TGA) and carbonation depth measurements through the phenolphthalein method in prisms and cylinders of natural hydraulic lime mortars at different curing periods and under different curing conditions would be of interest.

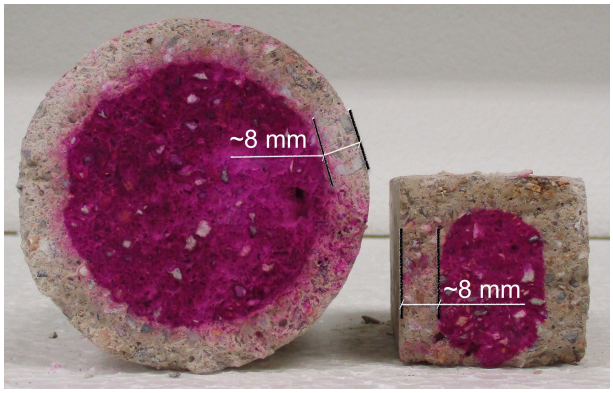

Figure 7.2: Carbonation depth by means of the phenolphthalein method in prisms and cylinders at 614 days.

7.4. Discussion and analysis

7.4.1. Numerical analysis

The composition and manufacturing process of NHL mortars lead to the hypothesis that their behavior in fracture corresponds to a cohesive material. The mechanical properties measured in this study would correspond with a cohesive material that is quite sensitive to the geometry size of the specimen, as the differences in the compressive strength from prisms and cylinders indicate [78, 155]. In particular, the characteristic length is quite larger than the depth of the prisms and than the diameter of the cylinders, which may mean that the extension of the fracture processes before failure are commensurate with the dimensions of the specimens.

In order to verify this and further improve the understanding of this material, an exhaustive numerical analysis was carried out by modelling two of the experimental tests: the three-point bending (TPB) test for measuring the fracture energy (G_F) and the compressive test for measuring the compressive strength on prisms (f_{cpr}), as described above.

7.4.2. Numerical model of the TPB test

The consideration of a NHL mortar as a typical cohesive material means that the appearance and propagation of cracks must be related to the progressive damage generated in what is known as the Fracture Process Zone (FPZ), directly governed by a softening law, that is a constitutive function that relates the tension transmitted across the lips of the crack with the crack opening, $\sigma(w)$. A numerical model of a TPB test needs this function as input data. By setting the proper softening curve, a good fit of the results yielded by such a model with the experimental ones would confirm the existence of a FPZ and a cohesive behavior.

The numerical simulation of the TPB test was made through a model successfully used in previous works [155–158], based on the smeared crack-tip method of Planas and Elices [77, 159]. It considers cohesive fracture, where only one discrete crack propagates. The numerical formulation consists in an improvement of the influence method of Petersson [160] by a triangulation of the system of equations which can be solved by direct substitution.

From the many expressions available in the bibliography, the bilinear softening law proposed by Guinea, Planas and Elices in [161] (Figure 7.3) was chosen, as it provides a good fit of the peak

load and the tail of a load-displacement curve. It is defined by four parameters: two of them are experimentally measured for both types of NHL mortar, the tensile strength f_t and the specific fracture energy G_F, and the other two are inferred as explained as follows. The slope of the initial section is defined by the intercept with the horizontal axis at $w = w_1$, see Figure 7.3. For the specific case of the beam geometry with $S = 2.5D$ and $a = D/2$, w_1 can be obtained as detailed as follows, while for a general case with $S = 4D$ and $a = D/2$ as in [161]. First, a coefficient β is interpolated from the model in reference [159] according to the value of the non-dimensional load P^*, defined as:

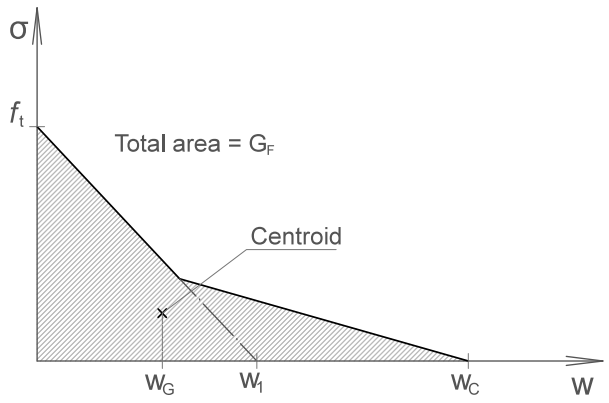

Figure 7.3: Bilinear softening law.

$$P^* = \frac{3SP_{max}}{2f_tBD^2} \tag{7.1}$$

where P_{max} is the maximum load obtained in the TPB test. Then, the variable l_1, with a nature similar to l_{ch}, is computed as:

$$l_1 = \frac{D}{\beta} \tag{7.2}$$

With l_1, w_1 is obtained as:

$$w_1 = 2\frac{f_t l_1}{E} \tag{7.3}$$

The rest of the defining points of the bilinear cohesive law is determined with the abscisa of the centroid of the area under the softening function w_G (Figure 7.3), which is computed as:

$$w_G = \frac{A}{G_F} \tag{7.4}$$

where A is the constant obtained by fitting the function defined with Eq. 7.5 to the tail of the $P - \delta$ curve to obtain the fracture energy. Such a function describes the asymptotic behavior of the curve approaching a load $P = 0$;

$$P = A(\frac{1}{\sigma^2} - \frac{1}{\sigma_u^2}) \tag{7.5}$$

where A is a constant, as already mentioned, P is the load, δ is the displacement of the load application point and δ_u is the displacement of the last point of the experimental $P - \delta$ curve to obtain the fracture energy. These measurements are referred to the axes labelled as $P_m - \delta_m$ in Figure 2.8, which are placed after the correction of the initial linear ramp of the experimental curve and making that $P = 0$ at the point $\delta = \delta_u$.

Finally, the critical crack opening w_c can be obtained from the previous defined parameters of the softening curve as:

$$w_c = \frac{3w_g G_F - 0.5 f_t w_1^2}{2G_F - w_1 f_t} - 2w_1 \tag{7.6}$$

The obtained parameters for both mortars to define the softening curves are shown in Table 7.3.

Table 7.3: Parameters of two NHL mortars to infer their softening curves.

Type of mortar	f_t (MPa)	G_F (N/mm)	w_1 (mm)	w_G (mm)
H08C04M	0.51	0.013	0.036	0.055
H11C04M	0.24	0.005	0.025	0.046

With the model adapted to the specific specimen dimensions and implementing the proper mechanical properties, the load-displacement and load-CMOD curves were obtained and compared with the experimental ones. The results for both NHL mortars are shown in Figure 7.4. In both cases, the numerical curves fit very well the experimental results, especially attending to initial slopes, maximum loads and curve tails, with even long overlapped sections. This validates the applicability of a softening law for this material and its cohesive fracture behavior.

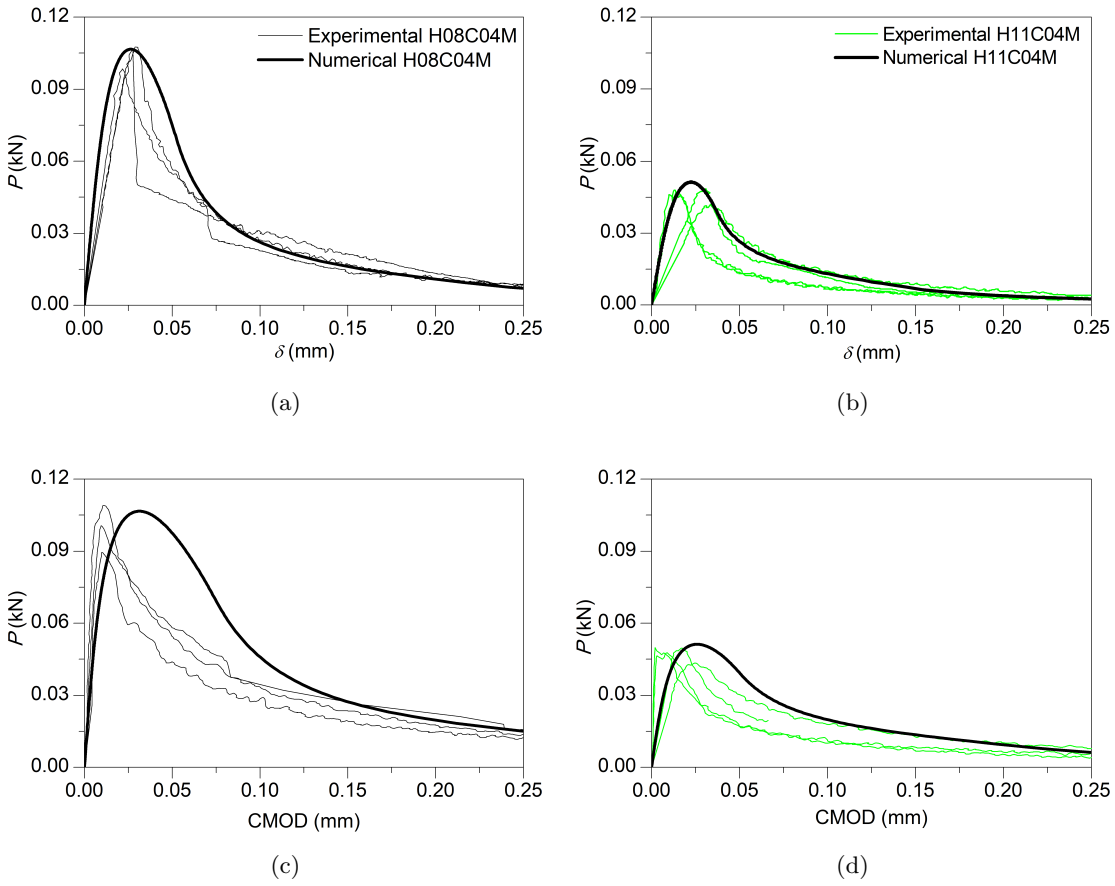

Figure 7.4: Experimental and numerical (a and b) load-displacement and (c and d) load-CMOD curves of (a and c) H08C04M and (b and d) H11C04M.

7.4.3. Numerical model of the compressive test on prisms

The interest in modeling the compressive test for prisms emerges from the difference observed between the values of compressive strength measured with these prisms and cylinders. Specifically, the strength given by prisms of the H08C04M mortar is almost the double of the strength obtained with cylinders. This could be due to improper curing throughout the specimen in the case of the cylinders [21], which are more massive than prisms, although the curing time in this research (of 56 days) should be enough. Presumably, it is not neither due to different carbonation processes as explained in Section 7.3.5, nor due to possible differences in the compaction of the material as the densities of both specimens differ by less than 1% (see Section 7.3.1 and Table 2.6 of Chapter 2). Instead, our hypothesis is that this type of mortars presents a strong size and geometry effect, which could justify the observed difference in the compressive strength measured from prismatic and cylindrical specimens of different sizes. This phenomenon can be analyzed through a numerical model, which also offers the opportunity to study the damage in the mortar matrix in the form of crack patterns.

The model was made with the commercial program ATENA [162], already used before for modeling laboratory tests [163]. ATENA uses the Finite Element Method and has non-linear constitutive material models implemented, especially aimed for cohesive materials. It also models fracture in an explicit way by representing cracks, determined with the crack band model [164], taking the crack band size L_t as the projection of the element size on the crack direction, see Figure 7.5. By default, the program uses a Rankine failure criterion in tension combined with a plasticity one of Menétrey and William [165] in compression (Figure 7.6a). In such a failure criterion $f_c'^{ef}$ and $f_t'^{ef}$ are, respectively, the maximum compressive and tensile stresses. Figure 7.6a represents the failure criterion for two dimensions, while Figure 7.6b is the translation into an equivalent uniaxial law. Cracks initiate when the tensile resistance is reached. Prior to cracking, the material is treated as isotropic with a modulus of elasticity derived from the equivalent uniaxial law using the lowest principal stress. Then, after cracking, the material is orthotropic. The exponential softening law proposed by Hordijk *et al.* [166] for cohesive materials is used (Figure 7.7), where $w_0 = w_c$ is the crack opening at the state of complete stress release.

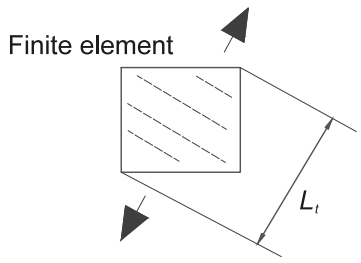

Figure 7.5: Projection of the element size on the crack direction.

The geometry of the model consists of three piled bodies, see Figure 7.8. The one at the bottom represents the supporting steel plate of dimensions 10 mm × 40 mm × 40 mm. The mortar specimen with dimensions of 40 mm × 40 mm × 80 mm lies in horizontal position centered on that plate. Finally, another plate the same as the first one serves as the element that transmits the load to the specimen. Symmetry was used in order to reduce the number of finite elements and the computing cost. Thus, only a quarter defined by the two vertical planes of symmetry of the total geometry was modeled.

Therefore, regarding the boundary conditions, the displacements of the surfaces of each body corresponding to the planes of symmetry are prevented in the perpendicular direction to those planes. The movements of the bottom surface of the supporting plate are also restrained. The load is applied as a prescribed downward displacement on the node placed in the intersection of the two orthogonal symmetry planes, on the upper face of the loading plate. This node corresponds to the central point of the complete surface.

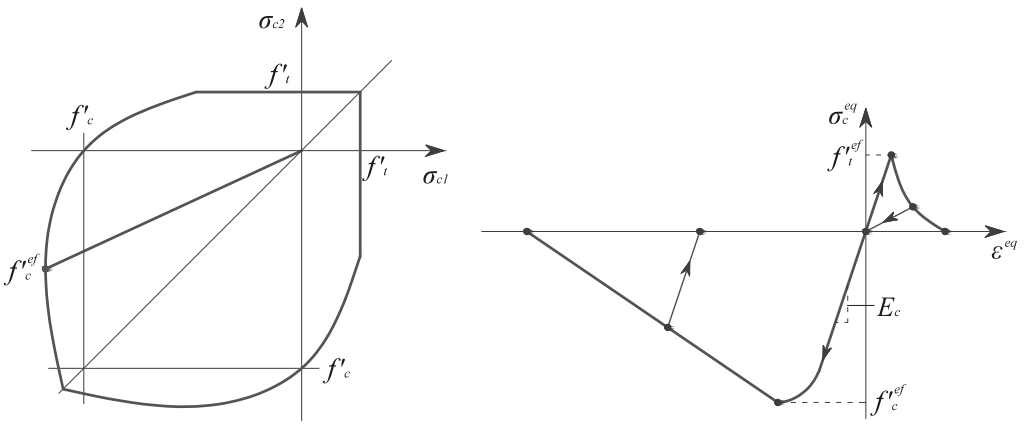

(a) (b)

Figure 7.6: Failure criterion: (a) combined Rankine failure criterion in tension and plasticity of Menetrey William in compression, (b) equivalent uniaxial law.

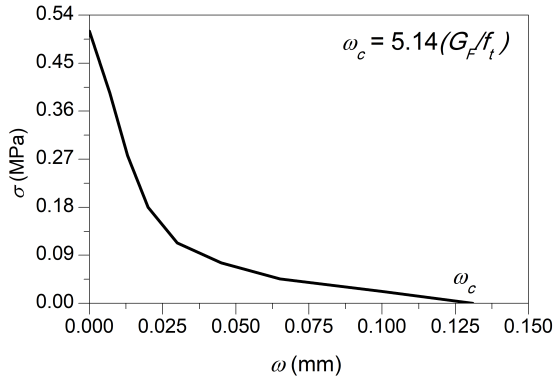

Figure 7.7: Schematic exponential softening law of Hordijk.

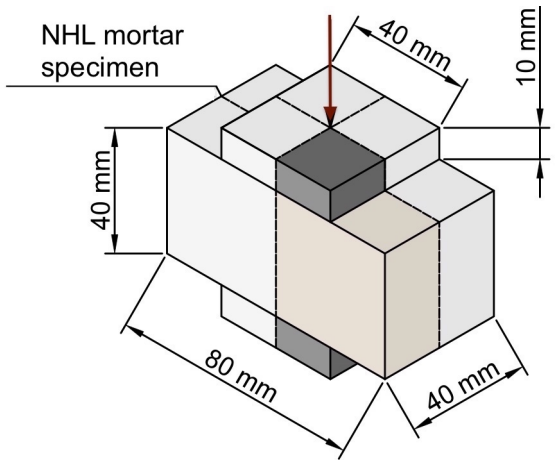

Figure 7.8: Geometry of the model.

The material properties of the specimen element were taken from the experimental results (see Table 7.2), for E, G_F, f_t and f_c. Regarding the discrepancy between the prismatic and cylindrical compressive strengths (f_{cpr} and f_{ccy}, respectively), it was assumed the existence of a size effect and, thus, f_{ccy} was chosen for the compressive strength in the model, as a value closer to the actual intrinsic mortar strength. The other two elements were defined with a same perfect linear elastic material, as their only function was to distribute and transmit the load to the mortar specimen and their resistance was much greater than the mortar one. Its elastic modulus was set as 210 GPa. The contacts between these three elements were also defined, with no adherence between them and a friction angle of 0.45.

Cubic 8-node finite elements were employed, owing to their accuracy with a relative small number of elements in comparison with the 4-node tetrahedral ones, as the regular prismatic geometry allowed it. In order to determine the appropriate finite element size, a mesh-sensitivity study was performed. Figure 7.9 shows the peak load obtained with different element sizes. The curve defined has an increasing tendency with the size of the elements and it seems that it would only converge for very small sizes. Furthermore, the peak load in that size range is under the experimental band. The dependency on the band size is a common drawback of the crack band model [167]. However, each material has its optimal band width, which is commensurate to the maximum aggregate size [77]. Regarding the crack pattern (Figure 7.10), the main cracks are the compression arches on the sides of the directly compressed zone, which start from the same locations for the element sizes of 2 and 5 mm. However, for the size of 8 mm, that arch is placed further from the edge of the loading and supporting plates, which is not the real behavior. Then, the finite element size of 5 mm was chosen, as it provides a peak load within the experimental range and yields proper results for the crack pattern.

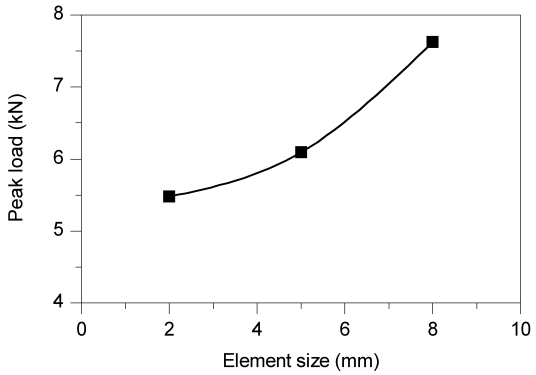

Figure 7.9: Mesh study: peak load vs. element size.

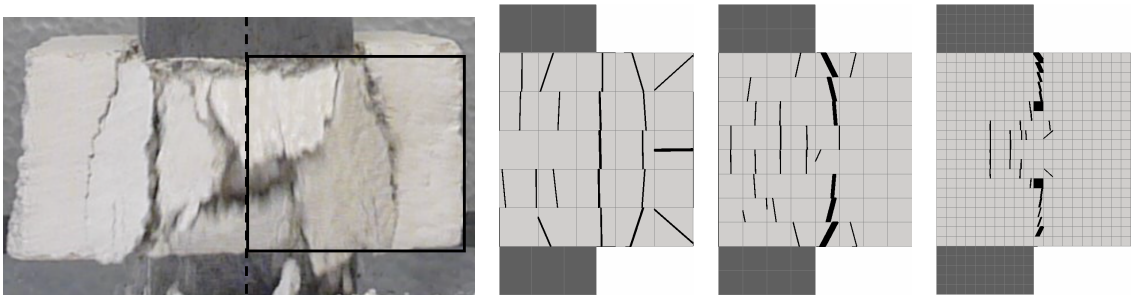

Figure 7.10: Mesh study: crack pattern. (a) Experimental specimen and numerical simulation: cubes of size of (b) 8 mm, (c) 5 mm and (d) 2 mm.

The final results of load-displacement curves offered by the model for both lime mortars are presented in Figure 7.11. These results fit very well the experimental curves, which is especially relevant because by using the cylindrical compressive strength (f_{ccy}) for the mortar in the model, it is possible to attain the correct maximum load with a prism. If we divide this maximum load by the corresponding loading area (40×40 mm^2), the result is the compressive strength from prisms (f_{cpr}), which is significantly greater than f_{ccy}. This proves the existence of a size and geometry effect in NHL mortars.

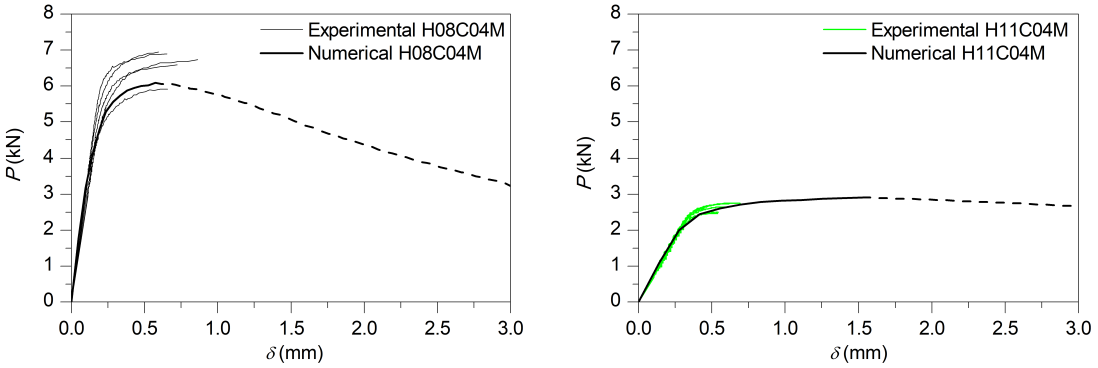

(a) (b)

Figure 7.11: Experimental and numerical load-displacement curves of (a) H08C04M and (b) H11C04M in compression.

In the case of the mortar H08C04M, the peak load lies within the experimental band, so this result means that its cylindrical compressive strength is very close to the actual material strength. In the case of the mortar H11C04M, the use of f_{ccy} (1.4 MPa) as the model mortar strength does not provide a fit of the peak load as good as in the first case, as it results in a higher maximum load than the corresponding to $f_{cpr} = 1.7$ MPa. However, it is possible to set this parameter so as to have in consideration both compression results, accepting the usual experimental scatter. This way, with a value of $f_c = 1.3$ MPa, a nominal prismatic strength of 1.8 MPa is obtained, which represent each a variation of just 0.1 MPa with respect to the corresponding mean compressive strength.

From the peak load on, the numerical models also provide an estimation of the post-peak trajectory, which complements experimental information. Another interesting result is crack patterns, which reproduce appropriately the real fracture observed in tests, comparing Figure 7.10a with Figure 7.10c. All these results validate the models for representing the compressive test with prisms and certifies once again the cohesive fracture behavior of NHL mortars.

7.4.4. Size effect in compression

The size effect in compression evidenced in experimental tests and verified by the numerical model is studied in order to discover its influence in prismatic specimens and the relation with the compressive strength obtained from cylinders of 75 mm in diameter and 150 mm in height. Variations in the crack pattern are also analyzed. This study is made by following the procedure described in the work by Del Viso, Carmona and Ruiz [78]. Two additional numerical analyses were performed for each one of the NHL mortars, where the dimensions of the original models were doubled once (80 mm$\times$ 80 mm $\times$ 160 mm) and twice (160 mm $\times$ 160 mm$\times$ 320 mm), respectively, but maintaining the finite element size.

With the maximum loads of each model, their corresponding nominal strength, σ_N, is obtained, which has a decreasing tendency for larger sizes. By plotting σ_N^2 against the inverse of the Hillerborg's brittleness number, i.e. $1/\beta_H$ or ℓ_{ch}/D (Figure 7.13), it is possible to deduce the

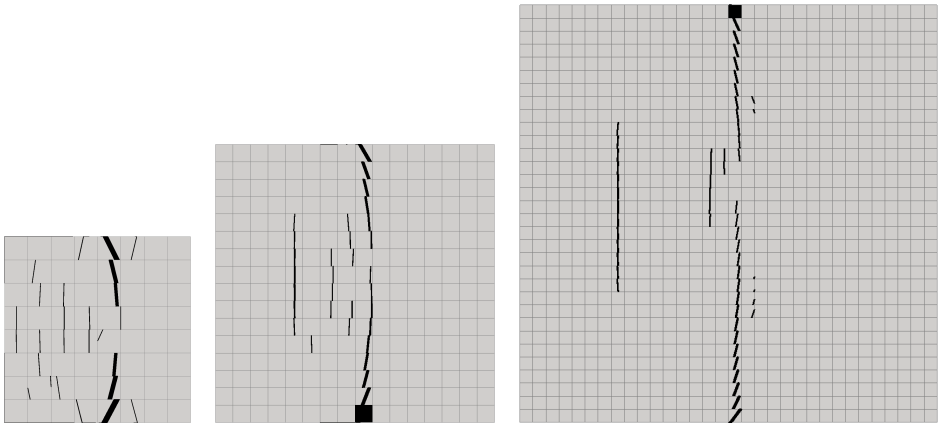

(a) (b) (c)

Figure 7.12: Crack patterns of the numerical models. Sizes of (a) 40, (b) 80 and (c) 160 mm. Picture of half of the specimen. Relative proportions of 3/2 in the figure (of 2 in reality).

assimptotic value of the compressive strength when $D \to \infty$ [78], in other words, the intrinsic compressive strength of the material, denoted here as σ_{inf}.

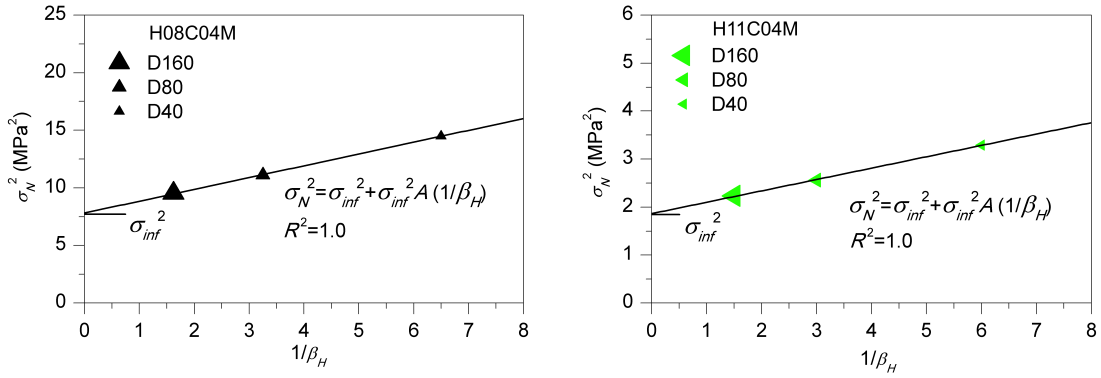

(a) (b)

Figure 7.13: Regression for setting σ_{inf} and A for (a) H08C04M and (b) H11C04M

In Figure 7.14, the non-dimensional values of σ_N are plotted related to β_H (with a logarithmic scale) for both mortars. These results allow fitting the analytical curves that represent their size effect laws. As shown by these curves, the size effect tends to disappear for large sizes. The compressive strength converges in both cases to the value used in the models for f_c. In other words, these simulations prove that the experimental value for the compressive strength on cylinders can be roughly considered as σ_{inf}, whereas the compressive strength from prisms is reproduced by the model as a structural response and, thus, it cannot be regarded as a true material property.

Crack patterns have also been compared between the three scaled specimens (Figure 7.12). For both mortars, the results are quite similar within each size. In the three different sizes, a compression arch appears from the vertex of the loading element to the vertex of the supporting one (denoting the presence of the main tension cracks).

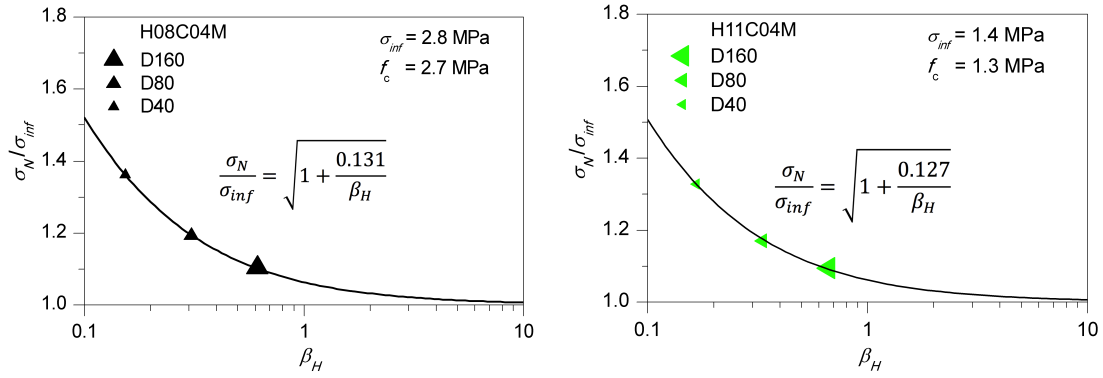

(a) (b)

Figure 7.14: Size effect laws for (a) H08C04M and (b) H11C04M

7.5. Conclusions

In this research, the mechanical properties of two NHL mortars have been studied extensively. The water/lime ratios were 0.8 and 1.1 respectively. It has been observed that the water/lime ratio has a great influence on the mechanical properties of NHL mortars. Flexural strength of H11C04M was 33% lower than the one of H08C04M, compressive strength of prisms and of cylinders decreased by 61% and by 48% respectively for the water/lime ratio of 1.1, fracture energy decreased by 61% and the elastic modulus and the splitting tensile strength got around 50% less.

This experimental characterization has been verified with an exhaustive numerical analysis. The objective was to further understand the behavior of NHL mortars and to verify the hypothesis of a cohesive material. In the first place, the TPB test for measuring G_F has been simulated with a cohesive numerical model by implementing suitable materials' softening laws with four parameters. The compressive tests on prisms have also been simulated with a finite element model for both types of mortars. In both cases, the results show good agreement with the experimental ones. This confirms that NHL mortars behave as cohesive materials.

In the second place, the marked difference in the experimental results of compression tests on prisms and cylinders, f_{cpr} and f_{ccy}, could evidence the existence of size effects in NHL mortars. This hypothesis has also been verified with a numerical analysis with two additional models by doubling the size of the samples once and twice, respectively, but maintaining the finite element size. The results show that larger specimens resist less in terms of stress than smaller ones. It has also been observed that for big sizes the compressive strength in prisms converges to the compressive strength obtained with the cylinders. Finally, the crack pattern has also been studied in the three different scaled numerical models and compared with the experimental one when appropriate, showing also a good agreement.

Part III

Conclusions and future research

Chapter 8

Conclusions and main contributions

In the thesis, an advanced mechanical characterization of natural hydraulic and aerial lime mortars has been performed. On the one hand, important properties not normally studied have been measured, such as splitting tensile strength, fracture energy and static elastic modulus. They are useful to define the fracture behavior, the ductility and the deformability of the material. On the other hand, advanced techniques have been applied when measuring all the mechanical properties in order to avoid the influence of the boundary conditions. For instance, it was used anti-torsion supports for the tests to obtain the normalized flexural strength and the fracture energy, ball-and-socket joint to reduce eccentricity in the standardized compressive strength test, narrow wooden strips in the Brazilian tests to avoid size effects, application of the corrections of Planas, Guinea and Elices in the three-point point bending test to obtain the fracture energy with no influence of size effects and strain gauge extensometers in the middle height of the cylinders to avoid the influence of friction effects in the compression test to obtain the static elastic modulus. Furthermore, such mechanical properties have been related to other important physical ones such as density, open porosity, UPV, etc. when possible.

Different aspects have been analyzed, such as: the influence of five factors affecting the dosage and fabrication process of seven types of natural hydraulic and aerial lime mortars on their mechanical properties; the evolution of some mechanical properties at early ages and in the long-term, and the loading rate effect on the fracture energy. Furthermore, the shape and size effect on the compressive strength of two natural hydraulic lime mortars was disclosed by numerical simulation and experiments.

1. Regarding five influence factors on the mechanical properties, the results show that high water/lime ratios produce structural weakening and reduce the mechanical properties. High relative humidity (97 $\pm$ 0.5%) is more suitable than ambient laboratory conditions for the hydration of the compounds of NHL mortars and for the increase of its ductility; however, in the case of aerial lime mortars, such high humid conditions are less favorable than drier ones for the carbonation process. Moreover, using wooden molds also improves these properties as they absorb the excess of free water, although this effect seems to be local and results in a non-homogeneous material. When maintaining constant water/lime ratios, introducing aggregates with higher grain size (in this case a well-graded sand with maximum grain size of 4 mm) improves the mechanical properties. Mortars with river sand have lower mechanical properties than crushed limestone aggregates as the interlocking among particles is not so effective. Certainly, if the water/lime ratio also varies at the same time, the tendency would be different. Furthermore, some empirical formulas are proposed for the first time among several mechanical properties of the lime mortars and the compressive strength from prisms. They can be useful to predict some mechanical properties just by measuring the compressive strength from prisms due to the convenience of conducting the test.
2. Referring the study of the mechanical and physical properties of three NHL mortars at early ages, EMM-ARM has been applied for the first time to measure deformability of NHL mortars since casting. It is concluded that this technique has shown feasible potential of application for NHL mortars, especially at early ages (up to 3 or 7 curing days), with very good comparability with results from the cyclic compression tests from cylinders. The initial dormant period was well captured as the kinetics of the stiffness increase. Also,

different fabrication and curing methods were analyzed to compare the standard procedures (compaction and unsealing) and the ones followed for EMM-ARM (vibration and sealing). A general trend was observed: specimens with higher water content provided lower stiffness and strengths. Moreover, evolution laws of normalized flexural and compressive strength up to 7 days were obtained. Some relationships were also obtained among results of density, UPV and open porosity on the one hand and evolution of free portlandite by means of TGA and compressive strength of the mortar on the other. Such analysis enhances the comprehension of the NHL mortars behavior at early ages.

3. Additionally, some important mechanical properties, such as splitting tensile strength, fracture energy and elastic modulus were measured in the long term on one natural hydraulic and an aerial lime mortars for the first time. It is observed that for both mortars, all the measured mechanical properties increase considerably up to around 56 curing days. From this period up to 224 days, the evolution is more or less constant and with slight increase for the NHL mortars. Finally, up to 448 days, most of the mechanical properties remain almost constant for the aerial lime mortar while they experiment some increase for the NHL one. The main differences between both mortars are mainly due to the different hardening processes: aerial lime mortars mainly harden by carbonation while NHL ones also by hydration of its mineral compounds. The evolution of the mechanical properties was compared with the development of the carbonation depth by means of the phenolphthalein method. Also, empirical formulas describing the evolution of the mechanical properties up to 448 days were obtained for the first time.

4. With respect to the loading rate effect, it was measured for the first time on the fracture energy in bending of one natural hydraulic and an aerial lime mortars. The loading rates were ranged from 5.0×10^{-4} to 1.6×10^{1} mm/s. It is obvious that the materials are rate sensitive. The DIFs of the peak load are 1.4 and 1.6, respectively for the natural hydraulic and the aerial lime ones and 1.9 for both in the fracture energy. Additional specimens were dried and tested at the lowest and the highest loading rates to analyze the possible phenomena of such rate sensitivity. The results show that it is mainly because of the viscous effects caused by the presence of free water in the porous structure in the case of natural hydraulic lime mortar and due to effect of crack propagation in the case of the aerial one. Furthermore, SEM analyses show that the failure is intergranular, which means that the material breaks through the matrix instead of through the aggregates grains.

5. Furthermore, it has been observed a big variation on the compressive strengths from prisms and cylinders of the NHL mortars, the ratio could reach 1.6. A numerical simulation of the compressive test on prisms of two NHL mortars was performed to analyze such difference. Three specimen sizes were simulated by doubling the standard size once and twice but maintaining the finite element size. The results show that larger specimens resist less in terms of stress than smaller ones and therefore the difference found between prisms and cylinders is mainly due to geometry and size effects. It has also been observed that the compressive strength from cylinders provides roughly the real compressive strength of the material. Furthermore, the size effect laws of both mortars were obtained for the first time. Another numerical model of the three-point bending test on beams was performed by implementing suitable materials' softening laws with four parameters. The good agreement found between the experimental and numerical results confirms that NHL mortars behave as cohesive materials.

It can be concluded that this thesis provides significant improvements in the techniques to measure the mechanical properties of materials of the civil and architectural patrimony, such as lime mortars. Different effects affecting the mechanical properties of the material have been analyzed and empirical formulas have been proposed for the first time. Such analyses and formulas could be useful to define with more realism and precision the numerical simulations of masonry structures built with lime mortars.

8.1. Future research

After the elaboration of this thesis, new research works can be proposed. On the one hand to improve and continue with the topics already proposed and on the other hand to extend to new ones.

In this thesis different aspects affecting the dosage and fabrication process of lime mortars have been studied. However, there is still much work to do to develop a dosage methodology like the ones present for other materials, such as concrete, with which it is possible to define a particular dosage to satisfy a target compressive strength or consistency [168]. To start with such a concern, it would be useful to define a function relating the obtained compressive strength according to the water/lime ratio used. This would facilitate the fabrication process of lime mortars with the consequently improvement of precision of the restoration works. Then, it could also be possible to study the statistically significance of each dosage factor (water/lime ratio, aggregate type and size, etc.) on the resulting mechanical properties. For such a purpose the software Minitab could be applied, which has successfully been used for concrete [169, 170].

Regarding the stiffness evolution measurement of NHL mortar at early ages, another concern already mentioned in Chapter 4 is the need of demolding the specimens used in EMM-ARM after 2 or 3 curing days. Such an objective was not within the scope of this thesis but it would allow applying EMM-ARM to NHL mortars for longer periods of time and to pure aerial lime mortars to consider other hardening mechanisms such as drying and carbonation. Related to the work presented in Chapter 4, it has also been mentioned the need of further research on the influence of the curing conditions (especially concerning different sealing methods that cause various humid states) on the mechanical properties of natural hydraulic lime mortars at early ages.

As for the measurement of the mechanical properties of lime mortars in the long-term, in this thesis two mortars were tested due to the limited time available, but this research could be improve by increasing the number of mortars tested and the period of time studied. Furthermore, it would also be interesting to perform other tests, such as TGA and/or SEM analyses to relate better the evolution of the mechanical properties with the mineralogical changes of the mortars.

Referring the study of the loading rate effects on lime mortars, improvements can be done by increasing also the number of mortars tested and by enlarging the range of loading rates applied, for example by using a drop-weight impact machine. Also, a Digital Image Correlation (DIC) with a high-speed video camera could be interesting to be applied in lime mortars to analyze the displacements and strains near the fracture zone. Furthermore, having verified the cohesive behavior of lime mortars, it would also be of interest to propose a loading rate dependent cohesive model for lime mortars, similar to the one created for concrete by Rosa, Yu, Ruiz, *et al.* [156]. In such a way, it could be possible to define a softening law and a corresponding constitutive model for lime mortars by considering also loading rate effects.

Concerning the study of the size effect on NHL mortars, it would be necessary to perform an experimental verification on specimens of different sizes, as the ones modeled within the numerical simulation (specimens of 40 mm, 80 mm and 160 mm in depth), to check if possible different hardening processes (specially different carbonation states) may take place on natural hydraulic lime mortars at different ages and under different curing conditions. For the purpose, carbonation depth could be measured through TGA and with the phenolphthalein test. In this sense, the possible different hardening processes could be considered together with the size effect in a numerical model similar to the one created for aerial quicklime mortars by Oliveira [62] and previously on masonry towers by Ferretti and Bažant [63]. The application of this study to hydrated aerial lime mortars would also be of interest.

There are other topics beyond the scope of this thesis, which can also be proposed for future analysis:

1. The application of the empirical formulas proposed in this thesis to numerical simulation of historical masonry structures. Examples of such numerical simulations can be seen in [1–5].

2. The inclusion of fibers on lime mortars. The research on such topic is increasing in interest as shown in [171–173].

3. The study of fatigue in lime mortars. To our knowledge, such topic is not already investigated

and could be of significance as many masonry structures, such as bridges and towers, are subjected to fatigue loads. Research of fatigue behavior of concrete can be seen in [174–176] and we have found a reference about fatigue on brick masonry [177].

8.2. Work published in Journals

As a result of the work performed in the thesis, different publications listed below have been produced.

1. L. Garijo, X. X. Zhang, G. Ruiz, J. J. Ortega, R. C. Yu. Advanced mechanical characterization of NHL mortars and cohesive simulation of their failure behavior. *Construction and Building Materials*, 153:569-577, 2017. doi: 10.1016/j.conbuildmat.2017.07.127.
2. L. Garijo, X. X. Zhang, G. Ruiz, J. J. Ortega, Z. M. Wu. The effects of dosage and production process on the mechanical and physical properties of natural hydraulic lime mortars. *Construction and Building Materials*, 169:325-334, 2018. doi: 10.1016/j.conbuildmat.2018.03.016.
3. G. Ruiz, X. X. Zhang, W. F. Edris, I. Cañas, L. Garijo. A comprehensive study of mechanical properties of compressed earth blocks. *Construction and Building Materials*, 176: 566-572, 2018. doi: 10.1016/j.conbuildmat.2018.05.077.
4. L. Garijo, M Azenha, M. Ramesh, P. B. Lourenço, G. Ruiz. Stiffness evolution of natural hydraulic lime mortars at early ages measured through EMM-ARM. *Construction and Building Materials*, 216: 405-415, 2019. doi: 10.1016/j.conbuildmat.2019.04.258.

8.3. Work submitted to Journals

1. L. Garijo, X. X. Zhang, G. Ruiz, J. J. Ortega. Age effect on the physical and mechanical properties of a natural hydraulic and an aerial lime mortars. *Construction and Building Materials*, submitted on 29/04/2019.
2. X. X. Zhang, L. Garijo, G. Ruiz, J. J. Ortega. Loading rate effect on the fracture response of natural hydraulic and aerial lime mortars. *Journal of Materials in Civil Engineering*, submitted on 09/07/2019.
3. L. Garijo, X. X. Zhang, G. Ruiz, J. J. Ortega. The influence of dosage and production process on the physical and mechanical properties of aerial lime mortars. *Construction and Building Materiasl*, submitted on 11/07/2019.

8.4. Book chapter

1. L. Garijo, X. X. Zhang, G. Ruiz, J. J. Ortega, R. C. Yu. Mechanical behaviour of natural hydraulic lime mortars. *Sustainable Construction and Building Materials*, 1-20, 2018. doi: 10.5772/intechopen.80852.

8.5. Work published in Conferences

1. L. Garijo, X. X. Zhang, G. Ruiz. Advanced mechanical characterization of lime mortars. *Anales de Mecánica de la Fractura*, 33, 521-526, 2016.
2. L. Garijo, X. X. Zhang, G. Ruiz. Caracterización mecánica avanzada de morteros de cal hidráulica natural. *A cal no espacio Ibérico: um futuro con história. V Jornadas FICAL – Fórum Ibérico da Cal. Livro de Atas*, 419-428, 2016.
3. J. J. Ortega, G. Ruiz, L. Garijo, X. X. Zhang, R. C. Yu. Size effect on the compressive strength of natural hydraulic lime mortars. *Anales de Mecánica de la Fractura*, 34, 279-285, 2017. ISSN: 0213-3725.

4. L. Garijo, X. X. Zhang, G. Ruiz. Influence of dosage and production process on the mechanical properties of natural hydraulic lime mortars. *Anales de Mecánica de la Fractura*, 34, 256-263, 2017. ISSN: 0213-3725.
5. G. Ruiz, X. X. Zhang, I. Cañas, W. A. Fouad, L. Garijo. Advanced study of the mechanical properties of compressed earth block. *SOStierra 2017, International Conference on vernacular earthen architecture, conservation and sustainability*, CRC Press, 797-802, 2017. ISBN: 978-1-138-03546-1.
6. L. Garijo, X. X. Zhang, G. Ruiz. Efecto de la velocidad de solicitación en el comportamiento en fractura de morteros de cal. *Anales de Mecánica de la Fractura*, 35, 112-114, 2018. ISSN: 0213-3725.
7. L. Garijo, X. X. Zhang, G. Ruiz, J. J. Ortega. Evolución de las propiedades mecánicas de morteros de cal aérea e hidráulica natural. *Anales de Mecánica de la Fractura*, 36, 120-123, 2019. ISSN: 0213-3725.
8. J. J. Ortega, L. Garijo, G. Ruiz. Simulación con modelos de fractura cohesiva de la rotura de una losa de hormigón armado con un orificio. *Anales de Mecánica de la Fractura*, 36, 136-139, 2019. ISSN: 0213-3725.

8.6. Prize “Cátedra ECSA”

1. J. J. Ortega, L. Garijo. Prize “Cátedra ECSA. Cátedra de Construcción Sostenible y Avanzada”, 2018, competition organised by the Polytechnic University of Valencia and directed to students of technical schools of Spanish universities and to national and international professional teams. The objective was to analyse the mechanical behavior of a concrete slab and to predict its failure load. The proposed solution was based on the techniques of Fracture Mechanics.

Bibliography

[1] B. Panto, F. Cannizzaro, I. Calio, and P. B. Lourenço. Numerical and experimental validation of a 3D macro-model for the in-plane and out-of-plane behavior of unreinforced masonry walls. *International Journal of Architectural Heritage*, 11(7):946–964, 2017. doi: 10.1080/15583058.2017.1325539.

[2] P. Medeiros, G. Vasconcelos, P. B. Lourenço, and J. Gouveia. Numerical modelling of non-confined and confined masonry walls. *Construction and Building Materials*, 41:968–976, 2013. doi: 10.1016/j.conbuildmat.2012.07.013.

[3] P. Roca, M. Cervera, G. Gariup, and L. Pelà. Structural analysis of masonry historical constructions. Classical and advanced approaches. *Archives of Computational Methods in engineering*, 17(3):299–325, 2010. doi: 10.1007/s11831-010-9046-1.

[4] C. Molins and P. Roca. A numerical model for the study of ancient masonry structures. In Brebbia, CA and Leftheris, B, editor, *Structural Studies of Historical Buildings IV - Vol 2: Dynamics, Repairs & Restoration*, pages 275–282, 1995. ISBN 1-85312-426-5.

[5] E. Reyes. *Rotura de la fábrica de ladrillo bajo solicitaciones de tracción y cortante*. PhD thesis, Universidad de Castilla-La Mancha, 2004.

[6] A. Kalagri, I. Karatasios, and V. Kilikoglou. The effect of aggregate size and type of binder on microstructure and mechanical properties of NHL mortars. *Construction and Building Materials*, 53:467–474, 2014. doi: 10.1016/j.conbuildmat.2013.11.111.

[7] R. Veiga. Air lime mortars: What else do we need to know to apply them in conservation and rehabilitation interventions? A review. *Construction and Building Materials*, 157:132–140, 2017. doi: 10.1016/j.conbuildmat.2017.09.080.

[8] J. Lanas, J. L. P. Bernal, M. A. Bello, and J. I. A. Galindo. Mechanical properties of natural hydraulic lime-based mortars. *Cement and Concrete Research*, 34(12):2191–2201, 2004. doi: 10.1016/j.cemconres.2004.02.005.

[9] J. Lanas and J. I. Alvarez. Masonry repair lime-based mortars: Factors affecting the mechanical behavior. *Cement and Concrete Research*, 33(11):1867–1876, 2003. doi: 10.1016/S0008-8846(03)00210-2.

[10] R. Chan and V. Bindiganavile. Toughness of fibre reinforced hydraulic lime mortar. Part-1: Quasi-static response. *Materials and Structures*, 43(10):1435–1444, 2010. doi: 10.1617/s11527-010-9598-4.

[11] G. Ruiz, X. X. Zhang, W. F. Edris, I. Canas, and L. Garijo. A comprehensive study of mechanical properties of compressed earth blocks. *Construction and Building Materials*, 176:566–572, 2018. ISSN 0950-0618. doi: 10.1016/j.conbuildmat.2018.05.077.

[12] *BS EN 459-1, Building lime - Part 1: Definitions, specifications and conformity criteria.* 2015.

[13] A. Arizzi, G. Cultrone, M. Bruemmer, and H. Viles. A chemical, morphological and mineralogical study on the interaction between hemp hurds and aerial and natural hydraulic lime particles: Implications for mortar manufacturing. *Construction and Building Materials*, 75: 375–384, 2015. doi: 10.1016/j.conbuildmat.2014.11.026.

[14] B. A. Silva, A. P. Ferreira Pinto, and A. Gomes. Influence of natural hydraulic lime content on the properties of aerial lime-based mortars. *Construction and Building Materials*, 72: 208–218, 2014. doi: 10.1016/j.conbuildmat.2014.09.010.

[15] J. Lanas, R. Sirera, and J. I. Alvarez. Compositional changes in lime-based mortars exposed to different environments. *Thermochimica Acta*, 429(2):219–226, 2005. doi: 10.1016/j.tca.2005.03.015.

[16] A. Arizzi, G. Martinez-Huerga, E. Sebastian-Pardo, and G. Cultrone. Mineralogical, textural and physical-mechanical study of hydraulic lime mortars cured under different moisture conditions. *Materiales De Construccion*, 65(318), 2015. doi: 10.3989/mc.2015.03514.

[17] J. Lanas, M. Arandigoyen, J. I. Alvarez, J. L. P. Bernal, and M. A. Bello. Mechanical behavior of masonry repair mortars: aerial and hydraulic lime-based mixtures. In 10^{th} *International Congress on Deterioration and Conservation of Stones*, Stockholm, 2004.

[18] J. R. Rosell. Algunas consideraciones de la cal y sus morteros. In Fórum Ibérico de la cal, editor, *Jornadas FICAL*, volume II, pages 6–16, 2011.

[19] J. R. Rosell, L. Haurie, M. Bosch, A. Rattazzi, and I. Cantalapiedra. ¿ existen diferencias en las cales apagadas por distintos métodos tradicionales?: la experiencia de zone (bs). In Fórum Ibérico de la cal, editor, *Jornadas FICAL*, volume II, pages 41–54, 2011.

[20] URL `https://limes.us/technical-info/hydraulicity-properties/`.

[21] A. Drougkas, P. Roca, and C. Molins. Compressive strength and elasticity of pure lime mortar masonry. *Materials and Structures*, 49(3):983–999, 2016. doi: 10.1617/s11527-015-0553-2.

[22] L. Pelà, K. Kasioumi, and P. Roca. Experimental evaluation of the shear strength of aerial lime mortar brickwork by standard tests on triplets and non-standard tests on core samples. *Engineering Structures*, 136:441–453, 2017. doi: 10.1016/j.engstruct.2017.01.028.

[23] D. Marastoni, L. Pelà, A. Benedetti, and P. Roca. Combining Brazilian tests on masonry cores and double punch tests for the mechanical characterization of historical mortars. *Construction and Building Materials*, 112:112–127, 2016. doi: 10.1016/j.conbuildmat.2016.02.168.

[24] L. Pelà, E. Canella, A. Aprile, and P. Roca. Compression test of masonry core samples extracted from existing brickwork. *Construction and Building Materials*, 119:230–240, 2016. doi: 10.1016/j.conbuildmat.2016.05.057.

[25] J. Grilo, A. S. Silva, P. Faria, A. Gameiro, R. Veiga, and A. Velosa. Mechanical and mineralogical properties of natural hydraulic lime-metakaolin mortars in different curing conditions. *Construction and Building Materials*, 51:287–294, 2014. doi: 10.1016/j.conbuildmat.2013.10.045.

[26] D. Marastoni, A. Benedetti, L. Pelà, and G. Pignagnoli. Torque Penetrometric Test for the in-situ characterisation of historical mortars: fracture mechanics interpretation and experimental validation. *Construction and Building Materials*, 157:509–520, 2017. doi: 10.1016/j.conbuildmat.2017.09.120.

[27] M. Apostolopoulou, E. Aggelakopoulou, L. Siouta, A. Bakolas, M. Douvika, P. G. Asteris, and A. Moropoulou. A methodological approach for the selection of compatible and performable restoration mortars in seismic hazard areas. *Construction and Building Materials*, 155:1–14, 2017. doi: 10.1016/j.conbuildmat.2017.07.210.

[28] V. G. Haach, G. Vasconcelos, and P. B. Lourenço. Influence of aggregates grading and water/cement ratio in workability and hardened properties of mortars. *Construction and Building Materials*, 25(6):2980–2987, 2011. doi: 10.1016/j.conbuildmat.2010.11.011.

[29] L. Binda, I. Papayianni, E. Toumbakari, and R. Van Hees. *Characterization of Old Mortars with Respect to Their Repair. Final Report of RILEM TC 167-COM*, chapter Mechanical tests on mortars and assemblages. 2004.

[30] *DIN 18555-9. Testing of mortar containing mineral binders - Part 9: Determining the compressive strength of hardened mortar.* 1999.

[31] *BS EN 1015-11, Methods of test for mortar for masonry - Part 11: Determination of flexural and compressive strength of hardened mortar.* 1999/A1:2006.

[32] I. Papayianni and M. Stefanidou. Strength-porosity relationships in lime-pozzolan mortars. *Construction and Building Materials*, 20(9):700–705, 2006. doi: 10.1016/j.conbuildmat.2005.02.012.

[33] P. Maravelaki-Kalaitzaki, A. Bakolas, I. Karatasios, and V. Kilikoglou. Hydraulic lime mortars for the restoration of historic masonry in Crete. *Cement and Concrete Research*, 35(8): 1577–1586, 2005. doi: 10.1016/j.cemconres.2004.09.001.

[34] J. R. Rosell and I. R. Cantalapiedra. Simple method of dynamic Young's modulus determination in lime and cement mortars. *Materiales De Construccion*, 61(301):39–48, 2011. doi: 10.3989/mc.2010.53509.

[35] V. Nežerka, Z. Slizkova, P. Tesarek, T. Plachy, D. Frankeova, and V. Petranova. Comprehensive study on mechanical properties of lime-based pastes with additions of metakaolin and brick dust. *Cement and Concrete Research*, 64:17–29, 2014. doi: 10.1016/j.cemconres.2014.06.006.

[36] J. S. Pozo-Antonio. Evolution of mechanical properties and drying shrinkage in lime-based and lime cement-based mortars with pure limestone aggregate. *Construction and Building Materials*, 77:472–478, 2015. doi: 10.1016/j.conbuildmat.2014.12.115.

[37] M. P. Pereira, J. B. Aguiar, A. Camões, and P. B. Lourenço. Influence of type of binder and sand on the characteristics of masonry mortars. *Revista Romana De Materiale-Romanian Journal of Materials*, 45(2):117–122, 2015.

[38] J. M. Pereira and P. B. Lourenço. Experimental characterization of masonry and masonry components at high strain rates. *Journal of Materials in Civil Engineering*, 29(2), 2017. doi: 10.1061/(ASCE)MT.1943-5533.0001755.

[39] D. Asprone, E. Cadoni, F. Iucolano, and A. Prota. Analysis of the strain-rate behavior of a basalt fiber reinforced natural hydraulic mortar. *Cement & Concrete Composites*, 53:52–58, 2014. doi: 10.1016/j.cemconcomp.2014.06.009.

[40] A. Moropoulou, A. S. Cakmak, G. Biscontin, A. Bakolas, and E. Zendri. Advanced Byzantine cement based composites resisting earthquake stresses: the crushed brick/lime mortars of Justinian's Hagia Sophia. *Construction and Building Materials*, 16(8):543–552, 2002. doi: 10.1016/S0950-0618(02)00005-3.

[41] L. Garijo, X. X. Zhang, G. Ruiz, J. J. Ortega, and Z. Wu. The effects of dosage and production process on the mechanical and physical properties of natural hydraulic lime mortars. *Construction and Building Materials*, 169:325–334, 2018. doi: 10.1016/j.conbuildmat.2018.03.016.

[42] A. Gameiro, A. Santos Silva, P. Faria, J. Grilo, T. Branco, R. Veiga, and A. Velosa. Physical and chemical assessment of lime-metakaolin mortars: Influence of binder:aggregate ratio. *Cement & Concrete Composites*, 45:264–271, 2014. doi: 10.1016/j.cemconcomp.2013.06.010.

[43] A. R. Santos, M. R. Veiga, A. S. Silva, J. De Brito, and J. Ignacio Alvarez. Evolution of the microstructure of lime based mortars and influence on the mechanical behaviour: The role of the aggregates. *Construction and Building Materials*, 187:907–922, 2018. doi: 10.1016/j.conbuildmat.2018.07.223.

[44] M. Arandigoyen and J. I. Alvarez. Pore structure and mechanical properties of cement-lime mortars. *Cement and Concrete Research*, 37(5):767–775, 2007. doi: 10.1016/j.cemconres.2007.02.023.

[45] G. Cultrone, E. Sebastian, and M. O. Huertas. Durability of masonry systems: A laboratory study. *Construction and Building Materials*, 21(1):40–51, 2007. doi: 10.1016/j.conbuildmat.2005.07.008.

[46] A. Arizzi and G. Cultrone. The influence of aggregate texture, morphology and grading on the carbonation of non-hydraulic (aerial) lime-based mortars. *Quarterly Journal of Engineering Geology and Hydrogeology*, 46(4):507–520, 2013. doi: 10.1144/qjegh2012-017.

[47] M. Stefanidou and I. Papayianni. The role of aggregates on the structure and properties of lime mortars. *Cement & Concrete Composites*, 27(9-10):914–919, 2005. doi: 10.1016/j.cemconcomp.2005.05.001.

[48] S. Xu, J. Wang, and Y. Sun. Effect of water binder ratio on the early hydration of natural hydraulic lime. *Materials and Structures*, 48(10):3431–3441, 2015. doi: 10.1617/s11527-014-0410-8.

[49] R. M. H. Lawrence and P. Walker. The impact of the water/lime ratio on the structural characteristics of air lime mortars. In DAyala, D and Fodde, E, editor, *Structural Analysis of Historic Construction: Preserving Safety and Significance, Vols 1 and 2*, pages 885–889, 2008. ISBN 978-0-415-46872-5.

[50] T. S. Nagaraj and Z. Banu. Generalization of Abrams' law. *Cement and concrete research*, 26(6):933–942, 1996. doi: 10.1016/0008-8846(96)00065-8.

[51] M. P. Raposo Pacheco Algarvio. Influence of water/lime ratio on the characteristics of lime mortars for use as substitution renders in ancient buildings. Technical report, Universidade Técnica de Lisboa, 2010.

[52] J. Lanas, R. Sirera, and J. I. Alvarez. Study of the mechanical behavior of masonry repair lime-based mortars cured and exposed under different conditions. *Cement and Concrete Research*, 36(5):961–970, 2006. doi: 10.1016/j.cemconres.2005.12.003.

[53] J. Grilo, P. Faria, R. Veiga, A. S. Silva, V. Silva, and A. Velosa. New natural hydraulic lime mortars - Physical and microstructural properties in different curing conditions. *Construction and Building Materials*, 54:378–384, 2014. doi: 10.1016/j.conbuildmat.2013.12.078.

[54] D. R. Moorehead. Cementation by the carbonation of hydrated lime. *Cement and Concrete Research*, 16(5):700–708, 1986. doi: 10.1016/0008-8846(86)90044-X.

[55] K. Van Balen and D. Vangemert. Modeling lime mortar carbonation. *Materials and Structures*, 27(171):393–398, 1994. doi: 10.1007/BF02473442.

[56] A. V. Saetta, B. A. Schrefler, and R. V. Vitaliani. 2-D Model for carbonation and moisture heat-flow in porous materials. *Cement and Concrete Research*, 25(8):1703–1712, DEC 1995. doi: 10.1016/0008-8846(95)00166-2.

[57] O. Cizer, K. V. Balen, and D. V. Gemert. Competition between hydration and carbonation in hydraulic lime and lime-pozzolana mortars. In 7^{th} *International Conference on Structural Analysis of Historical Constructions (SAHC 2010)*, Tongji University, Shanghai, 2010.

[58] G. Cultrone, E. Sebastian, and M. O. Huertas. Forced and natural carbonation of lime-based mortars with and without additives: Mineralogical and textural changes. *Cement and Concrete Research*, 35(12):2278–2289, 2005. doi: 10.1016/j.cemconres.2004.12.012.

[59] P. Faria and A. Martins. Influence of curing conditions on lime and lime-metakaolin mortars. In *International Conference on Durability of Building Materials and Components*, Porto (Portugal), 2011.

[60] P. Faria and A. Martins. Influence of type of air lime and curing conditions on lime and lime-metakaolin mortars. In *Durability of Building Materials and Components: Building Pathology and Rehabilitation*, pages 105–26, Porto (Portugal), 2013.

[61] O. Cizer. *Competition between carbonation and hydration on the hardening of calcium hydroxide and calcium silicates binders*. PhD thesis, Katholieke Universiteit Leuven, Haverlee (Belgium), 2009.

[62] M. A. Oliveira. *A Multi-Physics Approach Applied to Masonry Structures with Non-Hydraulic Lime Mortars*. PhD thesis, University of Minho, Guimarães, Portugal, 2015.

[63] D Ferretti and Z. P. Bažant. Stability of ancient masonry towers: Moisture diffusion, carbonation and size effect. *Cement and Concrete Research*, 36(7):1379–1388, 2006. doi: 10.1016/j.cemconres.2006.03.013.

[64] R. M. H. Lawrence, T. J. Mays, P. Walker, and D. D'Ayala. Determination of carbonation profiles in non-hydraulic lime mortars using thermogravimetric analysis. *Thermochimica Acta*, 444(2):179–189, 2006. doi: 10.1016/j.tca.2006.03.002.

[65] M. Karaveziroglou-Weber and I. Papayianni. Long-term strength of mortars and grouts used in interventions. In *Proceedings of IABSE symposium on structural preservation of the architectural heritage*, pages 527–532, Rome, Italy, 1993.

[66] P. Manita and T. C. Triantafillou. Influence of the design materials on the mechanical and physical properties of repair mortars of historic buildings. *Materials and Structures*, 44(9): 1671–1685, 2011. doi: 10.1617/s11527-011-9726-9.

[67] R. Chan and V. Bindiganavile. Toughness of fibre reinforced hydraulic lime mortar. Part-2: Dynamic response. *Materials and Structures*, 43(10):1445–1455, 2010. doi: 10.1617/s11527-010-9599-3.

[68] Md. T. Islam and V. Bindiganavile. Dynamic Fracture Toughness of Sandstone Masonry Beams Bound with Fiber-Reinforced Mortars. *Journal of Materials in Civil Engineering*, 26 (1):125–133, 2014. doi: 10.1061/(ASCE)MT.1943-5533.0000704.

[69] M. T. Islam, R. Chan, and V. Bindiganavile. Stress rate sensitivity of stone masonry units bound with fibre reinforced hydraulic lime mortar. *Materials and Structures*, 45(5):765–776, 2012. doi: 10.1617/s11527-011-9796-8.

[70] E. Cadoni, L. Fenu, and D. Forni. Strain rate behaviour in tension of austenitic stainless steel used for reinforcing bars. *Construction and Building Materials*, 35:399–407, 2012. doi: 10.1016/j.conbuildmat.2012.04.081.

[71] D. Asprone, E. Cadoni, and A. Prota. Experimental analysis on tensile dynamic behavior of existing concrete under high strain rates. *ACI Structural Journal*, 106(1):106–113, 2009.

[72] X. X. Zhang, A. M. Abd Elazim, G. Ruiz, and R. C. Yu. Fracture behaviour of steel fibre-reinforced concrete at a wide range of loading rates. *International Journal of Impact Engineering*, 71:89–96, 2014. doi: 10.1016/j.ijimpeng.2014.04.009.

[73] *FIB Model Code 2010, Final draft. Volumes 1-2*. FIB-Fédération Internationale du Béton, Lausanne, Switzerland, 2012.

[74] N Jones. *Structural Impact*. Cambridge University Press, New York, USA, second edition, 2011.

[75] P. H. Bischoff and S. H. Perry. Compressive behavior of concrete at high-strain rates. *Materials and Structures*, 24(144):425–450, 1991. doi: 10.1007/BF02472016.

[76] J. F. Kalthoff. On the measurement of dynamic fracture toughnesses - a review of recent work. *International Journal of Fracture*, 27(3-4):277–298, 1985. doi: 10.1007/BF00017973.

[77] Z. P. Bažant and J. Planas. *Fracture and Size Effect in Concrete and Other Quasibrittle Materials*. CRC Press, Boca Raton, Florida, 1998.

[78] J. R. Del Viso, J. R. Carmona, and G. Ruiz. Shape and size effects on the compressive strength of high-strength concrete. *Cement and Concrete Research*, 38(3):386–395, 2008. doi: 10.1016/j.cemconres.2007.09.020.

[79] G. Mohamad, P. B. Lourenço, A. Camões, and H. R. Troman. Estudo de caracterização mecânica das argamassas de assentamento para alvenaria estrutural. In *VII Simpósio Brasileiro de Tecnologia das Argamassas – VII SBTA*, Recife, Brasil, 2007.

[80] L. Garijo, X. X. Zhang, G. Ruiz, J. J. Ortega, and R. C. Yu. Advanced mechanical characterization of NHL mortars and cohesive simulation of their failure behavior. *Construction and Building Materials*, 153:569–577, 2017. doi: 10.1016/j.conbuildmat.2017.07.127.

[81] M. Azenha, F. Magalhães, R. Faria, and A. Cunha. Measurement of concrete E-modulus evolution since casting: A novel method based on ambient vibration. *Cement and Concrete Research*, 40(7):1096–1105, 2010. doi: 10.1016/j.cemconres.2010.02.014.

[82] M. Ramesh, M. Azenha, and P. B. Lourenço. Mechanical properties of lime-cement masonry mortars in their early ages. *Materials and Structures*, 52(1), 2019. doi: 10.1617/s11527-019-1319-z.

[83] *ACI 318-11. Building code requirements for structural concrete and commentary.* ACI-American Concrete Institute, Farmington Hills, Michigan, USA, 2011.

[84] *BS EN 1015-1, Methods of test for mortar for masonry - Part 1: Determination of particle size distribution by sieve analysis.* 1998/A1:2006.

[85] *BS EN 1097-6, Tests for mechanical and physical properties of aggregates - Part 6: Determination of particle density and water absorption.* 2013.

[86] *BS EN 1097-3, Tests for mechanical and physical properties of aggregates. Part 3: Determination of loose bulk density and voids.* 1998.

[87] B. Bails. *Diccionario de Arquitectura Civil. Obra póstuma.* Colegio de Aparejadores y Arquitectos Técnicos de Asturias, Oviedo, Spain, 1973.

[88] *BS EN 1015-3, Methods of test for mortar for masonry - Part 3: Determination of consistence of fresh mortar (by flow table).* 1999/A2:2006.

[89] *BS EN 1015-6, Methods of test for mortar for masonry - Part 6: Determination of bulk density of fresh mortar.* 1998/A1:2006.

[90] *BS EN 1015-2, Methods of test for mortar for masonry - Part 2: Bulk sampling of mortars and preparation of test mortars.* 1998/A1:2006.

[91] *BS EN 459-2, Building lime - Part 2: Tests methods.* 2010.

[92] *BS EN 12390-13, Testing hardened concrete. Part 13: Determination of secant modulus of elasticity in compression.* 2012.

[93] RILEM Committee on Fracture Mechanics of Concrete, Determination of the fracture energy of mortar and concrete by means of the three-point bend tests on notched beams, Draft recommendation, TC 50-FMC. *Materials and Structures*, (18):285–290, 1985.

[94] M. Elices, G. V. Guinea, and J. Planas. Measurement of the fracture energy using three-point bend tests: Part 3-Influence of cutting the P-δ tail. *Materials and Structures*, 25(150): 327–334, 1992. doi: 10.1007/BF02472591.

[95] G. V. Guinea, J. Planas, and M. Elices. Measurement of the fracture energy using three-point bend tests: Part 1-Influence of experimental procedures. *Materials and Structures*, 25 (148):212–218, 1992. doi: 10.1007/BF02473065.

[96] J. Planas, M. Elices, and G. V. Guinea. Measurement of the fracture energy using three-point bend tests: Part 2-Influence of bulk energy-dissipation. *Materials and Structures*, 25 (149):305–312, 1992. doi: 10.1007/BF02472671.

[97] M. Elices, G. V. Guinea, and J. Planas. On the measurement of concrete fracture energy using three-point bend tests. *Materials and Structures*, 30(200):375–376, 1997. doi: 10.1007/BF02480689.

[98] X. X. Zhang, G. Ruiz, R. C. Yu, and M. Tarifa. Fracture behaviour of high-strength concrete at a wide range of loading rates. *International Journal of Impact Engineering*, 36(10-11): 1204–1209, 2009. doi: 10.1016/j.ijimpeng.2009.04.007.

[99] Hillerborg, A. Results of three comparative test series for determining the fracture energy G_F of concrete. *Material and Structures*, 18:407–413, 1985.

[100] G. V. Guinea, J. Y. Pastor, J. Planas, and M. Elices. Stress intensity factor, compliance and CMOD for a general three-point-bend beam. *International Journal of Fracture*, 89(2): 103–116, 1998. doi: 10.1023/A:1007498132504.

[101] RILEM TC89:FMT Committee on Fracture Mechanics of Concrete–Test Methods. Determination of the fracture parameters (K_{Ic}^s and CTOD_c) of plain concrete using three-point bend tests. *Materials and Structures*, (23):457–60, 1991.

[102] *BS EN 12390-6, Testing hardened concrete - Part 6: Tensile splitting strength of test specimens.* 2009.

[103] C. Rocco, G. V. Guinea, J. Planas, and M. Elices. Size effect and boundary conditions in the Brazilian test: Theoretical analysis. *Materials and Structures*, 32(220):437–444, 1999. doi: 10.1007/BF02482715.

[104] C. Rocco, G. V. Guinea, J. Planas, and M. Elices. Size effect and boundary conditions in the Brazilian test: Experimental verification. *Materials and Structures*, 32(217):210–217, 1999. doi: 10.1007/BF02481517.

[105] I. Iglesias, B. Acosta, R. Yu, G. Ruiz, M. Aineto, and A. Acosta. Study of mechanical characterization of ceramic specimens from a Brazilian test adaptation. *Materiales De Construccion*, 61(303):417–429, 2011. doi: 10.3989/mc.2011.55809.

[106] C. Rocco, G. V. Guinea, J. Planas, and M. Elices. Mechanisms of rupture in splitting tests. *Aci Materials Journal*, 96(1):52–60, 1999.

[107] A. Hillerborg, M. Modéer, and P. E. Petersson. Analysis of crack formation and crack growth in concrete by means of fracture mechanics and finite elements. *Cement and Concrete Research*, 6(6):773–781, 1976. doi: 10.1016/0008-8846(76)90007-7.

[108] D. Gulotta, S. Goidanich, C. Tedeschi, T. G. Nijland, and L. Toniolo. Commercial NHL-containing mortars for the preservation of historical architecture. Part 1: Compositional and mechanical characterisation. *Construction and Building Materials*, 38:31–42, 2013. doi: 10.1016/j.conbuildmat.2012.08.029.

[109] *UNE 83980. Concrete durability. Test methods. Determination of the water absorption, density and accesible porosity for water in concrete.* 2014.

[110] M. Stefanidou. Methods for porosity measurement in lime-based mortars. *Construction and Building Materials*, 24(12, SI):2572–2578, 2010. doi: 10.1016/j.conbuildmat.2010.05.019.

[111] *AutoPore IV 9500 Operator's Manual.* Micromeritics Instrument Corporation, 2001.

[112] *BS EN 1015-18, Methods of test for mortar for masonry - Part 18: Determination of water absorption coefficient due to capillary action of hardened mortar.* BSI, 2002.

[113] A. Benazzouk, O. Douzane, and M. Queneudec. Transport of fluids in cement-rubber composites. *Cement & Concrete Composites*, 26(1):21–29, 2004. doi: 10.1016/S0958-9465(02)00119-1.

[114] N. S. Martys and C. F. Ferraris. Capillary transport in mortars and concrete. *Cement and Concrete Research*, 27(5):747–760, 1997. doi: 10.1016/S0008-8846(97)00052-5.

[115] P. Pipilikaki and M. Beazi-Katsioti. The assessment of porosity and pore size distribution of limestone Portland cement pastes. *Construction and Building Materials*, 23(5):1966–1970, 2009. doi: 10.1016/j.conbuildmat.2008.08.028.

[116] J. I. Alvarez, J. M. Fernandez, I. Navarro-Blasco, A. Duran, and R. Sirera. Microstructural consequences of nanosilica addition on aerial lime binding materials: Influence of different drying conditions. *Materials Characterization*, 80:36–49, 2013. doi: 10.1016/j.matchar.2013.03.006.

[117] S. Mindess, J. F. Young, and D. Darwin. *Concrete.* Pearson Education, Upper Saddle River, New Jersey, USA, second edition, 2002.

[118] A. Isebaert, W. De Boever, F. Descamps, J. Dils, M. Dumon, G. De Schutter, E. Van Ranst, V. Cnudde, and L. Van Parys. Pore-related properties of natural hydraulic lime mortars: an experimental study. *Materials and Structures*, 49(7):2767–2780, 2016. doi: 10.1617/s11527-015-0684-5.

[119] X. Zhang, G. Ruiz, R. C. Yu, E. Poveda, and R. Porras. Rate effect on the mechanical properties of eight types of high-strength concrete and comparison with FIB MC2010. *Construction and Building Materials*, 30:301–308, 2012. doi: 10.1016/j.conbuildmat.2011.11.037.

[120] M. G. Margalha. *Ligantes aéreos minerais. Processos de extinção e o factor tempo na sua qualidade.* PhD thesis, Lisbon University, Portugal, 2010.

[121] R. Ramalho. A resistência mecânica e a porosidade das argamassas bastardas com baixo teor de cimento. Master's thesis, Évora University, Portugal, 2013.

[122] M. Azenha, L. F. Ramos, R. Aguilar, and J. L. Granja. Continuous monitoring of concrete E-modulus since casting based on modal identification: A case study for in situ application. *Cement & Concrete Composites*, 34(7):881–890, 2012. doi: 10.1016/j.cemconcomp.2012.04.004.

[123] M. Azenha, R. Faria, F. Magalhães, L. Ramos, and A. Cunha. Measurement of the E-modulus of cement pastes and mortars since casting, using a vibration based technique. *Materials and Structures*, 45(1-2):81–92, 2012. doi: 10.1617/s11527-011-9750-9.

[124] M. Azenha. *Numerical Simulation of the Structural Behavior of Concrete since its Early Ages.* PhD thesis, Faculty of Enginnering of the University of Porto, 2009.

[125] M. Azenha, F. Magalhães, and L. Ramos. Method based in ambient vibration for quantifying the evolution of E-modulus of hardening materials. In *Portugal patent application 104413*, 2009.

[126] L. Maia, M. Azenha, R. Faria, and J. Figueiras. Influence of the cementitious paste composition on the E-modulus and heat of hydration evolutions. *Cement and Concrete Research*, 41(8):799–807, 2011. doi: 10.1016/j.cemconres.2011.03.008.

[127] L. Maia, M. Azenha, M. Geiker, and J. Figueiras. E-modulus evolution and its relation to solids formation of pastes from commercial cements. *Cement and Concrete Research*, 42(7): 928–936, 2012. doi: 10.1016/j.cemconres.2012.03.013.

[128] J. L. Granja, M. Azenha, C. De Sousa, and C. Ferreira. Comparison between different experimental techniques for stiffness monitoring of cement pastes. *Journal of Advanced Concrete Technology*, 12(2):46–61, 2014. doi: 10.3151/jact.12.47.

[129] J. Granja and M. Azenha. Towards a robust and versatile method for monitoring E-modulus of concrete since casting: Enhancements and extensions of EMM-ARM. *Strain*, 53(4), 2017. doi: 10.1111/str.12232.

[130] J. L. Granja. *EMM-ARM User's Guide. Version 2.0.1. Appendix-A. PhD Thesis. Continuous characterization of stiffness of cement - based materials: experimental analysis and micro-mechanics modelling.* University of Minho, Guimarães, Portugal, 2016.

[131] *ASTM. C403/C 403M-99. Standard Test Method for Time od Setting of Concrete Mixtures by Penetration Resistance.* ASTM, West Conshohocken, United States, 1999.

[132] M. A. Meyers and K. K. Chawla. *Mechanical Behavior of Materials.* Cambridge University Press, New York, USA, second edition, 2008.

[133] C. Montoya, J. Lanas, M. Arandigoyen, I. Navarro, P. J. G. Casado, and J. I. Alvarez. Study of ancient dolomitic mortars of the church of Santa Maria de Zamarce in Navarra (Spain): comparison with simulated standards. *Thermochimica Acta*, 398(1-2):107–122, 2003. doi: 10.1016/S0040-6031(02)00321-0.

[134] M. A. Oliveira, M. Azenha, P. B. Lourenço, A. Meneghini, E. T. Guimaraes, F. Castro, and D. Soares. Experimental analysis of the carbonation and humidity diffusion processes in aerial lime mortar. *Construction and Building Materials*, 148:38–48, 2017. doi: 10.1016/j.conbuildmat.2017.04.120.

[135] D. A. Silva, H. R. Wenk, and P. J. M. Monteiro. Comparative investigation of mortars from Roman Colosseum and cistern. *Thermochimica Acta*, 438(1-2):35–40, 2005. doi: 10.1016/j.tca.2005.03.003.

[136] K. Scrivener, R. Snellings, and B. Lothenbach. *A practical Guide to Microstructural Analysis of Cementitious Materials.* CRC Press Taylor & Francis Group, Boca Raton, Florida, USA, 2016.

[137] J. L. Granja. *Continuous characterization of stiffness of cement-based materials: experimental analysis and micro-mechanics modelling.* PhD thesis, Universidade do Minho, Escola de Engenharia, Guimarães, Portugal, 2016.

[138] N. Sathiparan and U. Rumeshkumar. Effect of moisture condition on mechanical behavior of low strength brick masonry. *Journal of Building Engineering*, 17:23–31, 2018. doi: 10.1016/j.jobe.2018.01.015.

[139] S. Popovics. *Strength and Related Properties of Concrete: A Quantitative Aproach.* New York, USA, 1998.

[140] C. Moler. *Matlab. R2016b.* MathWorks, 2016.

[141] U. Lencis, A. Udris, and A. Korjakins. Moisture effect on the ultrasonic pulse velocity in concrete cured under normal conditions and at elevated temperature. *Construction Science*, (14):71–78, 2013. doi: 10.2478/cons-2013-0011.

[142] Z. Lafhaj, M. Goueygou, A. Djerbi, and M. Kaczmarek. Correlation between porosity, permeability and ultrasonic parameters of mortar with variable water/cement ratio and water content. *Cement and Concrete Research*, 36(4):625–633, 2006. doi: 10.1016/j.cemconres.2005.11.009.

[143] J. H. Bungey. The validity of ultrasonic pulse velocity testing of in-place concrete for strength. *Ndt International*, 13(6):296–300, 1980. doi: 10.1016/0308-9126(80)90021-8.

[144] S. Boualleg, M. Bencheikh, L. Belagraa, A. Daoudi, and M. A. Chikouche. The combined effect of the initial cure and the type of cement on the natural carbonation, the portlandite content, and nonevaporable water in blended cement. *Advances in Materials Science and Engineering*, pages 1–17, 2017. doi: 10.1155/2017/5634713.

[145] D. G. Albert. A comparison between wave-propagation in water-saturated and air-saturated porous materials. *Journal of Applied Physics*, 73(1):28–36, JAN 1 1993. doi: 10.1063/1.354035.

[146] O. Cazalla. *Morteros de cal. Aplicación en el Patrimonio Histórico.* PhD thesis, Universidad de Granada, Spain, 2002.

[147] R. M. Dheilly, J. Tudo, Y. Sebai, and M. Queneudec. Influence of storage conditions on the carbonation of powdered $Ca(OH)_2$. *Construction and Building Materials*, 16(3):155–161, 2002. doi: 10.1016/S0950-0618(02)00012-0.

[148] V. Rostami, Y. Shao, A. J. Boyd, and Z. He. Microstructure of cement paste subject to early carbonation curing. *Cement and Concrete Research*, 42(1):186–193, 2012. doi: 10.1016/j.cemconres.2011.09.010.

[149] P. J. P. Gleize, A. Mullier, and H. R. Roman. Microstructural investigation of a silica fume-cement-lime mortar. *Cement & Concrete Composites*, 25(2):171–175, 2003. doi: 10.1016/S0958-9465(02)00006-9.

[150] K. S. Wang, K. L. Lin, T. Y. Lee, and B. Y. Tzeng. The hydration characteristics when C_2S is present in MSWI fly ash slag. *Cement & Concrete Composites*, 26(4):323–330, 2004. doi: 10.1016/S0958-9465(02)00144-0.

[151] A. El-Turki, M. A. Carter, M. A. Wilson, R. J. Ball, and G. C. Allen. A microbalance study of the effects of hydraulicity and sand grain size on carbonation of lime and cement. *Construction and Building Materials*, 23(3):1423–1428, 2009. doi: 10.1016/j.conbuildmat.2008.07.006.

[152] C. Rodriguez-Navarro, O. Cazalla, K. Elert, and E. Sebastian. Liesegang pattern development in carbonating traditional lime mortars. *Proceedings of the Royal Society A-Mathematical Physical and Engineering Sciences*, 458(2025):2261–2273, 2002. doi: 10.1098/rspa.2002.0975.

[153] O. Cazalla, C. Rodriguez-Navarro, E. Sebastian, G. Cultrone, and M. J. De La Torre. Aging of lime putty: Effects on traditional lime mortar carbonation. *Journal of the American Ceramic Society*, 83(5):1070–1076, 2000.

[154] X. Zhang, G. Ruiz, M. Tarifa, D. Cendon, F. Galvez, and W. H. Alhazmi. Dynamic Fracture Behavior of Steel Fiber Reinforced Self-Compacting Concretes (SFRSCCs). *Materials*, 10 (11), 2017. doi: 10.3390/ma10111270.

[155] G. Ruiz. Propagation of a cohesive crack crossing a reinforcement layer. *International Journal of Fracture*, 111(3):265–282, 2001. doi: 10.1023/A:1012260410704.

[156] A. L. Rosa, R. C. Yu, G. Ruiz, L. Saucedo, and J. L. A. O. Sousa. A loading rate dependent cohesive model for concrete fracture. *Engineering Fracture Mechanics*, 82:195–208, 2012. doi: 10.1016/j.engfracmech.2011.12.013.

[157] G. Ruiz, J. J. Ortega, R. C. Yu, S. Xu, and Y. Wu. Effect of size and cohesive assumptions on the double-K fracture parameters of concrete. *Engineering Fracture Mechanics*, 166:198–217, 2016. doi: 10.1016/j.engfracmech.2016.09.001.

[158] G. Ruiz, J. J. Ortega, R. C. Yu, S. Xu, and Y. Wu. Loading rate effect on the double-K fracture parameters of concrete. *FRAMCOS-9*, page doi 10.21012/FC9.038, 2016.

[159] J. Planas and M. Elices. Nonlinear fracture of cohesive materials. *International Journal of Fracture*, 51(2):139–157, 1991.

[160] P. E. P. E. Petersson. Crack growth and development of fracture zone in plain concrete and similar materials. *Lund Institute of Technology*, (Report No. TVBM-100), 1981.

[161] G. V. Guinea, J. Planas, and M. Elices. A general bilinear fit for the softening curve of concrete. *Materials and Structures*, 27(166):99–105, 1994. doi: 10.1007/BF02472827.

[162] V. Cervenka, L. Jendele, and J. Cervenka. Computer program of nonlinear finite element analysis of reinforced concrete structures. *Cervenka Consulting Prague*, pages 1–142, 2009.

[163] E. Poveda, J. J. Ortega, G. Ruiz, R. Porras, and J. R. Carmona. Normal and tangential extraction of embedded anchor plates from precast facade concrete panels. *Engineering Structures*, 110:21–35, 2016. doi: 10.1016/j.engstruct.2015.11.045.

[164] Z. P. Bažant and B. H. Oh. Crack band theory for fracture of concrete. *Mater Struct*, 16: 155–177, 1983.

[165] P. Menétrey and K. J. William. Triaxial failure criterion for concrete and its generalization. *ACI Structural Journal*, 92(6):311–318, 1995.

[166] D. A. Hordijk. *Local approach to fatigue of concrete. PhD thesis.* PhD thesis, 1991.

[167] R. C. Yu, G. Ruiz, and E. W. V. Chaves. A comparative study between discrete and continuum models to simulate concrete fracture. *Engineering Fracture Mechanics*, 75(1): 117–127, 2008. doi: 10.1016/j.engfracmech.2007.03.031.

[168] A. de la Rosa, E. Poveda, G. Ruiz, and H. Cifuentes. Proportioning of self-compacting steel-fiber reinforced concrete mixes based on target plastic viscosity and compressive strength: Mix-design procedure & experimental validation. *Construction and Building Materials*, 189: 409–419, 2018. doi: 10.1016/j.conbuildmat.2018.09.006.

[169] G. Ruiz, A. de la Rosa, S. Wolf, and E. Poveda. Model for the compressive stress–strain relationship of steel fiber-reinforced concrete for non-linear structural analysis. *Hormigón y Acero*, 69(S1):75–80, 2019. doi: 10.1016/j.hya.2018.10.001.

[170] G. Ruiz, A. de la Rosa, and E. Poveda. Relationship between residual flexural strength and compression strength in steel-fiber reinforced concrete within the new Eurocode 2 regulatory framework. *Theoretical and Applied Fracture Mechanics*, Submitted.

[171] A. Izaguirre, J. Lanas, and J. I. Alvarez. Effect of a polypropylene fibre on the behaviour of aerial lime-based mortars. *Construction and Building Materials*, 25(2):992–1000, 2011. doi: 10.1016/j.conbuildmat.2010.06.080.

[172] M. L. Santarelli, F. Sbardella, M. Zuena, J. Tirillo, and F. Sarasini. Basalt fiber reinforced natural hydraulic lime mortars: A potential bio-based material for restoration. *Materials & Design*, 63:398–406, 2014. doi: 10.1016/j.matdes.2014.06.041.

[173] F. Iucolano, B. Liguori, and C. Colella. Fibre-reinforced lime-based mortars: A possible resource for ancient masonry restoration. *Construction and Building Materials*, 38:785–789, 2013. doi: 10.1016/j.conbuildmat.2012.09.050.

[174] J. J. Ortega, G. Ruiz, R. C. Yu, N. Afanador-Garcia, M. Tarifa, E. Poveda, X. X. Zhang, and F. Evangelista Jr. Number of tests and corresponding error in concrete fatigue. *International Journal of Fatigue*, 116:210–219, 2018. doi: 10.1016/j.ijfatigue.2018.06.022.

[175] E. Poveda, G. Ruiz, H. Cifuentes, R. C. Yu, and X. X. Zhang. Influence of the fiber content on the compressive low-cycle fatigue behavior of self-compacting SFRC. *International Journal of Fatigue*, 101(1):9–17, 2017. doi: 10.1016/j.ijfatigue.2017.04.005.

[176] L. Saucedo, R. C. Yu, A. Medeiros, X. X. Zhang, and G. Ruiz. A probabilistic fatigue model based on the initial distribution to consider frequency effect in plain and fiber reinforced concrete. *International Journal of Fatigue*, 48:308–318, 2013. doi: 10.1016/j.ijfatigue.2012.11.013.

[177] Joan R. Casas. A probabilistic fatigue strength model for brick masonry under compression. *Constructiona and Building Materials*, 23(8):2964–2972, 2009. doi: 10.1016/j.conbuildmat.2009.02.043.